Universitat Autònoma de Barcelona

Quantum Metrology and Thermometry in Open Systems. Thermal Equilibrium and Beyond

Mohammad Mehboudi

Universitat Autònoma de Barcelona

Quantum Metrology and Thermometry in Open Systems

Thermal Equilibrium and Beyond

by

Mohammad Mehboudi

under supervision of

Dr. Anna Sanpera Trigueros

A thesis submitted in partial fulfillment for the
degree of Doctor of Philosophy

in

Unitat de Física Teòrica: Informació i Fenòmens Quàntics
Departament de Física
Facultat de Ciències

Bellaterra, April 2017

Abstract

In my thesis I explore quantum metrology in open systems, with a special focus on quantum temperature estimation, or *thermometry*. For this aim, I categorize my study in two different regimes of *thermal equilibrium* and *beyond thermal equilibrium*. In both cases, my collaborators and I, raise questions of fundamental and technological interest.

Among such questions, I point out the followings: What are the ultimate precision bounds on thermometry with individual (single) probes? Is it possible to improve these bounds by using quantum resources such as *quantum correlations* and *quantum criticality*?

We not only find the ultimate precision bound on thermometry, posed by physical laws of nature, but also show how to exploit quantum resources to surpass the classical bounds on precision, even at finite temperature. Furthermore, we identify experimentally feasible measurements which can achieve these bounds. Specifically, our results show that in a many-body sample, the collective quantum correlations can become optimal observables to accurately estimate the temperature. In turn, the collective spin correlations can be read out with the non-demolishing *quantum Faraday spectroscopy*. Hence, our method offers inferring maximum information about the temperature, yet leaving the sample unperturbed.

Out of thermal equilibrium, we address both *static* and *dynamic* systems. In the former case, we find the limitations/opportunities for estimation of low temperature, and small *temperature gradient* in a sample. Particularly, we identify that the thermometric precision at low temperature can be significantly enhanced by strengthening the probe-sample coupling. Our observations may find applications in practical nanoscale thermometry at low temperature—a regime which is particularly relevant to quantum technologies.

With a more applied point of view, such non equilibrium protocols give rise to *autonomous quantum heat pumps*. Hence, we also give thought to probing the quality of such heat pumps with the tiniest probes, i.e., a single spin. Although at the first glance a spin seems to be a very small probe, we confirm its efficiency in probing quantum heat pumps. Our techniques may find applications in the emerging field of quantum thermal engineering, as they facilitate the diagnosis and design optimization of complex thermodynamic cycles.

When it comes to dynamic systems, we have formulate a (fluctuation-dissipation) theory with the help of which one can identify the smallest external perturbation which affects a quantum system. Our proposal might be found useful in quantum force detection, for instance, interferometric detection of gravitational waves.

Resumen

En mi tesis exploro la metrología cuántica en sistemas abiertos, con especial enfoque en la estimación de temperatura cuántica o *termometría*. Para este objetivo, voy a clasificar mi estudio en dos regímenes diferentes de *equilibrio térmico* y *más allá del equilibrio térmico*. En ambos casos, mis colaboradores y yo planteamos cuestiones de interés fundamental y tecnológico.
Entre estas preguntas, señalo lo siguiente: ¿Cuáles son los límites de precisión máximos en la termometría con sondas individuales? ¿Es posible mejorar estos límites utilizando recursos cuánticos tales como las *correlaciones cuánticas* y la *criticalidad cuántica*?
No sólo encontramos la máxima precisión ligada a la termometría, planteada por las leyes físicas de la naturaleza, sino también muestramos cómo explotar los recursos cuánticos para superar los límites clásicos en la precisión, incluso a temperatura finita. Además, identificamos medidas experimentalmente viables que pueden alcanzar estos límites. Específicamente, nuestros resultados muestran que en una muestra de muchos cuerpos, las correlaciones cuánticas colectivas pueden convertirse en observables óptimos para estimar con precisión la temperatura. A su vez, las correlaciones de spin colectivo se pueden observar con *espectroscopia cuántica de Faraday* no destructiva. Por lo tanto, nuestro método ofrece la posibilidad de inferir la máxima información sobre la temperatura, dejando la muestra sin perturbar.
Fuera del equilibrio térmico, abordamos sistemas *estáticos* y *dinámicos*. En el primer caso, encontramos limitaciones/oportunidades para la estimación a baja temperatura, y bajo *gradiente de temperatura* en una muestra. Particularmente, identificamos que la precisión termométrica a baja temperatura puede ser significativamente mejorada mediante el fortalecimiento del acoplamiento sonda-muestra. Nuestras observaciones pueden encontrar aplicaciones prácticas en termometría a nanoescala y baja temperatura—un régimen que es particularmente relevante para tecnologías cuánticas.
Con un punto de vista más aplicado, tales protocolos de no equilibrio dan lugar a *bombas de calor cuánticas autónomas*. Por lo tanto, también pensamos en explorar la calidad de tales bombas de calor con las sondas más pequeñas, es decir, un solo spin. Aunque a primera vista un spin parece ser una sonda muy pequeña, confirmamos su eficiencia explorando bombas de calor cuánticas. Nuestras técnicas pueden encontrar aplicaciones en el campo emergente de la ingeniería térmica cuántica, ya que facilitan el diagnóstico y la optimización del diseño de ciclos termodinámicos complejos.
Cuando se trata de sistemas dinámicos, hemos formulado una teoría (fluctuación-disipación) con la ayuda de la cual se puede identificar la mínima perturbación externa que afecta a un sistema cuántico. Nuestra propuesta puede ser útil en la detección de la fuerzas cuánticas, como por ejemplo, la detección interferométrica de ondas gravitatorias.

In memory of Mohammad Shafie Mehboudi

I entwined mind and soul indeed
Then planted the resulting seed
In this marriage the outcome is joy
Beauty and soulfulness employ

Hafez

Contents

Chapter 1

Introduction

The field of *parameter estimation* or *metrology* deals with optimizing measurement and post measurement strategies in order to infer the value of an unknown parameter ξ. Metrology lies at the core of cutting-edge applications including ultra precise clocks, global positioning, or sensing of tiny signals in biological systems to name a few [1–3]. In practice, technological advances are bringing the attainable measurement resolutions to a whole new level, as showcased, for instance, by the recent interferometric detection of gravitational waves [4]. The active exploitation of quantum effects in high precision measurements, or *quantum* metrology, holds promise for further improving the current metrological standards. Quantum metrology is becoming one of the pillars of future quantum technologies [5, 6].

The most generic metrological setting consists in coupling a probe to a sample on which the parameter ξ is registered. The outcomes of measurements performed on the probe form a dataset, using which an estimate ξ_{est} of the unknown parameter is inferred. On account of the fact that, imperfections, practical limitations, and other sources of *error* are inescapable in reality, an essential aim of metrology is to enhance accuracy of data acquisition and inference, thus boosting the level of estimation [7].

Apart from the indispensable task of upgrading measurement instruments, *statistics* plays its own crucial role in exceeding better precisions. For instance, as a consequence of the celebrated central limit theorem, the error in the estimation of the parameter ξ, denoted by $\delta\xi$, decreases as the number of independent measurement realizations, denoted by N, increases. This fact leads to the *shot-noise* scaling $\delta\xi \sim 1/\sqrt{N}$ [8]. What is even more compelling, is the restriction (or even new possibilities to exploit) imposed by the physics of the system under study. These restrictions typically set bounds on the ultimate achievable accuracy, which are commonly described through a 'Cramér-Rao bound' (CRB) [9]).

In the framework settled by quantum physics, measurements act differently than in classical systems. In particular, *quantum correlations* can affect the outcomes of measurements [10], suggesting new possibilities to explore in parameter estimation. For instance, one of the most remarkable outcomes of quantum metrology is exploiting entanglement in parameter estimation. Using entangled systems could drastically improve the shot-noise limit, leading to an error $\delta\xi \sim 1/N$. This is conventionally termed the *Heisenberg limit*, the counter part of the classical shot-noise limit (also know as the *standard quantum limit*) [11].

Beating the shot-noise scaling is very difficult to be realized in practice [12]. This is primarily due to the fragility of entanglement to environmental noise [13], although, in some instances noise can allow for better-than-shot-noise performance [14–21]. An additional problem arises from the fact that the optimal measurements to be performed on the N probes, i.e., those that minimize the uncertainty in the estimation, are often highly non-local measurements and thus, harder to implement. Nevertheless, multiple experiments have accomplished sub-shot-noise limit error by utilizing features of quantum physics [22].

As the interaction with environment gets substantial, the underlying *open* dynamics originates complications in having a neat theory of parameter estimation [23–26]. In principle, one might consider the environment large enough, such that the compound *system-environment* forms a "bigger closed system". In turn, the evolution of this bigger closed system is described with a unitary operation. The state of the system at any moment is given by tracing over the environment, namely $\rho_S(t) = \mathrm{Tr}_E[U_{SE}(t,t_0)\rho_{SE}(t_0)U_{SE}^\dagger(t,t_0)]$, where ρ_{SE} is the state of the system-environment (SE), and $U_{SE}(t,t_0)$ is its corresponding unitary evolution [27, 28]. (See Chapter 3 for a review.) Under some conditions, this dynamics transfers any system to a unique *stationary/steady state*. The characteristics of this stationary state not only depend on the Hamiltonian of the system, but also on that of the environment and its interaction with the system. In particular, the stationary state might be at (i) *thermal equilibrium*, or (ii) *out of equilibrium*. In this thesis, we address parameter estimation in both scenarios as well as in (iii) *dynamic* systems.

(i) Thermal equilibrium

This occurs when the environment is in a thermal state and weakly interacts with the system. With quantum[1] thermal systems being usually described by few parameters, i.e., the *conserved charges* or *generalized chemical potentials*, quantum metrology can play a crucial role to identify them. Specifically there is a growing interest in obtaining accurate temperature readings with nanometric spatial resolution [3, 30, 31], which would pave the way towards many groundbreaking applications in medicine, biology or material science. This motivates the development of precise quantum thermometric techniques.

[1] Here we use the term "quantum" to also emphasize that the conserved charges might be non-commuting [29], in contrast with a classical thermal state.

On one hand, the recent progress in the manipulation of *individual* quantum systems has made it possible to use them as temperature probes, thus minimizing the undesired disturbance on the sample. Fluorescent thermometry may be implemented, for instance, on a single quantum dot to accurately estimate the temperature of fermionic [32, 33] and bosonic [34] reservoirs. Similarly, the ground state of colour centres in nano-diamonds has already been used as a fluorescent thermometer [3, 30, 31], achieving precisions down to the millikelvin scale, and a spatial resolution of few hundreds of nanometers. Thermometry applied to micro-mechanical resonators [35–37] has also been subject of investigation. Other studies have focused on more fundamental questions such as the scaling of the precision of temperature estimation with the number of quantum probes [38], and the potential role played by coherence and entanglement in simple thermometric tasks [39].

On the other hand, many-body systems empower the feasibility of realizing *super-extensive* accuracy, (i.e., precisions better than the Heisenberg scaling). This accuracy may be attained even without correlations in the input state, as the *non-local* Hamiltonian of a many body system produces quantum correlations amongst any input state [22, 40–42]. Concretely, by enabling k-body interactions, one can reach an estimation error as small as $\delta\xi \sim 1/\sqrt{N^k}$ [43], if the system is entangled, while uncorrelated inputs reach errors down to $\delta\xi \sim 1/\sqrt{N^{k-1}}$. Notwithstanding that these findings substantially rely on the non-local structure of the Hamiltonian, and the measurement that is performed [43–45], few experiments have achieved super-Heisenberg limit [22].

Thus, many-body systems, and in particular, strongly correlated ones present several features that are starting to be explored for quantum sensing and quantum metrology purposes [46–48]. With the advent of quantum simulators based on *ultracold* atoms and ions, several paradigmatic Hamiltonians representing simple spin models are being implemented in a very controllable manner [49–52], which paves the way towards practical quantum-enhanced sensing. Hence, in a fraction of this thesis we have explored the possibilities that strongly correlated systems provide for quantum metrological purposes.

At zero temperature, quantum fluctuations can push the system to a new order by means of quantum phase transitions. For second order phase transitions, the emergence of a new order is reflected by the presence of quantum correlations at all length scales in the critical point. It is known, that *criticality* emerged around a quantum phase transition point, is a powerful resource for metrology [46, 53], as it allows for super-extensive scaling in the estimation of Hamiltonian parameters, and external magnetic fields. At finite temperature, however, such emergence gradually fades away due to the presence of thermal fluctuations. As a result, for low dimensional systems, critical points signaling quantum phase transitions often broaden into *critical regions*. Those regions still separate different phases which keep track of their ground state correlations.

Hence, the transition between those phases might appear as smooth crossovers [54, 55], nonetheless carrying a footprint of the quantum phase transition occurring at zero temperature. In view of these facts, the behavior of quantum correlations at finite temperatures could be used as a way to estimate the it. Therefore, a natural question to pose, both for fundamental as well as for technological reasons, is how well can the temperature be determined in these systems. The second question is about precise estimation of many-body Hamiltonian couplings, rather than temperature itself. Namely, what are the fundamental bounds on the precision of the estimation? Is it possible to beat the shot-noise limit at finite temperatures? Our results show that this is indeed the case.

Having the ultimate bound on precision at hand, a third question arises concerning its attainability: Are there experimentally feasible measurement strategies that can saturate those bounds? Generally this is not the case. For instance, the minimal error in temperature estimation of a thermal sample is realized by a projective measurement on its energy eigenbasis. Typically, such type of measurement in ultracold lattice gases is not accessible. Instead, information about quantum phases and temperature is usually obtained from momentum and density distributions or from density-density (or spin-spin) correlations. These quantities can be extracted by using destructive methods such as time of flight imaging or in-situ imaging, the latter using single site addressability [56], for instance using single site addressability [57, 58]. Despite the huge relevance, these methods suffer some limitations for metrological pursposes due to their destructive character.

In this sense, quantum non demolition (QND) methods can provide clear advantages [59]. The quantum Faraday spectroscopy is a minimally disturbing matter-light interface that maps collective atomic quantum correlations into light quadrature fluctuations, the latter perceptible to be measured by homodyne detection. As a part of this thesis, we adapt this method to estimate the temperature and Hamiltonian couplings of a strongly correlated system simulated by an atomic lattice gas. Furthermore, to asses the reliability of our method for, we compare the signal-to-noise ratio obtained from the measurement of collective atomic correlations with the minimal possible error provided by the quantum Cramér-Rao bound. Our results show that the measurement of collective quantum correlations can become optimal for thermometry and magnetometry in some integrable models.

(ii) Non-equilibrium stationary states

Such states appear particularly, in the strong coupling limit, or due to the presence of multiple environments interacting simultaneously with the system. In the former occurrence, the strong coupling conducts a notable correlation between the system and the environment, therefore simplifications which lead to the Lindbladian master equation are not permitted any longer. Even

so, in numerous instances one might pinpoint the exact solution of the problem with the help of, say, quantum Langevin equations. The strong coupling regime is very difficult to address theoretically, but it conveys the idea that the system might acquire more information about its environment, thus, providing a more precise thermometer. Indeed, we prove such conjecture rigorously for low temperature thermometry and identify the measurements that saturate the CRB for specific systems. In addition, we suggest how the spectral density of the system-environment coupling may be engineered to further improve thermometric performance.

In contrast, when *multiple environments* appear, the Lindbladian master equation may be still valid. Rather, it is precisely the existence of multiple dissipators in the master equation that leads to non-equilibrium stationary states. In this occasion we investigate how the role of a system interacting with multiple baths at different temperatures translates into the estimation of temperature gradient between the baths, or the other way round, how the temperature gradient affects the quality of estimation in the system under scrutiny.

Further, with a more applied point of view, a tiny system coupled to several heat baths may be thought of as a *quantum heat pump*. Depending on the direction of its stationary heat flows, it may function as, e.g., a refrigerator or a heat transformer. These continuous heat devices can be arbitrarily complex multipartite systems, and yet, their working principle is always the same: they are made up of several elementary three-level stages operating in parallel. As a result, it is possible to devise external "black-box" testing strategies to learn about their functionality and performance regardless of any internal details. In this thesis, we propose testing such heat pump by coupling a two-level spin to one of its "contact transitions". The steady state of this external probe contains information about the presence of heat leaks and internal dissipation in the device and, also, about the direction of its steady-state heat currents. Provided that the irreversibility of the heat pump is low, one can further estimate its coefficient of performance. Our techniques may find applications in the emerging field of quantum thermal engineering, as they facilitate the diagnosis and design optimization of complex thermodynamic cycles.

(iii) Non-equilibrium systems with a *dynamic* state

There are two different situations in which we address also dynamic systems. In the first one, we assume that time is a finite resource, and we interrogate the system of interest before it reaches a stationary state. Such a situation demands different strategies for quantum metrology and quantum thermometry, which will be addressed later.

The second situation that we address deals with small time dependent perturbations around stationary state of a generic Markovian evolution. Often in such circumstances, the time dependence of the perturbation does not allow the system to rest at a stationary state. Yet still,

estimation of the strength of the perturbation itself is a fundamental goal. We achieve such a goal by means of a generalized *fluctuation dissipation theorem*.

The fluctuation-dissipation theorem (FDT) is a central result in statistical physics, both for classical and quantum systems. It establishes a relationship between the linear response of a system under a time-dependent perturbation and time correlations of certain observables in equilibrium. The FDT shows that the same information is obtained by measuring the response function of a system or its fluctuations, and depending on convenience one can choose one or the other. More recently, it has been proved useful to assess the entanglement of complex quantum systems and in parameter estimation and other problems in quantum metrology [60].

We derive a generalization of the FDT that can be applied to any Markov quantum system and makes use of the symmetric logarithmic derivative (SLD). There are several important benefits when FDTs are formulated in terms of the SLD. First, such a formulation clarifies the relation between classical and quantum versions of the equilibrium FDT. Second, and more important, it facilitates the extension of the FDT to arbitrary quantum Markovian evolution, as given by quantum maps. Third, it brings out the connection between the FDT and Fisher information, which plays a crucial role in quantum metrology. We prove a generalized FDT for generic quantum maps and illustrate these features in an example of two harmonic oscillators with a modulated interaction.

1.1 The structure of thesis

The thesis is structured as follows: Chapters 2 and 3 are aimed at introducing some concepts and tool boxes which are needed when presenting our original research contributions. In particular, Chapter 2 presents the basics of quantum metrology while Chapter 3 deals with the theory of open quantum systems. Namely, we review the definition of quantum maps and the derivation of the Lindbladian master equation. Further, we introduce some models with open dynamics, which are repeatedly used in the literature of open quantum systems. Specifically we present their Lindbladian master equation, and give their steady state solutions.

We present our results in the next four chapters. In Chapter 4, our findings about parameter estimation in systems at finite temperatures are given. We investigate which is the optimal quantum probe to estimate temperature of an arbitrary thermal system, in other words, which is the best quantum thermometer. We also characterize the smallest temperature fluctuations such a quantum thermometer might detect. Then we explore the role of quantum correlations between probes in thermometry, and certify their importance in precision enhancement. However, since such optimal precision inherently demands non-local measurements, we benchmark the performance of local measurements on any subsystem against the optimal one. We figure out that

such local measurements are very close to optimal. Finally, we address the estimation of other parameters in thermal systems. Namely we examine metrology of the coupling between two individual systems. We show that, unlike thermometry, local measurements are not very efficient in this case.

Chapter 5, is exclusively devoted to parameter estimation in many body systems. Among our results, the following two are remarkable: (i) We show it is possible to use a QND measurement to estimate the parameters of a spin chain with an almost optimal precision. We provide such a protocol for a experimentally relevant range of parameters. (ii) We propose an adaptive scheme to exploit critical phenomena in many-body systems in order to overcome the shot-noise-limit at finite temperature.

The last two chapters of this thesis address the problem of parameter estimation in systems out of equilibrium. We categorize them into two different classes: *static* and *dynamic*. By static or dynamic, we refer to the time dependence of the interrogated system. The static case is addressed in Chapter 6. In these scenarios, the reason for the system being out of equilibrium is, for instance, a strong coupling to the environment, or the presence of multiple baths. Hence the stationary state of the system is not thermal anymore, leading to a non-equilibrium stationary state. Most of the mathematically beautiful results of thermal systems are not valid for these models. In the first part of the chapter we study the strongly coupled systems, and we find out that increasing the coupling boosts the precision of thermometry significantly. In the second part, we work on systems which are coupled to multiple baths with different temperatures. Namely, we suggest a method to efficiently measure the temperature gradient of the baths. In the end, we propose the tiniest possible probe, i.e., a two level atom, to estimate the coefficient of performance of a quantum heat pump.

Finally, in the last chapter we present our results in parameter estimation of dynamic systems. In the first part, we give thought to a situation where a system is interrogated before it reaches an stationary state, such that the measurement time plays a considerable impact. No need to mention that the initial state of the system plays its own role as well, making it essential to prepare a more sensitive one. For the sake of thermometry, we show that an optimal probe shall be prepared on its ground state, and interrogated as fast as possible. In the next part we consider parameter estimation in systems with a Markovian dynamics. The system, initially resting at a stationary state, is perturbed by a time dependent term, whose strength is to be estimated. For this, we develop a general fluctuation dissipation theorem, which connects the linear response of the system to the static SLD, associated with a constant perturbation (i.e., with no time dependence). The theorem simplifies most calculations in quantum metrology. Namely, by knowing the linear ressponce of the system to a constant perturbation, we can characterize the linear response to any time dependent parameter. As a case study, we illustrate the power of

our generalized FDT considering two detuned harmonic oscillators coupled with a modulated perturbation.

Chapter 2

An overview on quantum metrology

In this chapter we provide some necessary toolboxes from theory of quantum metrology. Our focus is on the basic concepts, those which will be used in the upcoming chapters for presenting our results. Quantum metrology is a fairly large field, for seeing its achievements see for instance [61–63] and the references therein.

The structure is as follows: In Section 2.1 we review the precision bounds on classical and quantum parameter estimation. Namely, we introduce the (Quantum) Cramér Rao inequality, which sets a lower bound on the statistical error of parameter estimation. The quantum Fisher information, a key element in metrology, is placed under scrutiny in Section 2.2, where its classical and quantum parts are identified. Moreover, we provide some useful expressions for it which will be used frequently in the next chapters. Further, in Section 2.3, we address some properties of the quantum Fisher information such as "additivity" and "convexity".

2.1 Error bounds on metrology

Consider a sample whose state depends on a parameter ξ. The value of ξ is unknown to us. In order to identify the state precisely, one has to estimate ξ. Accumulation of information about this parameter, is not possible except by performing measurements. Typically, such a measurement is realized by exploiting an interaction between the sample and an external *probe*. On the account of such an interaction, the probing system, with an initial state ρ_0, will acquire a certain amount of information about the value of ξ, hence, we show its state after the interaction with $\rho(\xi)$. Subsequently, a measurement is performed on the probe to extract this information and infer an estimate ξ_{est} of the parameter. See Figure 2.1.

The measurement, in the most extensive case, is described by a positive-operator valued measurement (POVM), the outcomes of which occur randomly, with some probability distribution

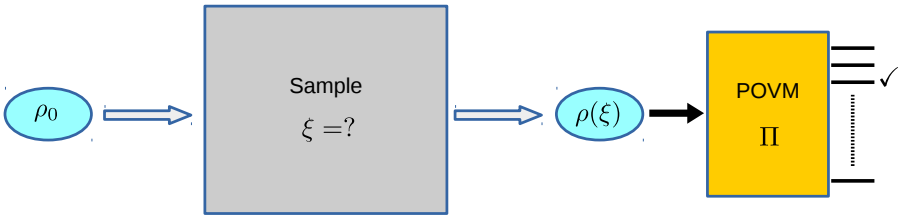

FIGURE 2.1: (Color online) A simple sketch of a probing scenario. The parameter ξ registered on the sample is unknown, and the aim is to estimate it as precise as possible. To this end, one must prepare a probe at an appropriate initial state ρ_0, which gains some information about ξ after interacting with the sample. Following this interaction one might show with ρ_ξ the state of the probe to account for the information it has acquired about ξ. This information will further be extracted by performing a POVM measurement on the probe, and due to the contribution of ξ in determining the statistics of the outcomes of such a measurement.

$\{p_m(\xi)\}$. More specifically, if the POVM elements are appointed by the set $\mathbf{\Pi} = \{\Pi_m\}$, then as maintained by the Born rule, $p_m(\xi) = \mathrm{Tr}\big(\Pi_m\, \rho(\xi)\big)$. This distribution is expected to depend on the parameter value. Repeating the whole measurement scenario a large number of times, N, provides us with a dataset $\mathbf{x}$. Eventually, one might use an *estimator* $\xi_{est}(\mathbf{x})$, in order to map the dataset to some estimate of the parameter ξ. The precision of this estimation is unfavorably affected by the randomness in the outcomes of the POVM measurement. This poses an error on the parameter estimation, which is typically quantified by the square mean error

$$\delta(\mathbf{\Pi};\, \xi_{est}) = \sqrt{\Big\langle \big(\xi_{est}(\mathbf{x}) - \langle \xi_{est}(\mathbf{x})\rangle_{\mathbf{x}}\big)^2 \Big\rangle_{\mathbf{x}}}. \tag{2.1}$$

Here the upper index $\mathbf{\Pi}$ reminds that this error depends on the specific POVM measurement. On the right hand side, the averages are evaluated over all possible data outcomes, i.e., $\langle f(\mathbf{x})\rangle_{\mathbf{x}} = \sum_{\mathbf{x}} p(\mathbf{x}|\xi) f(\mathbf{x})$, with $p(\mathbf{x}|\xi)$ being the probability of $\mathbf{x}$ given the exact value of the parameter is ξ. Hereafter we focus on unbiased estimators, for which $\langle \xi_{est}(\mathbf{x})\rangle_{\mathbf{x}} = \xi$.

The first relevant question is, how small could the error get? To answer this question, let us begin with a case where the POVM measurement is fixed. The Cramér-Rao bound (CRB) puts a lower bound on the estimation error of any unbiased estimator as follows

$$\delta(\mathbf{\Pi};\, \xi_{est}) \geq \frac{1}{\sqrt{N\mathcal{F}_c(\mathbf{\Pi};\, \xi)}}. \tag{2.2}$$

The $1/\sqrt{N}$ dependence on the repeats is a direct result of the central limit theorem. This is a very classical behavior, which leads to the well known *shot-noise* limit (also known as the standard quantum limit). Moreover $\mathcal{F}_c(\mathbf{\Pi};\, \xi)$, the so called *Fisher information*, takes into account the response of the probability distribution p to a small change in the parameter ξ. It is defined as

follows

$$\mathcal{F}_c(\mathbf{\Pi};\,\xi) \equiv \left\langle \left(\partial_\xi \log p(\mathbf{x}|\xi)\right)^2 \right\rangle_{\mathbf{x}} = \sum_{\mathbf{x}} \frac{\left(\partial_\xi p(\mathbf{x}|\xi)\right)^2}{p(\mathbf{x}|\xi)}. \tag{2.3}$$

The role of the Fisher information becomes more clear by considering its relation with the *fidelity* between two probability distributions. The fidelity between two probability distribution quantifies their closeness, and is defined as follows

$$F(p,q) = \sum_{\mathbf{x}} \sqrt{p_{\mathbf{x}} q_{\mathbf{x}}}. \tag{2.4}$$

It is easy to see that $0 \leq F(p,q) = F(q,p) \leq 1$, with the equality to one holding iff $p = q$, while equality to zero happens iff the two distributions have no common support, i.e., $p_{\mathbf{x}} \neq 0 \Rightarrow q_{\mathbf{x}} = 0$, and $q_{\mathbf{x}} \neq 0 \Rightarrow p_{\mathbf{x}} = 0$. As we will see in Section 2.3.3 for a more general quantum case, the $\mathcal{F}_c(\mathbf{\Pi},\xi)$ is related to the fidelity of two probability distributions at ξ and $\xi + \delta\xi$. Concretely

$$\mathcal{F}_c(\mathbf{\Pi};\,\xi) = -4 \lim_{\delta\xi \to 0} \left(1 - \frac{F\Big(p(\xi), p(\xi+\delta\xi)\Big)}{\delta\xi^2} \right). \tag{2.5}$$

The CRB can be asymptotically saturated using a maximum likelihood estimator [63].

It is essential to note that the CRB depends on the POVM measurement through the probability distributions. It is very interesting to identify the POVM measurement which optimizes the CRB, and its corresponding *minimum error*. The latter is provided by the Quantum Crémer-Rao bound (QCRB), which puts a lower bound on the CRB, independent of any specific measurement. The bound reads as

$$\delta\xi_{est} \geq \frac{1}{\sqrt{N\mathcal{F}(\xi)}}. \tag{2.6}$$

The term $\mathcal{F}(\xi)$ is the *quantum Fisher information* (QFI) associated with the parameter ξ, and is an optimization of the Fisher information over all possible measurements, such that $\mathcal{F}(\xi) = \max_{\mathbf{\Pi}} \mathcal{F}_c(\mathbf{\Pi};\,\xi)$. More importantly, the QFI might could be explicitly calculated using the density matrix of the probe

$$\mathcal{F}(\xi) = \mathrm{Tr}\Big(\rho(\xi)\,\Lambda_\xi^2\Big). \tag{2.7}$$

The self adjoint operator Λ_ξ is termed the *symmetric logarithmic derivative* (SLD) and is defined as

$$\Lambda_\xi\,\rho(\xi) + \rho(\xi)\,\Lambda_\xi \equiv 2\partial_{\xi'}\rho(\xi')\Big|_{\xi'=\xi}. \tag{2.8}$$

Proof of the Cramér Rao bound

Consider an unbiased estimator for which $\sum_{\mathbf{x}} p(\mathbf{x}|\xi)\Big(\xi_{est}(\mathbf{x}) - \xi\Big) = 0$. By taking derivative of this equality with respect to ξ one finds that

$$\begin{aligned} 0 &= \partial_\xi \sum_{\mathbf{x}} \Big(\xi_{est}(\mathbf{x}) - \xi\Big) p(\mathbf{x}|\xi) \\ &= -1 + \sum_{\mathbf{x}} \Big(\xi_{est}(\mathbf{x}) - \xi\Big) \partial_\xi p(\mathbf{x}|\xi), \\ \Rightarrow\ 1 &= \sum_{\mathbf{x}} \Big(\xi_{est}(\mathbf{x}) - \xi\Big) p(\mathbf{x}|\xi) \partial_\xi \log p(\mathbf{x}|\xi) \\ &= \sum_{\mathbf{x}} \Big[\Big(\xi_{est}(\mathbf{x}) - \xi\Big) \sqrt{p(\mathbf{x}|\xi)}\Big] \Big[\sqrt{p(\mathbf{x}|\xi)} \partial_\xi \log p(\mathbf{x}|\xi)\Big]. \end{aligned} \tag{2.9}$$

Now using the Cauchy-Schwartz for the two terms inside the brackets one finds

$$\delta^2(\mathbf{\Pi};\ \xi) \geq \frac{1}{\sum_{\mathbf{x}} p(\mathbf{x}|\xi) \Big(\partial_\xi \log p(\mathbf{x}|\xi)\Big)^2}. \tag{2.10}$$

Reminding that the term in the denominator of the right hand side is $\mathcal{F}_c(\xi)$, the CRB for an unbiased estimator is proved. ♣

Proof of the quantum Cramér Rao bound

The QCRB can be proved with the help of the CRB, together with the Born rule, and the Cauchy-Schwartz inequality. We start by substituting $p(\mathbf{x}|\xi) = \mathrm{Tr}\,(\rho(\xi)\ \Pi_{\mathbf{x}})$ in the expression of the Fisher information

$$\mathcal{F}_c(\xi) = \sum_{\mathbf{x}} \frac{\Big(\partial_\xi \mathrm{Tr}\,(\rho(\xi)\ \Pi_{\mathbf{x}})\Big)^2}{\mathrm{Tr}\,(\rho(\xi)\ \Pi_{\mathbf{x}})}. \tag{2.11}$$

Next, we change the order of the derivative and the trace, and make use of the definition of the SLD

$$\mathcal{F}_c(\xi) = \sum_{\mathbf{x}} \frac{\Big(\Re \mathrm{Tr}\Big(\Lambda_\xi\ \rho(\xi)\ \Pi_{\mathbf{x}}\Big)\Big)^2}{\mathrm{Tr}\,(\rho(\xi)\ \Pi_{\mathbf{x}})} \leq \sum_{\mathbf{x}} \frac{\Big|\mathrm{Tr}\Big(\Lambda_\xi\ \rho(\xi)\ \Pi_{\mathbf{x}}\Big)\Big|^2}{\mathrm{Tr}\,(\rho(\xi)\ \Pi_{\mathbf{x}})}. \tag{2.12}$$

By writing down $\Lambda_\xi\ \rho(\xi)\ \Pi_{\mathbf{x}} = \Lambda_\xi\ \sqrt{\rho(\xi)}\ \sqrt{\rho(\xi)}\ \sqrt{\Pi_{\mathbf{x}}}\ \sqrt{\Pi_{\mathbf{x}}}$, and with the help of the cyclic property of trace, a further use of Cauchy-Schwartz inequality gives

$$\mathcal{F}_c(\xi) \leq \sum_{\mathbf{x}} \frac{\mathrm{Tr}\,(\rho(\xi)\ \Pi_{\mathbf{x}})\,\mathrm{Tr}\Big(\Lambda_\xi\ \rho(\xi)\ \Lambda_\xi\ \Pi_{\mathbf{x}}\Big)}{\mathrm{Tr}\,(\rho(\xi)\ \Pi_{\mathbf{x}})} = \mathrm{Tr}\left(\Lambda_\xi\ \rho(\xi)\ \Lambda_\xi \sum_{\mathbf{x}} \Pi_{\mathbf{x}}\right) = \mathcal{F}(\xi). \tag{2.13}$$

Where in the last line we use the completeness of a POVM set, $\sum_{\mathbf{x}} \Pi_{\mathbf{x}} = \mathbb{I}$, and the cyclic property of the trace. ♣

2.2 The QFI for a general density matrix: Classical and quantum contributions

One can write down the QFI with a more explicit relation to the density matrix of the system. With the help of Eq. .(2.8), and using the spectral decomposition of ρ, one might find the matrix elements of the SLD to be

$$\begin{aligned} &\Lambda_\xi \rho + \rho \Lambda_\xi = 2\partial_\xi \rho, \\ \Rightarrow\ &(\Lambda_\xi)_{mn} p_n |m\rangle\langle n| + (\Lambda_\xi)_{mn} p_m |m\rangle\langle n| = 2(\partial_\xi \rho)_{mn} |m\rangle\langle n|, \\ \Rightarrow\ &(\Lambda_\xi)_{mn} = 2\frac{(\partial_\xi \rho)_{mn}}{p_m + p_n}, \qquad p_m \neq 0 \wedge p_n \neq 0. \end{aligned} \tag{2.14}$$

If both p_m and p_n are zero we have the freedom to let $(\Lambda_\xi)_{mn} = 0$. Substituting to the QFI gives

$$\mathcal{F}(\xi) = 2\sum_{mn} \frac{\left|\partial_\xi \rho_{mn}\right|^2}{p_m + p_n}. \tag{2.15}$$

Eq. (2.15) describes the QFI of a general density matrix. It is very interesting to expand this expression in order to see the classical and quantum contributions to the QFI. To begin with, let us consider the simplest case, where the density matrix is pure $\rho = |\psi\rangle\langle\psi|$. We will denote the QFI for such a state with $\mathcal{F}_{Q,|\psi\rangle}$, where the index "$Q$" denotes the fact that the QFI is purely quantum in this case and we have dropped the ξ dependence of the QFI to lighten the notation. Simple algebra yields

$$\begin{aligned} \mathcal{F}_{Q,|\psi\rangle} &= 2\sum_{nm} \frac{\left|\left(\partial_\xi |\psi\rangle\langle\psi|\right)_{nm}\right|^2}{p_n + p_m} \\ &= 2\left(\langle\partial_\xi\psi|\psi\rangle + \langle\psi|\partial_\xi\psi\rangle\right)^2 + \frac{1}{2}\sum_{m\neq 0}\left(\left|\langle\partial_\xi\psi|\psi_m\rangle\right|^2 + \left|\langle\psi_m|\partial_\xi\psi\rangle\right|^2\right) \\ &= 4\langle\partial_\xi\psi|\left(\mathbb{I} - |\psi\rangle\langle\psi|\right)|\partial_\xi\psi\rangle = 4\langle\partial_\xi\psi|\partial_\xi\psi\rangle - \langle\partial_\xi\psi|\psi\rangle\langle\psi|\partial_\xi\psi\rangle \\ &= 4\langle\partial_\xi\psi|\left(\mathbb{I} - |\psi\rangle\langle\psi|\right)|\partial_\xi\psi\rangle. \end{aligned} \tag{2.16}$$

It is very easy to check that for a unitary parametrization, where the parameter dependence of $|\psi\rangle$ is generated by the operator $U = \exp(-iG)$ on some initial state $|\psi_0\rangle$, which does not depend on the parameter, we have $\mathcal{F} = 4\mathrm{Var}(G)_{\psi_0}$.

For a mixed quantum state, it is more convenient to work in the diagonal basis of the density matrix, such that $\rho = p_k \left|\psi_k\right\rangle\left\langle\psi_k\right|$. Thus one can write

$$\begin{aligned}
\mathcal{F} &= 2\sum_{nm} \frac{\left|\left(\partial_\xi \sum_k p_k \left|\psi_k\right\rangle\left\langle\psi_k\right|\right)_{nm}\right|^2}{p_n + p_m} \\
&= 4\sum_m \frac{\left(\partial_\xi p_m\right)^2}{p_m} + 2\sum_{nm} \frac{\left|p_m \left\langle\psi_m|\partial_\xi\psi_n\right\rangle + p_n \left\langle\partial_\xi\psi_m|\psi_n\right\rangle\right|^2}{p_n + p_m} \\
&= 4\sum_m \frac{\left(\partial_\xi p_m\right)^2}{p_m} + 2\sum_{nm} \frac{(p_n - p_m)^2}{p_n + p_m} \left|\left\langle\psi_m|\partial_\xi\psi_n\right\rangle\right|^2 \\
&= \mathcal{F}_c + \mathcal{F}_Q.
\end{aligned} \tag{2.17}$$

Again, to go from the second to the third line we use the fact that $\left\langle\psi_m|\partial_\xi\psi_n\right\rangle = -\left\langle\partial_\xi\psi_m|\psi_n\right\rangle$. This last equation is very helpful to distinguish between the classical and quantum parts of the quantum Fisher information. The first term, which we display by $\mathcal{F}_c$, is the *classical* Fisher information of the probability distribution $p = \{p_1, p_2, \dots\}$. This term is clearly zero for the pure states. Moreover, any unitary operation on the density matrix, being it parameter dependent or not, will keep this term unchanged, though it might change the diagonal basis of the density matrix. The second term, $\mathcal{F}_Q$, which represents the quantum contribution takes into account the parameter dependence of the basis. This term might be rewritten in the following form

$$\begin{aligned}
\mathcal{F}_Q &= 2\sum_{nm} \frac{(p_n - p_m)^2}{p_n + p_m} \left|\left\langle\psi_m|\partial_\xi\psi_n\right\rangle\right|^2 \\
&= 2\sum_{nm} \frac{(p_n + p_m)^2}{p_n + p_m} \left|\left\langle\psi_m|\partial_\xi\psi_n\right\rangle\right|^2 - 8\sum_{nm} \frac{p_n p_m}{p_n + p_m} \left|\left\langle\psi_m|\partial_\xi\psi_n\right\rangle\right|^2 \\
&= 4\sum_m p_m \left\langle\partial_\xi\psi_m|\partial_\xi\psi_m\right\rangle - 4\sum_m p_m \left|\left\langle\psi_m|\partial_\xi\psi_m\right\rangle\right|^2 - 8\sum_{n\neq m} \frac{p_n p_m}{p_n + p_m} \left|\left\langle\psi_m|\partial_\xi\psi_n\right\rangle\right|^2.
\end{aligned} \tag{2.18}$$

The first two terms together can be described as the average of the QFI of the density matrix spectra as described by (2.16). Hence the quantum contribution is

$$\mathcal{F}_Q = \sum_m p_m \mathcal{F}_{Q,|\psi_m\rangle} - 8\sum_{n\neq m} \frac{p_n p_m}{p_n + p_m} \left|\left\langle\psi_m|\partial_\xi\psi_n\right\rangle\right|^2. \tag{2.19}$$

The second term is zero for any pure state. It is also zero for a unitary parametrization, where the generator of the unitary has the same spectra as the density matrix. In such cases clearly $\mathcal{F} \leq \sum_m p_m \mathcal{F}_{Q,|\psi_m\rangle} \leq \max_{\psi_m} \mathcal{F}_{Q,|\psi_m\rangle}$, i.e., for any mixed state there exist a pure state that has a larger QFI. In other words, the QFI of a *unitary* parametrization is always optimal for a pure probe. An alternative tool to prove this is provided by the extended convexity of the QFI.

2.3 Some useful properties of the QFI

2.3.1 Additivity of the QFI

A very important property of the FI and the QFI is their additivity. This is not so difficult to explain. Given N *independent* probability distributions, the probability that a set of outcomes $\mathbf{X} = \{\mathbf{x}_1, \mathbf{x}_2, \ldots, \mathbf{x}_N\}$ occurs is given by the product of the probabilities of individual outcomes, i.e., $p(\mathbf{X}|\xi) = \prod_{m=1}^{N} p(\mathbf{x}_m|\xi)$, with $p(\mathbf{x}_m|\xi)$ being the probability of having the subset $\mathbf{x}_m$ of outcomes from mth distribution. By substituting this in the definition of the Fisher information one finds

$$\begin{aligned}\mathcal{F}_c(\mathbf{X},\xi) &= \sum_{\mathbf{X}} \frac{\big(\partial_\xi p(\mathbf{X}|\xi)\big)^2}{p(\mathbf{X}|\xi)} = \sum_{\mathbf{X}} p(\mathbf{X}|\xi)\big(\partial_\xi \log p(\mathbf{X}|\xi)\big)^2 \\ &= \sum_{\mathbf{X}} p(\mathbf{X}|\xi)\Big(\partial_\xi \sum_{m=1}^{N} \log p(\mathbf{x}_m|\xi)\Big)^2 = \sum_{m=1}^{N}\sum_{\mathbf{x}_m} \frac{\big(\partial_\xi p(\mathbf{x}_m|\xi)\big)^2}{p(\mathbf{x}_m|\xi)} + 2\sum_{m\neq m'}\sum_{\mathbf{x}_m,\mathbf{x}'_m} \partial_\xi p(\mathbf{x}_m|\xi)\partial_\xi p(\mathbf{x}'_m|\xi) \\ &= \sum_{m=1}^{n} \mathcal{F}_c(\mathbf{x}_m). \end{aligned} \tag{2.20}$$

Further, since the QFI is equal to the Fisher information obtained with an optimal measurement, it is additive as well, i.e.,

$$\mathcal{F}_\xi\Big(\otimes_{m=1}^{N} \rho^m\Big) = \sum_{m=1}^{N} \mathcal{F}_\xi(\rho^m). \tag{2.21}$$

Another way to prove this is by using Eqs. (2.7), (2.8), and the fact that the independent probability distributions means that the density matrix before the measurements should have been a product state $\rho(\xi) = \otimes_m \rho^m(\xi)$. This leads to a SLD of direct sum form, i.e., $\Lambda_\xi = \oplus_m \Lambda^m_\xi$. Substituting in the QFI definition proves the additivity.

2.3.2 Extended convexity of the QFI

For any positive set $\{P_m\}$ which sums up to one, and a corresponding set of density matrices $\{\rho_m(\xi)\}$, we have

$$\mathcal{F}\Big(\sum_m p_m \rho_m(\xi)\Big) \leq \mathcal{F}_c(\{p_m\}) + \sum_m p_m \mathcal{F}(\rho_m(\xi)). \tag{2.22}$$

with $\mathcal{F}_c(\{p_m\}) = \sum_m p_m(\partial_\xi p_m)^2$ being the classical Fisher information of the probability distribution $\{p_m\}$, as described in Eq. (2.3). ■

If $\{p_m\}$ is independent of the parameter, as is the case for a unitary parametrization, this classical term vanishes, leading to the *convexity of the quantum Fisher information*. Namely, if the unitary

parametrization is given by $U = \exp(-i\xi G)$, then for any ρ we have $\mathcal{F}(\rho) \leq \mathrm{Var}(G)_\rho$. This can be seen by writing the spectral decomposition of $\rho = \sum_m p_m \left|\psi_m\right\rangle\left\langle\psi_m\right|$, then by applying the theorem and using Eq. (2.19)

$$\mathcal{F}(\rho) \leq \sum_m p_m \mathcal{F}_{Q,|\psi_m\rangle} = \sum_m p_m \mathrm{Var}(G)_{|\psi_m\rangle} \leq \mathrm{Var}(G)_\rho. \tag{2.23}$$

Proof of the extended convexity—This theorem was introduced in [64] and we follow the same proof as presented in this reference. Let $\rho = \sum_m p_m \rho_m$ and $\tilde{\rho}_m = p_m \rho_m$. Differentiating with respect to ξ gives

$$\partial_\xi \tilde{\rho}_m = \frac{1}{2}\left(\Lambda_m \tilde{\rho}_m + \tilde{\rho}_m \Lambda_m\right), \tag{2.24}$$

with $\Lambda_m = \partial_\xi p_m / p_m + \Lambda_{\rho_m}$. Next, one shall focus on the Fisher information for an arbitrary set of POVM measurement $\mathbf{\Pi} = \{\Pi_1, \Pi_2, \dots\}$

$$\begin{aligned}
\mathcal{F}_c^{\mathbf{\Pi}}(\rho) &= \sum_k \frac{\partial_\xi \mathrm{Tr}(\rho\ \Pi_k)^2}{\mathrm{Tr}(\rho\ \Pi_k)} = \sum_k \frac{\sum_m \left(\Re \mathrm{Tr}(\Lambda_m\ \tilde{\rho}_m\ \Pi_k)\right)^2}{\mathrm{Tr}(\rho\ \Pi_k)} \\
&\leq \sum_k \frac{\sum_m \left|\mathrm{Tr}(\Lambda_m\ \tilde{\rho}_m\ \Pi_k)\right|^2}{\mathrm{Tr}(\rho\ \Pi_k)} \leq \sum_k \frac{\sum_m \mathrm{Tr}(\tilde{\rho}_m\ \Pi_k)\mathrm{Tr}(\tilde{\rho}_m\ \Lambda_m\ \Pi_k\ \Lambda_m)}{\mathrm{Tr}(\rho\ \Pi_k)} \\
&\leq \sum_k \sqrt{\frac{\sum_m \mathrm{Tr}(\tilde{\rho}_m\ \Pi_k)^2}{\mathrm{Tr}(\rho\ \Pi_k)}} \sqrt{\sum_m \mathrm{Tr}(\tilde{\rho}_m\ \Lambda_m\ \Pi_k\ \Lambda_m)^2}.
\end{aligned} \tag{2.25}$$

Now notice that the first term in the right hand side is less than one, hence, by once more using the triangle inequality one yields

$$\begin{aligned}
\mathcal{F}_c^{\mathbf{\Pi}}(\rho) &\leq \sum_k \sum_m \mathrm{Tr}(\tilde{\rho}_m\ \Lambda_m\ \Pi_k\ \Lambda_m) = \sum_m \mathrm{Tr}(\tilde{\rho}_m\ \Lambda_m\ \Lambda_m) \\
&= \mathcal{F}_c(\{p\}) + \sum_m p_m \mathcal{F}_Q(\rho_m).
\end{aligned} \tag{2.26}$$

The fact that the right hand side of $\mathcal{F}_c^{\mathbf{\Pi}}(\rho) \leq \mathcal{F}_c(\{p\}) + \sum_m p_m \mathcal{F}_Q(\rho_m)$, does not depend on the POVM measurements $\mathbf{\Pi}$, implies that the inequality is true for any POVM, including the one maximizing $\mathcal{F}_c^{\mathbf{\Pi}}$. This means that $\max_{\mathbf{\Pi}} \mathcal{F}_c^{\mathbf{\Pi}} = \mathcal{F}_Q(\rho) \leq \mathcal{F}_c(\{p\}) + \sum_m p_m \mathcal{F}_Q(\rho_m)$. ♣

2.3.3 Relation to fidelity, fidelity susceptibility and the Bures distance

Uhlmann fidelity

In quantum information theory, (Uhlmann) fidelity has been used as a measure of distance (closeness) between two quantum states [65, 66]. For any two *mixed* density matrices ρ and

σ, the Uhlmann fidelity is defined as [66]

$$F(\rho,\sigma) = \mathrm{Tr}\left[\sqrt{\sqrt{\rho}\,\sigma\,\sqrt{\rho}}\right]^2. \tag{2.27}$$

Obviously, for $\varrho = \sigma$ the Uhlmann fidelity is equal to one. Moreover, the symmetry of the fidelity under $\sigma \leftrightarrow \rho$ can be seen by defining $A = \sqrt{\rho}\,\sqrt{\sigma}$, which leads to

$$F(\rho,\sigma) = \mathrm{Tr}\left[\sqrt{AA^\dagger}\right]^2 = \mathrm{Tr}\,[|A|]^2 = \mathrm{Tr}\left[|A^\dagger|\right]^2 = \mathrm{Tr}\left[\sqrt{A^\dagger A}\right]^2 = F(\sigma,\rho). \tag{2.28}$$

It is clear from Eq. (2.27) that $0 \leq F(\rho,\sigma)$, with equality holding for the states which are diagonal in the same basis, with different supports. By using the Uhlmann theorem one can further see that $F(\rho,\sigma) \leq 1$. We refer the readers to [66] for proof of the theorem and more properties of the fidelity.

Relation to the Bures distance

With the help of the Uhlmann fidelity, one might define the Bures distance D_B between two quantum density matrices

$$D_B(\rho,\sigma) \equiv \sqrt{2\left(1 - \sqrt{F(\rho,\sigma)}\right)}. \tag{2.29}$$

Since we are interested in the distinguishability problem, we shall focus on the Bures distance of two states which are infinitesimally close to each other. We denote by d_B such a distance

$$d_B^2 \equiv D_B^2(\rho,\rho+\delta\rho). \tag{2.30}$$

Suppose that the variation in the density matrix, i.e., $\delta\rho$, is posed by the driving some parameter such as ξ. In order to have a measure which is independent of the magnitude of the driving $\delta\xi$, one might define the *Bures metric*, as follows

$$d_B^2 = g_\xi\,\delta\xi^2. \tag{2.31}$$

with g_ξ being the Bures metric.

The geometric meaning of the quantum Fisher information

The quantum Fisher information is four times the Bures metric i.e., $\mathcal{F}_\xi = 4g_\xi$. This gives a geometrical meaning to the QFI: For a parameter ξ, the smaller the QFI is, the closer are two quantum states $\rho(\xi)$ and $\rho(\xi+\delta\xi)$, hence the more difficult it is to distinguish them from one

another.

Proof of $\mathcal{F}_\xi = 4g_\xi$—We follow the proof of reference [67]. By substituting the two density matrices in the definition of the fidelity one finds

$$\sqrt{F(\rho,\rho+\delta\rho)} = \mathrm{Tr}\sqrt{\sqrt{\rho}(\rho+\delta\rho)\sqrt{\rho}}. \tag{2.32}$$

Next, we expand $\sqrt{\sqrt{\rho}(\rho+\delta\rho)\sqrt{\rho}}$ to the first order in $\delta\rho$

$$\sqrt{\sqrt{\rho}(\rho+\delta\rho)\sqrt{\rho}} \approx \rho + X, \tag{2.33}$$

With X being the linear term in $\delta\rho$, whose precise expression should be obtained. The fidelity is then $\mathrm{Tr}\sqrt{\sqrt{\rho}(\rho+\delta\rho)\sqrt{\rho}} = 1 + \mathrm{Tr}\, X$. By squaring both sides of Eq. (2.33) we obtain

$$\sqrt{\rho}\,\delta\rho\,\sqrt{\rho} = X\,\rho + \rho\,X. \tag{2.34}$$

In a basis where $\rho = \sum_i p_i |i\rangle\langle i|$, the elements of X are given by

$$X_{ij} = \frac{p_i^{1/2} p_j^{1/2}}{p_i + p_j}(\delta\rho)_{ij}. \tag{2.35}$$

This means that $\mathrm{Tr}X = 0$, which indeed should be the case, otherwise it was possible to have a fidelity greater than one. Hence, one should revise the Eq. (2.33), by adding a second order term to the right hand side: $Y \approx O(\delta\rho^2)$. Doing the same procedure, aside form Eq. (2.34) gives an additional equation for Y

$$\rho\,Y + Y\,\rho = -X^2. \tag{2.36}$$

One can simply see that the matrix elements of Y in the diagonal basis of ρ are

$$Y_{ij} = -\frac{1}{p_i + p_j}(X^2)_{ij}. \tag{2.37}$$

Therefore the Bures distance d_B^2 is given by

$$d_B^2 = -2\mathrm{Tr}Y = \frac{1}{2}\sum_{ij}\frac{\left|\delta\rho_{ij}\right|^2}{p_i + p_j} = g_\xi\,\delta\xi^2, \tag{2.38}$$

Comparing this with Eq. (2.15) proves the theorem. ♣

Fidelity susceptibility and quantum phase transitions

As we saw in the previous section, the linear response of the fidelity to any parameter driving is zero. Therefore, the leading order response of the fidelity, sometimes termed as the fidelity susceptibility, is a second order term and is given by

$$\chi_F \equiv -\lim_{\delta\xi\to 0} \partial^2_{\delta\xi^2} F(\rho_\xi, \rho_{\xi+\delta\xi}) = \sum_{nm} \frac{\left|\partial_\xi \rho_{nm}\right|^2}{p_n + p_m}. \tag{2.39}$$

which has been extensively used in the study of quantum phase transitions [68]. Notice that this is nothing but half of the quantum Fisher information associated to the deriving parameter, though typically in the study of quantum phase transitions it is referred to as the fidelity susceptibility. The motivation to investigate the fidelity in many-body systems is simple to express [46, 69, 70]. Once at the ground state of a many-body system, changing a parameter, such as an external magnetic field, will drive the system across a quantum phase transition. A relevant question is then, how to recognize the critical point where the phase transition happens. Furthermore, this problem can be extended to a thermal system whose state is not in the ground state anymore. In this situation the change in parameter drives the system across a *critical region* through which a *crossover* from one phase to another happens. In both cases, one expects the fidelity susceptibility to be a very good measure for quantifying the criticality. This is so, because the fidelity susceptibility measures the response of the system to the driving parameter. Remember that the fidelity of two very closed states with almost the same structure, should be very close to one. Indeed this is the case across a certain phase. However in a critical point, due to sudden change in the structure of the system, the fidelity shall drop notably, hinting a quantum phase transition.

Chapter 3

Preliminaries from open quantum systems

This chapter provides the necessary toolboxes for dealing with open quantum systems. In section 3.1 we review the properties of a generic quantum map. In section 3.2 we present the Lindbladian master equation, and overview the necessary conditions for it to hold. Section 3.3 is dedicated to introducing the bosonic heat bath at thermal equilibrium, a model to which we will refer frequently in the rest of this thesis. Next, we look at the dynamics and statics of different systems in contact with such a heat bath. These are mainly the systems which will be used for thermometry in chapter 4. Section 3.4 presents the solution of the simplest system, i.e., that of a two level atom. Further, in section 3.5 the solution of a quantum harmonic oscillator in contact with the bosonic bath is given. Finally in section 3.6, we look at two coupled harmonic oscillators interacting with a common bath. This system will be used for studying the role of quantum correlations in thermometry, as well as exploring the contribution of dissipation on estimation of the coupling between the two oscillators.

3.1 General quantum maps

First of all, we need to address the framework for evolution of an open quantum system. We remind that such a system might not be described by a unitary (Hamiltonian) dynamic anymore, and a sufficient knowledge about its environment is essential. Any open quantum system S, might be considered as a part of a sufficiently bigger isolated system. The latter includes S, with the Hamiltonian H_s, plus an environment (sometimes referred to as bath), which we represent by B, and is described by the Hamiltonian H_B. In addition to the free Hamiltonians, an interaction between S and B is also applied. We show the interaction Hamiltonian by H_I. See figure 3.1. The system-bath, hereafter SB, will undergo a unitary dynamics, generated by the

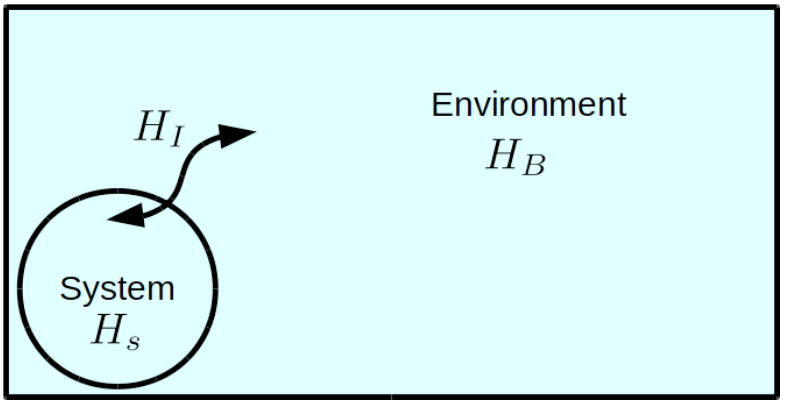

FIGURE 3.1: (Color online) An open quantum system with the Hamiltonian H_s. The dynamics of the system might be described with the help of an environment with H_B, with which the system interacts through the interaction Hamiltonian H_I. The whole system plus environment are isolated, hence having a closed dynamics described by a unitary evolution.

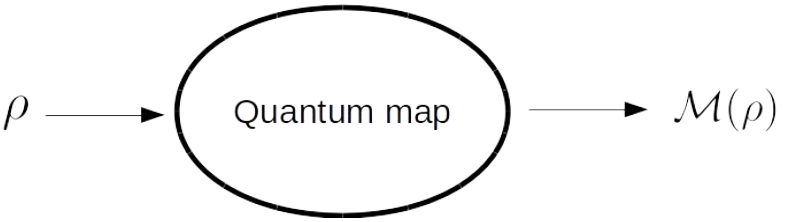

FIGURE 3.2: (Color online) Sketch of a general evolution of a density matrix under a quantum map. The process $\mathcal{M}$, maps any density matrix to another one. It should have the properties of a CPTP map, as described in the main text.

total Hamiltonian

$$H = H_s + H_B + H_I \tag{3.1}$$

By denoting by ρ_{SB} the density matrix of SB, which is defined on the Hilbert space $\mathcal{H}_S \otimes \mathcal{H}_B$, we know that its evolution is simply given by

$$\rho_{SB}(t) = U\rho_{SB}(0)U, \qquad U = \exp(-iH). \tag{3.2}$$

Since we are only concerned about S, we focus on its evolution by tracing out the B degrees of freedom $\rho_S(t) = \mathrm{Tr}_B(\rho_{SB}(t))$. Inspired by this equation, one could alternatively define a quantum map $\mathcal{M} : \mathcal{H} \to \mathcal{H}$, which describes the evolution of the system as follows (see figure 3.2)

$$\rho_S(t) \equiv \mathcal{M}\Big(\rho_S(0)\Big). \tag{3.3}$$

The map is consisting of operators and superoperators in the Hilbert space of the system. One way to show the map is using the Kraus representation as follows

$$\mathcal{M}(\rho) = \sum_k A_k \rho A_k^\dagger, \tag{3.4}$$

with the Kraus operators A_k satisfying $\sum_k A_k^\dagger A_k = \mathbb{I}$.

3.2 Lindbladian master equation

The aim is to find a differential equation, like the Schrodinger equation for the closed systems, with the help of which one might find the time evolution of the density matrix. The start point would be using the Kraus representation for a map which translates the density matrix infinitesimally in time, i.e., from t to $t+\delta t$. This can be written as

$$\rho(t+\delta t) = \mathcal{M}(t,\delta t)(\rho) = \sum_k A_k(t,\delta t)\rho A_k^\dagger(t,\delta t). \tag{3.5}$$

By assuming that the map is homogenous in time, we can drop the t dependence of $\mathcal{M}$, and A_k. On the other hand if we expand the density matrix wrt the translation time δt, we reach at $\rho(t+\delta t) = \rho(t) + \delta t\dot{\rho}(t) + O(\delta t^2)$. This means that the Kraus operators shall be $A_k(\delta t) = A_k^0 + \sqrt{\delta t}A_k^1 + O(\delta t)$. Since we have the freedom to choose the Kraus operators, we let $A_0 = \mathbb{I} + \sqrt{\delta t}(-iH_S + K) + O(\delta t^2)$, with H and K being Hermitian operators, and $A_k = \sqrt{\delta t}L_k \quad \forall k \neq 0$. Substituting in Eq. (3.5) yields

$$\rho(t) + \delta t\dot{\rho}(t) + O(\delta t^2) = [\mathbb{I} + \sqrt{\delta t}(-iH_S + K)]\rho[\mathbb{I} + \sqrt{\delta t}(+iH_S + K)] + \delta t\sum_{k>0} L_k\rho L_k^\dagger + O(\delta t). \tag{3.6}$$

Focusing on the linear contributions leads to an initial form of the desired master equation

$$\dot{\rho}(t) = -i[H,\rho] + \{K,\rho\} + \sum_{k>0} L_k\rho L_k^\dagger. \tag{3.7}$$

Finally, by focusing on the constraint on the Kraus operators, i.e., $\sum_k A_k^\dagger A_k = \mathbb{I}$, we can rewrite K in terms of all other operators L_k, leading to $K = -1/2\sum_k L_k^\dagger L_k$. Putting everything together we have the Lindbladian master equation

$$\dot{\rho}(t) = -i[H,\rho] + \sum_k \left(L_k\rho L_k^\dagger - \tfrac{1}{2}\left\{L_k^\dagger L_k,\rho\right\}\right). \tag{3.8}$$

Next, we aim at simplifying the master equation, such that we have a clear expression for the Lindbladian operators in terms of the environment characteristics and the interaction between S and B. For this we use the interaction picture to describe the density matrix and the operators. We remind that the interaction picture density matrix is related to the Schrodinger picture density matrix through

$$\rho_I(t) = e^{i(H_S+H_B)t}\rho(t)e^{-i(H_S+H_B)t}. \tag{3.9}$$

This is true for any other observable, like A, as well

$$A_I(t) = e^{i(H_S+H_B)t} A(t) e^{-i(H_S+H_B)t}. \tag{3.10}$$

The coherent dynamics of SB has a unitary shape, which in the interaction picture will takes the following form

$$\dot{\rho}_I(t) = -i[(H_{SB})_I(t), \rho_I(t)]. \tag{3.11}$$

Here $(H_{SB})_I(t)$ is the interaction Hamiltonian in the interaction picture. From now on let us replace it by $V_I(t)$ to lighten our notation. In the Schrodinger picture, the interaction Hamiltonian, in the most general case, might be written as $V = \sum_k A_k \otimes B_k$, where A_ks and B_ks, respectively, operate on the Hilbert space of S and B. In the interaction picture, one only needs to transform individual A_k and B_k in the Heisenberg picture corresponding to their Hamiltonian. We will refer to the interaction picture later, to make more simplifications. Integrating Eq. (3.11) one finds the integral form of the master equation

$$\rho_I(t) = \rho_I(0) - i \int_0^t dt' [V_I(t'), \rho_I(t')]. \tag{3.12}$$

One might further replace $\rho_I(t')$ appearing in the rhs by itself, leading to

$$\rho_I(t) = \rho_I(0) - i \int_0^t dt' [V_I(t'), \rho_I(0)] - \int_0^t \int_0^{t'} dt' dt'' [V_I(t'), [V_I(t''), \rho_I(t'')]]. \tag{3.13}$$

Now we assume that the system and environment are initially in a product state, i.e., $\rho(t) = \rho_S(0) \otimes \rho_B(0)$. Obviously this state is also product in the interaction picture. On top of that we restrict ourselves to the so called *weak coupling limit*, which states that the interaction between the system and the bath is weak enough, enabling us to write $\rho(t) = \rho_S(t) \otimes \rho_B(t)$ at any time. Further let's assume that τ_B, the correlation time of the bath, is so small that $\rho_B(t) \approx \rho_B(0)$ for $t \gg \tau_B$. Thus, since we are interested only in the state of the system, by tracing over the environment we forget about those degrees of freedom. Again, to lighten the notation, we drop the index I of the interaction picture, but we should be aware that the equations are in the interaction picture. We have

$$\rho_S(t) = \rho_S(0) - i \int_0^t dt' \mathrm{Tr}_B[V(t'), \rho_S(0) \otimes \rho_B(0)] - \int_0^t \int_0^{t'} dt' dt'' \mathrm{Tr}_B[V(t'), [V(t''), \rho_S(t'') \otimes \rho_B(0)]]. \tag{3.14}$$

With the help of the representation we introduced earlier for V, we might simplify the integrand appearing in the second term on the rhs, $\mathrm{Tr}_B[V(t'), \rho_S(0) \otimes \rho_B(0)] = \sum_k [A_k(t), \rho_S(0)] \langle B_k(t') \rangle_{\rho_B(0)}$. Notice that by the assumption we made earlier about the correlation time of the bath, one might drop the time dependence of $B_k(t)$. Also notice that it is always possible to choose the B_k

operators such that

$$\langle B_k \rangle_{\rho_B} = 0. \tag{3.15}$$

This may be done e.g., by $B_k \to B_k - \langle B_k \rangle$, and shifting the energy of the system accordingly to compensate. Hence, the second term in the rhs is zero. Taking the time derivative of Eq. (3.14) we obtain

$$\dot{\rho}_S(t) = -\int_0^t dt' \mathrm{Tr}_B[V(t),[V(t'),\rho_S(t')\otimes\rho_B(0)]], \tag{3.16}$$

which by replacing for $V(t)$ gives

$$\dot{\rho}_S(t) = \sum_{kk'}\int_0^t dt' \Big(A_k(t)\rho_S(t')A_{k'}(t') - A_{k'}(t')A_k(t)\rho_S(t')\Big)\Big\langle B_k(t)B_{k'}(t')\Big\rangle + h.c. \tag{3.17}$$

This equation is much simpler than what we started from, yet still the integrand depends on $\rho_S(t')$, which takes into account the memory effects of the dynamics. However, by Markov assumption, which assumes that in the integrand the dynamics of the system depends only on its current state, i.e., by replacing $\rho_S(t') \to \rho_S(t)$ in the rhs, we have

$$\dot{\rho}_S(t) = \sum_{kk'}\int_0^t dt' \Big(A_k(t)\rho_S(t)A_{k'}(t') - A_{k'}(t')A_k(t)\rho_S(t)\Big)G_{k,k'}(t,t') + h.c. \tag{3.18}$$

Here we have defined $G_{k,k'}(t,t') \equiv \langle B_k(t)B_{k'}(t')\rangle$. Next, by assuming that the correlation times of the bath are very small, such that $G_{k,k'}(t,t')$ has a significant value only around $t \approx t'$, we can shift the upper limit of the integral to infinity

$$\dot{\rho}_S(t) = \sum_{kk'}\int_0^\infty dt' \Big(A_k(t)\rho_S(t)A_{k'}(t') - A_{k'}(t')A_k(t)\rho_S(t)\Big)G_{k,k'}(t,t') + h.c. \tag{3.19}$$

Since the bath is considered to be at stationary, (which means $[H_B,\rho_B(0)] = 0$), the two time correlation function depends only on the time difference, i.e., $G_{k,k'}(t,t') = G_{k,k'}(t-t')$. Further, by writing the system interaction operators in terms of the Hamiltonian eigenoperators. The former is the Fourier transform of the latter, i.e., $A_k(t) = \sum_\omega \exp(i\omega t)A_k(\omega)$. Here

$$A_k(\omega) = \sum_{\epsilon_p - \epsilon_{p'} = \omega} \Pi_{\epsilon_p} A_k \Pi_{\epsilon_{p'}}, \tag{3.20}$$

with Π_{ϵ_p} being the projector into the eigenstate of the energy with the corresponding eigenvalue ϵ_p. It is easy to see that $[H,A_k(\omega)] = -\omega A_k(\omega)$ and $[H,A_k^\dagger(\omega)A_{k'}(\omega)] = 0$. By using the change

of variable $t' \to t - t'$, we reach at

$$\dot{\rho}_S(t) = \sum_{\omega\omega'}\sum_{kk'} e^{-i(\omega+\omega')t}\Big(A_k(\omega)\rho_S(t)A_{k'}(\omega') - A_{k'}(\omega')A_k(\omega)\rho_S(t)\Big)\int_0^\infty dt' e^{i\omega' t'} G_{k,k'}(t') + h.c. \tag{3.21}$$

In the rotating wave approximation, where the time scales of the system, characterized by typical values of $(\omega-\omega')^{-1}$ is very small, one might ignore the highly rotating terms, and only take into account the terms for which $\omega = \omega'$. The master equation is hence

$$\dot{\rho}_S(t) = \sum_{\omega}\sum_{kk'} J_{kk'}(\omega)\Big(A_k(\omega)\rho_S(t)A^\dagger_{k'}(\omega) - A^\dagger_{k'}(\omega)A_k(\omega)\rho_S(t)\Big) + h.c., \tag{3.22}$$

where we introduce the spectral density as the Fourier transform of the two times correlations of the bath, i.e., $J_{kk'}(\omega) \equiv \int_0^\infty dt' e^{i\omega t'} G_{k,k'}(t')$, and we used the fact that $A_k(-\omega) = A^\dagger_k(\omega)$. The spectral density can be rewritten as its real and imaginary parts such that $J_{kk'}(\omega) = {}^1/_2\gamma_{kk'}(\omega) + iS_{kk'}(\omega)$. With this one could write down the master equation as

$$\dot{\rho}_S(t) = -i[H_{LS}, \rho_S(t)] + \mathcal{D}(\rho_S(t)), \tag{3.23}$$

where the Lamb shift Hamiltonian H_{LS} is given by

$$H_{LS} = \sum_{\omega}\sum_{kk'} S_{kk'}(\omega)A^\dagger_{k'}(\omega)A_k(\omega). \tag{3.24}$$

and the dissipator $\mathcal{D}$ is defined as

$$\mathcal{D}(\rho_S(t)) = \sum_{\omega}\sum_{kk'} \gamma_{kk'}(\omega)\Big(A_{k'}(\omega)\rho_S(t)A^\dagger_k(\omega) - \tfrac{1}{2}\Big\{A^\dagger_{k'}(\omega)A_k(\omega), \rho_S(t)\Big\}\Big). \tag{3.25}$$

By diagonalising the $\gamma_{kk'}$ matrix, one may have a Lindbladian type master equation. The Schrodinger picture master equation is simply found by adding H_S to the Lamb shift Hamiltonian. Notice that $[H, H_{LS}] = 0$, which means that if the system is in a Gibbs state, only the dissipation part of the master equation matters. Moreover, if the environment also has a Gibbs state ρ_β, then, the KMS condition for the bath correlation functions holds

$$\begin{aligned}
\langle B_k(t)B_{k'}(0)\rangle &= \frac{1}{\mathcal{Z}}\mathrm{Tr}\Big(e^{-\beta H_B}e^{iH_B t}B_k e^{-iH_B t}B_{k'}\Big) \\
&= \frac{1}{\mathcal{Z}}\mathrm{Tr}\Big(e^{-\beta H_B}B_{k'}e^{-\beta H_B}e^{iH_B t}B_k e^{-iH_B t}e^{\beta H_B}\Big) \\
&= \langle B_{k'}(0)B_k(t-i\beta)\rangle\,.
\end{aligned} \tag{3.26}$$

By substituting in the Fourier transform one finds that

$$\gamma_{kk'}(\omega) = e^{\beta\omega}\gamma_{k'k}(-\omega). \tag{3.27}$$

Further, a thermal state of the system ρ_β^S satisfies

$$\rho_\beta^S A_k(\omega) = e^{\beta\omega} A_k(\omega)\rho_\beta^S, \tag{3.28}$$
$$\rho_\beta^S A_k^\dagger(\omega) = e^{-\beta\omega} A_k^\dagger(\omega)\rho_\beta^S. \tag{3.29}$$

Putting the last two equations into Eq. (3.25), one sees that the dissipator is also zero, proving that the stationary state of the system in contact with a thermal reservoir is a Gibbs state.

Another interesting property of the master equation (3.23) is that, for a non-degenerate system Hamiltonian, the populations of the density matrix have a closed dynamics. In other words, their equations of motion does not depend on the off-diagonal terms of the density matrix. This is true regardless of the stationary state of the environment, namely it does not need to be thermal. If the non-degenerate Hamiltonian is $H_S = \sum_n \epsilon_n |n\rangle\langle n|$, then p_n the population of nth level satisfies the following

$$\dot{p}_n = \sum_m \left(W(n|m)p_m - W(m|n)p_n\right), \tag{3.30}$$

with the transition rates $W(n|m)$ given by

$$W(n|m) = \sum_{kk'} \gamma_{kk'}(\epsilon_k - \epsilon_{k'})\langle m|A_k|n\rangle\langle n|A_{k'}|m\rangle. \tag{3.31}$$

Moreover, for a thermal bath, using (3.27), one can find the detailed balance criteria

$$W(m|n)e^{-\beta\epsilon_n} = W(n|m)e^{-\beta\epsilon_m}. \tag{3.32}$$

Therefore, at stationary the populations are given by the Boltzmann distribution

$$\frac{p_n(\infty)}{p_m(\infty)} = \frac{e^{-\beta\epsilon_n}}{e^{-\beta\epsilon_m}}. \tag{3.33}$$

3.3 Bosonic heat baths

As a paradigmatic case to which we will refer frequently in the rest of this chapter, and the future chapters, we address the bosonic heat bath. The environment consists of infinite number

of non-interacting bosonic modes, or simply harmonic oscillators, with the Hamiltonian

$$H_B = \sum_\mu \omega_\mu b_\mu^\dagger b_\mu. \tag{3.34}$$

Here b_μ is the annihilation operator of the μth mode in the bath. The environment is prepared in a thermal state. Moreover, the system, with the Hamiltonian H_S is coupled to the bath through the linear interaction Hamiltonian

$$H_I = X \otimes \sum_\mu g_\mu \left(b_\mu^\dagger + b_\mu\right), \tag{3.35}$$

with the operator X defined on $\mathcal{H}_S$, the Hilbert space of the system. This in general might have an spectrum given by $X = \sum_\omega A(\omega)$ with $A(\omega)$s being the Hamiltonian eigenoperators. Further we demand the ergodicity condition to hold, such that the system always relaxes to thermal equilibrium, regardless of the initial state. This condition translates to

$$[O, A(\omega)] = [A(\omega), O] = 0 \quad \forall\omega \quad \Rightarrow O \propto \mathbb{I}. \tag{3.36}$$

Before finding the spectral density, we notice that the criteria of Eq. (3.15) is satisfied for the bath operator $B = \sum_\mu g_\mu \left(b_\mu^\dagger + b_\mu\right)$, since it is evaluated over a thermal state. In order to find the two time correlation function $\langle B(t)B(0)\rangle$, we first notice that the time evolved of B is given by

$$B(t) = \sum_\mu g_\mu \left(e^{+i\omega_\mu t} b_\mu^\dagger + e^{-i\omega_\mu t} b_\mu\right). \tag{3.37}$$

which by substituting in the two time correlation function over the thermal state yields

$$\langle B(t)B(0)\rangle = \sum_\mu g_\mu^2 \left(e^{+i\omega_\mu t} N_\mu + e^{-i\omega_\mu t}(N_\mu + 1)\right). \tag{3.38}$$

Here $N_\mu = [\exp(\beta\omega_\mu) - 1]^{-1}$ is the average number of occupation in μth mode, over the thermal state. The one sided Fourier transform of the latter gives

$$\gamma(\omega) = \pi g_\omega^2 \left((N_\omega + 1)\,\Theta(\omega) - N_{-\omega}\Theta(-\omega)\right). \tag{3.39}$$

The dissipator Eq. (3.25) will be therefore

$$\begin{aligned}\mathcal{D}(\rho_S(t)) = \sum_{\omega>0} g_\omega^2 \Big[&(N_\omega + 1)\left(A(\omega)\rho A^\dagger(\omega) - \tfrac{1}{2}\left\{A^\dagger(\omega)A(\omega), \rho_S(t)\right\}\right) \\ &+ N_\omega \left(A^\dagger(\omega)\rho A(\omega) - \tfrac{1}{2}\left\{A(\omega)A^\dagger(\omega), \rho_S(t)\right\}\right)\Big],\end{aligned} \tag{3.40}$$

where we absorb the π coefficient into g_ω. The Lamb shift contribution is also given by

$$\begin{aligned} S(\omega) &= \sum_\mu g_\mu^2 \left(\frac{N(\omega_\mu)+1}{\omega-\omega_\mu} + \frac{N(\omega_\mu)}{\omega+\omega_\mu} \right) \\ &= \sum_\mu g_\mu^2 \frac{\omega_\mu + \omega \coth(\beta\omega_\mu)}{\omega^2-\omega_\mu^2}. \end{aligned} \tag{3.41}$$

This term will be responsible for a renormalization of the systems Hamiltonian. However, usually this renormalization is very small and might be neglected, due to the weak coupling limit [71].

3.4 Two level system in a radiation field

As the simplest scenario we consider a two dimensional system under the dissipative dynamics (3.40). Such a system could represent an atom whose dynamics could be studied effectively represented in a two level subspace. The system Hamiltonian is given by

$$H_2 = -\tfrac{1}{2}\omega\sigma_z = \tfrac{1}{2}\omega\left(|0\rangle\langle 0| - |1\rangle\langle 1|\right), \tag{3.42}$$

where the subscript 2 refers to the dimension of the system, σ_z being the Pauli matrix in z direction, and $|0\rangle$ ($|1\rangle$) standing for the ground (excited) state of the system. In turn, the bosonic environment might represent a radiation field, with each mode of the field associated with a quantum harmonic oscillator mode. The interaction Hamiltonian, which takes into account the system transitions from the ground state to the exited state, by absorbing an excitation from the radiation field, and vice verse through emitting an excitation to the bath, is given by

$$H_I = \sigma_x \otimes \sum_\mu g_\mu (b_\mu^\dagger + b_\mu), \tag{3.43}$$

with $\sigma_x = |0\rangle\langle 1| + |1\rangle\langle 0|$, being the Pauli matrix in the x direction. It is very easy to check that $\sigma_x = \sigma_+ + \sigma_-$, with $\sigma_+ = |1\rangle\langle 0|$ are the eigenoperators of the system Hamiltonian

$$[H_2, \sigma_\pm] = \mp\omega\sigma_\pm. \tag{3.44}$$

Therefore, by recognizing that there is only one operator with the positive eigenvalue, i.e., $A(\omega) = \sigma_-$, the master equation takes the form

$$\begin{aligned} \dot{\rho}_2(t) = g_\omega^2 \Big[&(N_\omega + 1)\left(\sigma_-\rho_2\sigma_+ - \tfrac{1}{2}\left\{\sigma_+\sigma_-, \rho_2\right\}\right) \\ &+ N_\omega\left(\sigma_+\rho_2\sigma_- - \tfrac{1}{2}\left\{\sigma_-\sigma_+, \rho_2\right\}\right)\Big]. \end{aligned} \tag{3.45}$$

Solving this simple equation gives the following time dependence for populations of the two levels

$$\begin{aligned} p_0(t) &= p_0^\infty \left(1 - e^{-\gamma t}\right) + e^{-\gamma t} p_0(0), \\ p_1(t) &= p_1^\infty \left(1 - e^{-\gamma t}\right) + e^{-\gamma t} p_1(0). \end{aligned} \tag{3.46}$$

Here we defined $p_0^\infty = {}^{(1+N_\omega)}/_{(1+2N_\omega)}$ and $p_1^\infty = {}^{N_\omega}/_{(1+2N_\omega)}$ to be stationary state populations, and $\gamma = g_\mu^2(1+2N_\omega)$. These diagonal terms are exactly the same in the Schrodinger picture. Moreover, for the off-diagonal terms, we have

$$p_{01}(t) = p_{10}^*(t) = e^{-{}^1/_2\gamma t} p_{01}(0). \tag{3.47}$$

or alternatively in the Schrodinger picture, one has to substitute $p_{01}(t) \to p_{01}(t)e^{-i\omega t}$, and $p_{10}(t) \to p_{10}(t)e^{i\omega t}$. Clearly, at stationary state, i.e., as $t \to \infty$, the coherences will vanish, leaving the density matrix diagonal. The corresponding stationary state populations are simply those of a two level system at thermal equilibrium, with the same temperature as the bath. This is so regardless of the initial preparation of the two level atom.

3.5 Damped harmonic oscillator

Another interesting model that we address is a damped harmonic oscillator (HO). The HO might represent a cavity mode, while the bosonic bath represents the radiation field, just like the previous section. The free Hamiltonian of the HO is $H_{ho} = \omega a^\dagger a$, and its interaction with the bath is realized by

$$H_I = (a + a^\dagger) \sum_\mu g_\mu \left(b_\mu + b_\mu^\dagger\right). \tag{3.48}$$

Neglecting the Lamb shift Hamiltonian, the master equation in the Schrodinger picture is

$$\dot{\rho}_{ho} = -i[H_{ho}, \rho_{ho}] + \gamma(\omega)\left(a\rho_{ho}a^\dagger - \tfrac{1}{2}\left\{a^\dagger a, \rho_{ho}\right\}\right) + \gamma(-\omega)\left(a^\dagger \rho_{ho} a - \tfrac{1}{2}\left\{aa^\dagger, \rho_{ho}\right\}\right), \tag{3.49}$$

where we have defined $\gamma_0 = g_\omega^2$, $\gamma(\omega) = \gamma_0(N_\omega + 1)$ and $\gamma(-\omega) = \gamma_0 N_\omega$ to simplify our notation. The stationary state of the HO is given by the Boltzmann distribution, since its energy spectrum is non-degenerate. The dynamics of the density matrix highly depends on the initial preparation, and in general one might not be able to address it, due to the infinite dimensional Hilbert space. Nevertheless, since the whole dynamic is quadratic, it preserves Gaussianity. So, we limit ourselves to Gaussian preparations. For such states, it is more convenient to work with the

covariance matrix σ, knowing which is equivalent to knowing the density matrix of the system

$$\sigma = \begin{pmatrix} \langle x^2 \rangle & 1/2\langle xp + px \rangle \\ 1/2\langle xp + px \rangle & \langle p^2 \rangle \end{pmatrix}, \tag{3.50}$$

where the *quadratures* x and p are Hermitian operators given by

$$x = 1/\sqrt{2}(a^\dagger + a), \qquad p = i/\sqrt{2}(a^\dagger - a), \tag{3.51}$$

$$a = 1/\sqrt{2}(x + ip), \qquad a^\dagger = 1/\sqrt{2}(x - ip). \tag{3.52}$$

For higher order moments, the following conversion relation between the two representations might be very useful

$$\begin{aligned} a^2 &= 1/2(x^2 - p^2 + ixp + ipx), & a^\dagger a &= 1/2(x^2 + p^2 - 1), \\ x^2 &= 1/2(a^2 + a^{\dagger\,2} + aa^\dagger + a^\dagger a), & p^2 &= -1/2(a^2 + a^{\dagger\,2} - aa^\dagger - a^\dagger a), \\ xp &= i/2(-a^2 + a^{\dagger\,2} + aa^\dagger - a^\dagger a), & px &= i/2(-a^2 + a^{\dagger\,2} - aa^\dagger + a^\dagger a). \end{aligned} \tag{3.53}$$

In order to evaluate the elements of σ, we need to know how second order operators like $\left\{a^2, a^{\dagger\,2}, aa^\dagger, a^\dagger a\right\}$ depend on time. To this end we remind that the Heisenberg picture equation of motion for any operator O_H defined on $\mathcal{H}_{ho}$ is

$$\frac{dO_H}{dt} = i[H_{ho}, O_H] + \gamma(\omega)\left(a^\dagger O_H a - \tfrac{1}{2}\left\{a^\dagger a, O_H\right\}\right) + \gamma(-\omega)\left(aO_H a^\dagger - \tfrac{1}{2}\left\{aa^\dagger, O_H\right\}\right). \tag{3.54}$$

Specifically for the creation and annihilation operators one might find

$$\begin{aligned} a_H(t) &= e^{(-i\omega - \gamma_0/2)t}a, \quad & a_H^2(t) &= e^{(-i2\omega - \gamma_0)t}a^2 \\ a_H^\dagger(t) &= e^{(i\omega - \gamma_0/2)t}a^\dagger, \quad & a_H^{\dagger\,2}(t) &= e^{(i2\omega - \gamma_0)t}a^{\dagger\,2} \\ a^\dagger a_H(t) &= e^{-\gamma_0 t}a^\dagger a + N(1 - e^{-\gamma_0 t}), \\ aa_H^\dagger(t) &= e^{-\gamma_0 t}aa^\dagger + (N+1)(1 - e^{-\gamma_0 t}). \end{aligned} \tag{3.55}$$

From here one can easily find the time evolution of the second moments of the quadratures, namely

$$\begin{aligned}
\left\langle x^2(t)\right\rangle &= \tfrac{1}{2}\left(\left\langle a_H^2(t)\right\rangle + \left\langle a_H^{\dagger\,2}(t)\right\rangle + \left\langle a^\dagger a_H(t)\right\rangle + \left\langle a a_H^\dagger(t)\right\rangle\right) \\
&= e^{-\gamma_0 t}\left(\cos^2(\omega t)x^2 + \sin^2(\omega t)p^2 + \frac{\sin(2\omega t)}{2}(xp+px)\right) + (N_\omega + \tfrac{1}{2})(1-e^{-\gamma_0 t}), \\
\left\langle p^2(t)\right\rangle &= \tfrac{1}{2}\left(-\left\langle a_H^2(t)\right\rangle - \left\langle a_H^{\dagger\,2}(t)\right\rangle + \left\langle a^\dagger a_H(t)\right\rangle + \left\langle a a_H^\dagger(t)\right\rangle\right) \\
&= e^{-\gamma_0 t}\left(\sin^2(\omega t)x^2 + \cos^2(\omega t)p^2 - \frac{\sin(2\omega t)}{2}(xp+px)\right) + (N_\omega + \tfrac{1}{2})(1-e^{-\gamma_0 t}), \\
\tfrac{1}{2}\left\langle px(t)+xp(t)\right\rangle &= \tfrac{-i}{2}\left(\left\langle a_H^2(t)\right\rangle - \left\langle a_H^{\dagger\,2}(t)\right\rangle\right) \\
&= \frac{e^{-\gamma_0 t}}{2}\left(\cos(2\omega t)\left\langle xp+px\right\rangle - \sin(2\omega t)\left(\left\langle x^2\right\rangle - \left\langle p^2\right\rangle\right)\right).
\end{aligned} \tag{3.56}$$

Again, from these sets of equation we revive the fact that at stationary state, i.e., $t \to \infty$, the off-diagonal terms vanish, while $\left\langle x^2(\infty)\right\rangle = \left\langle p^2(\infty)\right\rangle = N_\omega + 1/2$.

3.6 Coupled harmonic oscillators in a common bath

Here we address a system consisting of two interacting HO which are placed in a common bath. The Hamiltonian of the system is

$$H = \omega_1 a_1^\dagger a_1 + \omega_2 a_2^\dagger a_2 - J\left(a_1^\dagger a_2 + a_1 a_2^\dagger\right) + \frac{U}{2}\left(a_1^{\dagger 2} a_1^2 + a_2^{\dagger 2} a_2^2\right), \tag{3.57}$$

the first two terms refer to the free Hamiltonians of each oscillator, the third term takes into account the role of tunneling, and finally the last term is responsible for the self interaction in each mode. In what follows we let $\omega_1 = 1$, and allow for a detuning between the two frequencies $\Delta = \omega_2 - \omega_1$. At thermal equilibrium, the system is described by the following density matrix

$$\rho(\beta) = \frac{e^{-\beta H}}{\mathcal{Z}}, \text{ with the partition function } \mathcal{Z} = \mathrm{Tr}(e^{-\beta H}). \tag{3.58}$$

First of all, let us focus on the tunneling dominated regime. With $U = 0$, the Hamiltonian is quadratic, and we may benefit from the Gaussian stationary state. Very similar to the single HO of section 3.5, we define the quadratures associated with each mode as follows

$$x_j = 1/\sqrt{2}(a_j + a_j^\dagger), \text{ and } p_j = i/\sqrt{2}(a_j^\dagger - a_j). \tag{3.59}$$

The 4×4 covariance matrix, has the elements $\sigma_{lm} = \frac{1}{2}\langle R_l R_m + R_m R_l\rangle - \langle R_l\rangle\langle R_m\rangle$, where the R_l and R_m are chosen among any pair of the quadratures $R_l, R_m \in \{x_1, x_2, p_1, p_2\}$. One can show that

the stationary state covariance matrix is as follows

$$\sigma(\beta)=\frac{1}{2\mathcal{N}}\begin{pmatrix} K^{+} & 2J\sinh(C) & 0 & 0\\ 2J\sinh(C) & K^{-} & 0 & 0\\ 0 & 0 & K^{+} & 2J\sinh(C)\\ 0 & 0 & 2J\sinh(C) & K^{-}\end{pmatrix}, \tag{3.60}$$

with $\mathcal{N}=A\left(\cosh(B)-\cosh(C)\right)$, $K^{\pm}=A\sinh(B)\pm\Delta\sinh(C)$, $A=\sqrt{\Delta^2+4J^2}$, $B=\frac{1}{2}\beta(2+\Delta)$, and $C=\frac{1}{2}\beta\sqrt{\Delta^2+4J^2}$. Furthermore, once the two oscillators are at resonance, i.e., if $\Delta=0$, this takes the more compact form

$$\sigma_{\Delta=0}(\beta)=\frac{1}{2\left[\cosh(\beta)-\cosh(J\beta)\right]}\begin{pmatrix} \sinh(\beta) & \sinh(J\beta) & 0 & 0\\ \sinh(J\beta) & \sinh(\beta) & 0 & 0\\ 0 & 0 & \sinh(\beta) & \sinh(J\beta)\\ 0 & 0 & \sinh(J\beta) & \sinh(\beta)\end{pmatrix}. \tag{3.61}$$

Proof of Eq. (3.60)**—** One can easily bring the Hamiltonian of the coupled oscillators (with $U=0$) in the diagonal form by the mode mixing transformation. First we define the new ladder operators b_i to satisfy the following

$$\begin{pmatrix} a_1\\ a_2\end{pmatrix}=\begin{pmatrix} \cos\phi & \sin\phi\\ -\sin\phi & \cos\phi\end{pmatrix}\begin{pmatrix} b_1\\ b_2\end{pmatrix},\ \text{or equivalently}\ \begin{pmatrix} b_1\\ b_2\end{pmatrix}=\begin{pmatrix} \cos\phi & -\sin\phi\\ \sin\phi & \cos\phi\end{pmatrix}\begin{pmatrix} a_1\\ a_2\end{pmatrix}. \tag{3.62}$$

These new operators inherit the same commutation relations as a_js. By writing down the Hamiltonian in terms of the new ladder operators, and demanding the coefficients of the off diagonal terms to be zero. This leads to $\phi=\frac{1}{2}\arctan 2J/\Delta$ and

$$H=\Omega^1 b_1^{\dagger}b_1+\Omega^2 b_2^{\dagger}b_2,\ \text{with}\ \Omega^i=1+\left(\Delta\mp\sqrt{\Delta^2+(2J)^2}\right)/2. \tag{3.63}$$

with the minus sign for $i=1$, and plus sign for $i=2$. Once at thermal equilibrium, we can find the expectation value of the quadratic ladder operators

$$\left\langle b_1^{\dagger}b_1\right\rangle=\left\langle b_1 b_1^{\dagger}\right\rangle-1=N^1,\ \ \left\langle b_2^{\dagger}b_2\right\rangle=\left\langle b_2 b_2^{\dagger}\right\rangle-1=N^2,\ \text{with}\ N^i=(e^{\Omega^i/T}-1)^{-1}, \tag{3.64}$$

while all other quadratic operators have zero expectation value. In order to find the covariance matrix elements we need to know the expression for all the elements of the matrix in terms of

those appearing in Eq. (3.64). This can be done with the help of Eq. (3.62)

$$\begin{aligned}
\left\langle x_1^2 \right\rangle = \left\langle p_1^2 \right\rangle &= 1/2 + \left\langle a_1^\dagger a_1 \right\rangle = 1/2 + \cos^2\phi N^1 + \sin^2\phi N^2 \\
&= (1 + N^1 + N^2)/2 + \cos 2\phi (N^1 - N^2)/2, \\
\left\langle x_2^2 \right\rangle = \left\langle p_2^2 \right\rangle &= 1/2 + \left\langle a_2^\dagger a_2 \right\rangle = 1/2 + \cos^2\phi N^2 + \sin^2\phi N^1 \\
&= (1 + N^1 + N^2)/2 - \cos 2\phi (N^1 - N^2)/2, \\
\langle x_1 x_2 \rangle = \langle p_1 p_2 \rangle &= \left\langle a_1^\dagger a_2 + a_1 a_2^\dagger \right\rangle /2 = \sin 2\phi (N^2 - N^1)/2,
\end{aligned} \tag{3.65}$$

while any other element of the covariance matrix vanishes. Finally, this might be simplified to Eq. (3.60) by using

$$\begin{gathered}
1 + N^1 + N^2 = \frac{\sinh(\frac{\Omega^2+\Omega^1}{2T})}{\cosh(\frac{\Omega^2+\Omega^1}{2T}) - \cosh(\frac{\Omega^2-\Omega^1}{2T})}, \quad N^2 - N^1 = \frac{\sinh(\frac{\Omega^2-\Omega^1}{2T})}{\cosh(\frac{\Omega^2+\Omega^1}{2T}) - \cosh(\frac{\Omega^2-\Omega^1}{2T})}, \\
\cos 2\phi = \Delta / \sqrt{\Delta^2 + 4J^2}, \quad \sin 2\phi = 2J / \sqrt{\Delta^2 + 4J^2} \\
\clubsuit
\end{gathered} \tag{3.66}$$

In the next chapter we will use this covariance matrix in order to address the estimation of temperature as well as the interaction strength J.

Chapter 4

Quantum metrolgy at thermal equilibrium

This chapter is dedicated to our results regarding parameter estimation in thermal systems. By this, we mean that the parameter drivings happen adiabatically, keeping the thermal feature of the system. In general, on account of the structure of thermal states, the description of the problem is possible merely with the help of a small set of macroscopic parameters such as temperature, chemical potentials, and conserved quantities.

We classify metrology in thermal systems in two distinct categories:

1. Estimation of temperature, or thermometry.
2. Estimation of Hamiltonian couplings.

As we shall discuss below, thermometry is simpler to formulate and allows for universal results that have no dependence whatsoever on a specific model. This is so, because temperature enters as a global parameter in the expression of thermal states. On the contrary, the estimation of Hamiltonian couplings might become highly non trivial due to the non commutativity of the different terms in the Hamiltonian. In Section 4.1 we briefly review some fundamental definitions and properties of thermal systems. Specifically, Section 4.1.1 explains the difference of the two categories mentioned above.

The rest of this chapter is devoted to present our new results, which are mainly focused on thermometry. In Section 4.2 we investigate the ultimate temperature precision with individual quantum probes. We show that the best quantum thermometer corresponds to a two-level system with a single ground state and a highly degenerate excited state. Besides, we show that increasing the degeneracy always improves the thermometry precision. Such type of spectrum can be

easily implemented with e.g., alkaline atoms, which in the absence of an external magnetic field have a manifold of excited Zeeman hyperfine energy levels.

While for individual quantum probes, any thermometer cannot outperform the two-level system with a highly degenerate excited state, multipartite probes offers novel possibilities for thermometry. In order to examine this possibility, in Section 4.3 we investigate temperature sensitivity of a bipartite system, consisting of two coupled harmonic oscillators. The interaction between the two oscillators creates quantum correlations even at finite temperatures. We observe that, the presence of correlations appreciably enhances the thermometry precision, compared to two uncoupled probes. This enhanced precision is, however, achieved only by performing a global measurement on both oscillators, which might not be easy to implement in practice. Even so, we propose local measurements, that are more feasible experimentally, yet they perform close to optimal. We observe that quantum correlations boost the thermometry precision obtained even with local measurements.

Thermometry aside, in Section 4.3.2 we study the estimation of the interaction strength itself. Particularly, in the same system of coupled harmonic oscillators, we ask ourselves about the limitations on estimation of the coupling between the two modes. We observe that by increasing the temperature, the estimation gets less precise. In addition, unlike thermometry, local schemes fail to perform close to the global (optimal) ones. Finally, in Section 4.4 we conclude.

4.1 The canonical distribution

By stating that a (generic) system is at thermal equilibrium, we mean its density matrix is described by a *Gibbs state*. More precisely, if the Hamiltonian of the system is given by H, then the thermal state of the system would be

$$\rho^T = \frac{\mathrm{e}^{-H/k_B T}}{\mathcal{Z}}, \tag{4.1}$$

with k_B being the Boltzmann constant, T the temperature of the system, and $\mathcal{Z} = \mathrm{Tr}[\mathrm{e}^{-H/k_B T}]$ its the partition function. Throughout this thesis we set $k_B = \hbar = 1$, unless otherwise mentioned. Moreover, we regularly switch between T and the inverse temperature $\beta = 1/T$ to make notations simpler. The (Helmholtz) free energy is given

$$A = -T \log(\mathcal{Z}), \tag{4.2}$$

which is a very important quantity, specially in classical statistical mechanics. In fact the statistics (the expectation values and the uncertainties) about different physical quantities (observables) can be related to first and second derivatives of the free energy. We will discuss this in section 4.1.1 for classical systems, and try to find the non-trivial quantum counterpart.

4.1.1 Adiabatic driving and static susceptibilities

As we already mentioned, here we consider all parameters of interest change adiabatically, so that the system is always described by a Gibbs state. In particular, if the Hamiltonian of the system can be written as $H = \xi_1 H_1 + \xi_2 H_2$, then the driving parameters that allow to move within the Gibbs space correspond either to the temperature T or to the parameters $\{\xi_1, \xi_2\}$.

The temperature driving is simpler to study, because of the Gibbs structure of the state, and due to the fact that T appears as a global factor in the exponent of thermal states. In such case, one can explore $\chi_{B,T}$, the susceptibility of an arbitrary observable B associated to the temperature driving. This is defined as

$$\chi_{B,T} = \partial_T \langle B \rangle = \partial_T \mathrm{Tr}[B\, \rho^T]. \tag{4.3}$$

Traditionally, the temperature susceptibility (i.e., the susceptibility associated with temperature driving) of the Hamiltonian observable is called the heat capacity $C_T \equiv \chi_{H,T} = \partial_T \langle H \rangle$. One can easily confirm that the heat capacity is proportional to the variance of the Hamiltonian. More generally, for any observable B, the temperature susceptibility is nothing but its correlation with the Hamiltonian H. The proof is not complicated, one needs to substitute the thermal state (4.1) in (4.3), yielding

$$\begin{aligned} \chi_{B,T} &= \partial_T \mathrm{Tr}[B\, \mathcal{Z}^{-1} \mathrm{e}^{-H/T}] \\ &= \mathrm{Tr}[B\, \partial_T\, (\mathcal{Z}^{-1} \mathrm{e}^{-H/T})] \\ &= \beta^2\, \mathrm{Tr}[B\, (H - \langle H \rangle)\, (\mathcal{Z}^{-1} \mathrm{e}^{-H/T})] \\ &= \beta^2\, \mathrm{Corr}(B, H)_{\rho^T}, \end{aligned} \tag{4.4}$$

where we use $\partial_T\, \rho^T = \beta^2\, (H - \langle H \rangle) \rho^T$, and the standard definition of correlation, $\mathrm{Corr}(\circ, \bullet)_\sigma \equiv \frac{1}{2}\mathrm{Tr}[(\circ \bullet + \bullet \circ)\sigma] - \mathrm{Tr}[\circ\sigma]\mathrm{Tr}[\bullet\sigma]$. Straightforwardly, substituting $B \to H$, leads to the well-known expression for heat capacity $C_T = \beta^2\, \mathrm{Var}(H)_{\rho^T}$.

Before proceeding further, we remind that since H commutes with the density matrix, one can rewrite the derivative of the density matrix in the following symmetric shape

$$\partial_T\, \rho^T = \frac{\beta^2}{2} \Big((H - \langle H \rangle) \rho^T + \rho^T\, (H - \langle H \rangle) \Big). \tag{4.5}$$

As a result and by virtue of Eq. (2.8), the symmetric logarithmic derivative associated to temperature is simply

$$\Lambda_T = \frac{\beta^2}{2}\,(H - \langle H\rangle). \tag{4.6}$$

When it turns to Hamiltonian coupling estimation i.e., ξ_1 and ξ_2, to find analytical expressions for optimal observables become very involved and, generally, model dependent. This is so because $[H_1, H_2] \neq 0$ in general. However, there exist scenarios in which one is still able to find analytic solutions. We will address one of these occasions in Section 4.3.2, in the estimation of tunneling rate between two harmonic oscillators. Another occurrence which might be addressed with simple mathematics is when $[H_1, H_2] = 0$. Specifically, we explore parameter estimation under this circumstance in many body systems as presented in Section 5.5.

4.2 Ultimate precision of temperature estimation

In standard thermometry, a (sufficiently small) thermometer is simply allowed to equilibrate with the sample to be probed, so that the temperature of the latter is inferred from the state of the probe. In a quantum scenario, the same procedure can be applied. A first approximation to the sample temperature can be obtained by performing a suitable measurement on the steady state of the thermalized probe. As we know from Chapter 2, if a large number m of such independent experiments is carried out, one can refine the estimate T of the sample temperature. Its corresponding uncertainty δT is bounded from below by the quantum Fisher information $\mathcal{F}_T$, via the quantum Cramér-Rao inequality. We will then refer to $\mathcal{F}_T$ as *optimal thermal sensitivity* and consider it as a benchmark for maximum quality of estimation in the following analysis.

We write the Hamiltonian of our thermometer as $H = \sum_n \epsilon_n |\epsilon_n\rangle\langle\epsilon_n|$. A thermalization process leads to stationary states of the Gibbs form, as given by Eq. (4.1). The QFI for such a state is

$$\begin{aligned}\mathcal{F}_T &= \mathrm{Tr}\,[\Lambda_T^2 \rho^T] \\ &= \beta^4\ \mathrm{Var}(H)_{\rho^T} \\ &= \beta^2\ C_T,\end{aligned} \tag{4.7}$$

where in the last line we enter the heat capacity into the equation through $C_T = \beta^2\ \mathrm{Var}(H)_{\rho^T}$. Interestingly, in the single shot scenario of $\nu = 1$, one can combine Eqs. (2.6) and (4.7) to get the thermodynamic uncertainty relation $\delta^2 T\ \mathrm{Var}(H) \geq T^2$. Equivalently, the signal-to-noise ratio $T/\delta T$ is upper-bounded as $(T/\delta T)^2 \leq C(T)$ [72]. Note as well that, by the virtue of Eq. (4.6), the most informative measurement for thermometry is just a projection onto the energy eigenbasis.

In the light of Eq. (4.7), the maximization of the thermal sensitivity of a probe translates into finding the energy spectrum with the largest possible energy variance at thermal equilibrium, or equivalently, the N-dimensional probe with largest heat capacity. The heat capacity of the sample must be anyway much larger than that of the probe so as to minimize any disturbance arising from the estimation procedure.

For a general N-level probe, the energy variance writes as

$$\begin{aligned}\mathrm{Var}(H)_{\rho^T} &= \mathrm{Tr}[H^2\,\rho^T] - \mathrm{Tr}[H\,\rho^T]^2 = \sum_{k=0}^{N} p_k \epsilon_k^2 - \Big(\sum_{k=0}^{N} p_k \epsilon_k\Big)^2 \\ &= \mathcal{Z}^{-1} \sum_k \bar{\epsilon}_k^2 e^{-\bar{\epsilon}_k/T}\end{aligned} \tag{4.8}$$

with the populations defined as $p_k = \frac{\mathrm{e}^{-\beta\epsilon_k}}{\mathcal{Z}}$ and $\bar{\epsilon}_k \equiv \epsilon_k - \langle H\rangle$. The variance is bounded. In order to identify its maximum, we impose $\partial \mathrm{Var}(H)/\partial\bar{\epsilon}_l = 0$, which should hold for any l, resulting a set of N transcendental equations

$$\begin{aligned}0 &= -\beta p_l \sum_{k=1}^{N} (\delta_{kl} - p_k)\epsilon_k^2 + 2\epsilon_l p_l + 2\Big(\sum_{k=1}^{N} p_k\epsilon_k\Big)\Big(-\beta p_l \sum_{k=1}^{N}(\delta_{kl}-p_k)\epsilon_k + p_l\Big) \\ &= \epsilon_l^2 - \Big\langle H^2\Big\rangle - 2\frac{\epsilon_l}{\beta} - 2\langle H\rangle\left(\epsilon_l - \langle H\rangle - \frac{1}{\beta}\right) \\ &= \epsilon_l^2 - 2\Big(\frac{1}{\beta} + \langle H\rangle\Big)\epsilon_l + 2\langle H\rangle^2 - \Big\langle H^2\Big\rangle + \frac{2}{\beta}\langle H\rangle,\end{aligned} \tag{4.9}$$

By subtracting the lth equation from the l'th, we reach at

$$(\epsilon_l - \epsilon_{l'})[\epsilon_l - \epsilon_{l'} - 2(\langle H\rangle + T)] = 0. \tag{4.10}$$

That is, at the extremum points of $\mathrm{Var}(H)$, any two energy eigenvalues ϵ_l and $\epsilon_{l'}$ must be either equal, or sum up to a fixed value. This may only happen if the energy spectrum is that of an effective two-level atom with energies $\{\epsilon_-, \epsilon_+\}$ and some ground and excited-state degeneracies given by N_0 and $N - N_0$, respectively. Without loss of generality, we may always shift the energy spectrum so that $\epsilon_- = 0$, wherefore, the optimal gap becomes $x^*_{N,N_0} \equiv \Omega^*/T = 2(\langle H\rangle/T + 1) > 2$, since $\langle H\rangle > 0$. By virtue of this definition, it follows that

$$\mathrm{e}^{x^*_{N,N_0}} = \frac{N - N_0}{N_0}\frac{x^*_{N,N_0} + 2}{x^*_{N,N_0} - 2}. \tag{4.11}$$

Further, we note the expression for the energy variance reads as follows

$$\mathrm{Var}(H(x_{N,N_0})) = T^2 x^2_{N,N_0}\,\frac{N_0(N-N_0)\mathrm{e}^{x_{N,N_0}}}{\Big((N-N_0) + N_0\mathrm{e}^{x_{N,N_0}}\Big)^2}. \tag{4.12}$$

By exploiting Eq. (4.12) to the optimal frequency, one might compare the energy variance of two configurations with two different ground state degeneracies, namely N_0 and N_0-1, leading to

$$\mathrm{Var}(H(x^*_{N,N_0-1}))-\mathrm{Var}(H(x^*_{N,N_0}))=\frac{1}{4}\left(x^*_{N,N_0-1}-x^*_{N,N_0}\right)>0. \tag{4.13}$$

The last inequality is guaranteed by virtue of Eq. (4.11). Therefore, the maximum sensitivity is obtained from an effective two-level system with $N_0=1$ the degeneracy of the ground state, and $N-1$ the degeneracy of the excited states at the optimal gap, which satisfies (4.11).

At last let us show that the configuration we found here is indeed maximizing the energy variance, and does not correspond to a minimum or a saddle point. To this end, one should calculate the Hessian matrix $\mathbf{H}_{ij}=\partial_{\epsilon_i}\partial_{\epsilon_j}\mathrm{Var}(H)$. If it is negative definite, the extremum point that we found is indeed the maximum of the Hamiltonian variance. The diagonal elements of $\mathbf{H}$ are given by

$$\begin{aligned}\mathbf{H}_{ii}=\left(\frac{\mathrm{e}^{-\epsilon_i/T}}{T\mathcal{Z}}\right)^2\Bigg(&2\Big(\left\langle H^2\right\rangle-3\langle H\rangle^2-4T\langle H\rangle-T^2\Big)+8(T+\langle H\rangle)\epsilon_i-4\epsilon_i^2\\&+\mathcal{Z}\mathrm{e}^{\epsilon_i/T}\Big(2T^2+2\langle H\rangle(2T+\langle H\rangle)-\left\langle H^2\right\rangle-2(2T+\langle H\rangle)\epsilon_i\Big)+\epsilon_i^2\Bigg),\end{aligned} \tag{4.14}$$

while the off-diagonal terms read as

$$\mathbf{H}_{ij}=\frac{\mathrm{e}^{-(\epsilon_i+\epsilon_j)/T}}{T^2\mathcal{Z}^2}\Big(4\langle H\rangle(\epsilon_i+\epsilon_j-2T)+(\epsilon_i+\epsilon_j)(4T-\epsilon_i-\epsilon_j)+2\left\langle H^2\right\rangle-6\langle H\rangle^2-2T^2\Big). \tag{4.15}$$

The symmetry arising from $N-1$ degeneracy of the excited states simplifies the rest of the analysis. On this account, the Hessian matrix has four different types of elements, two of which are diagonal, corresponding to $a=\mathbf{H}_{11}$, and $b=\mathbf{H}_{ii}\ \ \forall i\neq 1$, and two off-diagonals, $c=\mathbf{H}_{1i}=\mathbf{H}_{i1},\forall i\neq 1$, and $d=\mathbf{H}_{ij}=\mathbf{H}_{ji},\ \ \forall i,j\neq 1$. Further, notice that $\mathcal{Z}=2x^*/(2+x^*)$, $\langle H\rangle=(x^*-2)T/2$, $\left\langle H^2\right\rangle=x^*(x^*-2)T^2/2$, and $\mathrm{e}^{x^*}=*(N-1)(x^*+2)/*(x^*-2)$. Putting everything together one obtains

$$\begin{aligned}a&=-\frac{1}{8}(x^*-4),\\ b&=-\frac{(x^*-2)(4N+x^*-6)}{8(N-1)^2},\\ c&=\frac{(x^{*2}-4)^2}{8(N-1)},\\ d&=-\frac{(x^*-2)^2}{8(N-1)^2}.\end{aligned} \tag{4.16}$$

Whence the eigenvalues of the Hessian matrix are $\lambda_1=0$, $\lambda_2=-(x^{*2}-4)/8(N-1)$, and $\lambda_3=-(x^*-2)/2(N-1)$, with λ_3 being $N-2$ folded degenerate. The fact that one of the eigenvalues

is zero, is a result of Var(H) being invariant under a constant energy-shift of all levels. Moreover, as it follows from (4.11), $x^* > 2$, which makes both λ_2 and λ_3 negative definite. That being the case, the configuration that we obtained earlier, is indeed maximizing the energy variance.

For an N-level system, by adapting the optimal $N_0 = 1$ structure, Eq. (4.12) suggests that, the optimal QFI reads as (actually one still needs to optimize over the energy gap, we rather refer to the optimality of the degeneracies)

$$\mathcal{F}_T^N = \frac{(N-1)\mathrm{e}^{\epsilon/T}}{((N-1)+\mathrm{e}^{\epsilon/T})^2}\frac{\epsilon^2}{T^4}. \tag{4.17}$$

4.2.1 Thermometry with a quantum harmonic oscillator

Another interesting example is a harmonic oscillator. The Hamiltonian is given by $H_{ho} = \sum_{n=1}^{\infty} n\epsilon_n |n\rangle\langle n|$, where we have considered the ground state energy to be zero. Once at thermal equilibrium at temperature T, the average energy is given by

$$\langle H_{ho}\rangle = \frac{\mathrm{e}^{-\epsilon/T}}{1-\mathrm{e}^{-\epsilon/T}}\epsilon. \tag{4.18}$$

By taking the derivative of the average energy with respect to temperature one may find the energy variance to be

$$\mathrm{Var}(H_{ho}) = \frac{\mathrm{e}^{-\epsilon/T}}{(1-\mathrm{e}^{-\epsilon/T})^2}\epsilon^2, \tag{4.19}$$

leading to a QFI given by

$$\mathcal{F}_T^{ho} = \frac{\mathrm{e}^{-\epsilon/T}}{(1-\mathrm{e}^{-\epsilon/T})^2}\frac{\epsilon^2}{T^4}. \tag{4.20}$$

All the dashed lines in Figure 4.1 shows the temperature sensitivity of the harmonic oscillator. In the left panel, we see that a h.o. with a specific frequency always over performs a qubit with the same energy gap. As already mentioned in the previous section, for small temperatures the qubit and the h.o. are equivalent in a thermometric point of view. In fact one can see this through the their QFIs as well. Concretely, for $T/\epsilon \ll 1$, we have $\mathcal{F}_T^{ho} \approxeq \mathcal{F}_T^2 \approxeq \frac{\epsilon^2}{T^4}e^{-\epsilon/T}$.

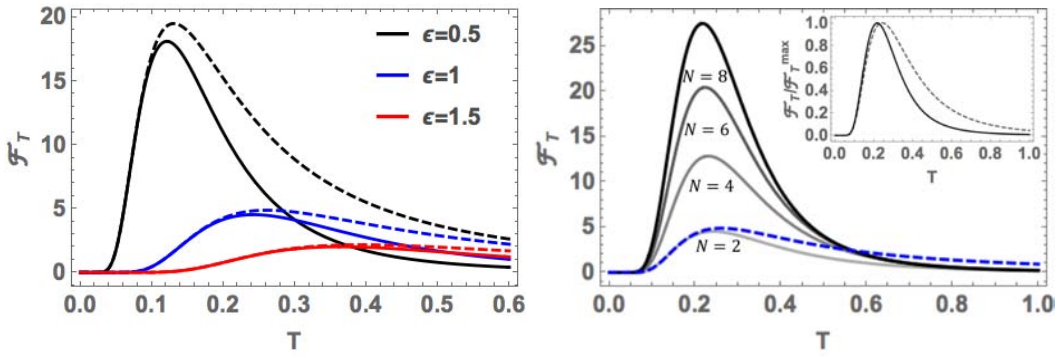

FIGURE 4.1: **Left:** (Solid) The temperature sensitivity, $\mathcal{F}_T$, of a two-level atom plotted versus temperature for different values of energy gap. At small temperatures, decreasing the energy gap improves appreciably the precision of thermometry. As temperature decreases, however, a small energy gap turns to a disadvantage. What is more, for a fixed energy gap, the sensitivity drops exponentially to zero as $T \to 0$, making it very challenging to estimate low temperatures. (Dashed) The same for a harmonic oscillator. Although it over performs the qubit predominantly, for small temperatures they have exactly the same operation quality. **Right:** (Solid) The temperature sensitivity of optimal N-level systems, with $N \in \{2,4,6,8\}$, and a fixed energy gap $\epsilon = 1$. (Dashed) The performance of a harmonic oscillator at the same frequency. (**Inset**) The normalized sensitivity of a qubit (Dashed) is compared to that of an $N = 8$ level system (Solid). It is evident that a two-level system performs close to its maximum value for a wider range of temperatures.

4.2.2 Analysis: Temperature sensitivity of multi-level systems and harmonic oscillators

Here we analyze the sensitivity of our optimal N-level system. To begin with, we look at a qubit's temperature sensitivity. Substituting $N \to 2$ into Eq. (4.17) yields

$$\mathcal{F}_T^2 = \frac{e^{\epsilon/T}}{(1+e^{\epsilon/T})^2}\frac{\epsilon^2}{T^4}. \tag{4.21}$$

The temperature sensitivity of a qubit as a function of temperature is depicted in the left panel of Figure 4.1, for different energy gaps ϵ between the ground and excited state. We also illustrate the performance of a harmonic oscillator with frequency $\Omega = \epsilon$ in the same picture. The first observation is that, for small temperatures, by decreasing the energy gap ϵ, the precision of the qubit improves. This can be easily explained by taking into account that at small temperatures thermal fluctuations are suppressed. Consequently, a system with a large energy gap remains in its ground sate, insensitive to temperature. In contrast, by diminishing the energy gap, it is more likely for the excited state to become occupied, making the qubit more sensitive to the temperature.

Second, at small temperatures, the qubit performs equivalent to a quantum harmonic oscillator with the same frequency. Again, this can be understood by noticing that at small temperatures and due to the small thermal fluctuations, only the first excited states of the h.o. is accessible.

Because of this, the h.o. might be thought of as an effective two-level system. Rigorously, for $T/\epsilon \ll 1$, Eqs. (4.21) and (4.20) suggest that $\mathcal{F}_T^{ho} \approxeq \mathcal{F}_T^2 \approxeq \frac{\epsilon^2}{T^4} e^{-\epsilon/T}$.

Beyond the scope of a qubit, in the right panel of Figure 4.1, we illustrate the thermal sensitivity of optimal multi level systems for different N. Evidently increasing N raises the temperature sensitivity albeit at the expense of reducing the temperature range within which it operates efficiently. One last remark regarding Figure 4.1: For very small temperatures, all of the sensitivities drop drastically. In fact it can be seen from Eq. (4.17) that for a finite N, even the best thermometer fails to estimate small temperatures with an exponential speed.

4.3 Metrology with bipartite systems: The role of interaction

So far we have identified the optimal individual thermometers. Here we put a step forward, and examine the role of *interaction* among constituents of a system in metrology. Our main motivation for investigating the effect of interaction is as follows: Although the individual probes have a unique Hamiltonian, whose structure might not be suitable for thermometry, the interaction among them can be manipulated in a favorable manner, so as to make them better thermometers.

In this section we address the simplest instance of a *bipartite* system, consisting of only two (interacting) parties. Systems with more parties, namely the *many-body* ones with *short range interactions*, are tackled exhaustively in the Chapter 5. The situation with long range interaction is beyond the scope of this thesis and it is subject for future works.

The bipartite system that we case study here is the coupled HOs of Section 3.6. For easiness we rewrite the Hamiltonian again

$$H = \omega a_1^\dagger a_1 + (\omega + \Delta) a_2^\dagger a_2 - J\left(a_1^\dagger a_2 + a_1 a_2^\dagger\right),$$

where we have ignore the self interaction term, and for simplicity we set $\omega = 1$ in what follows. Firstly we concentrate on thermometry, and then, for completeness, we address the estimation of the interaction strength J. We bear in mind that interaction between the two oscillators creates quantum correlations amongst them even if the full system is at thermal equilibrium. That being the case, the QFI is not additive. In other words the QFI of the bipartite system is not merely equal to the sum of the QFI of each individual HO. Nonetheless, thanks to such correlations, the thermometry precision improves noticeably, as we will see below in details.

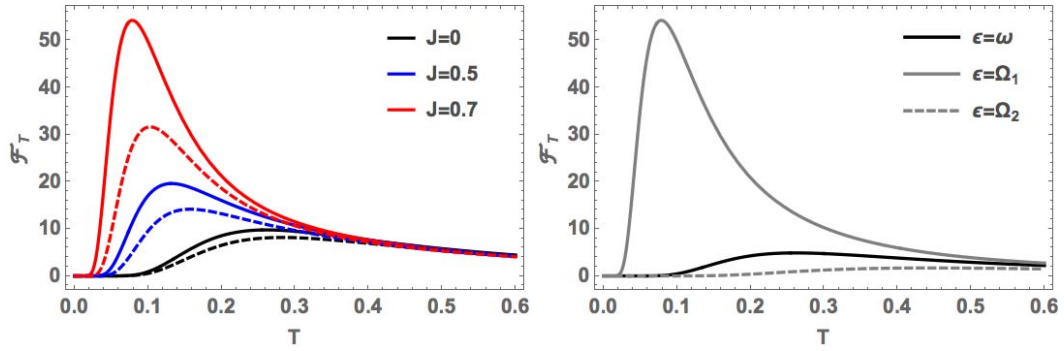

FIGURE 4.2: **Left:** $\mathcal{F}_T$ is plotted vs temperature. The solid lines belong to the resonance scenario with $\Delta = 0$, while the dashed curves represent a model with $\Delta = 0.2$. It is evident that, for having a better precision, one should keep the two oscillators at resonance. Moreover, we observe that by increasing the interaction strength between the two modes the precision boosts significantly. **Right:** We picture the performance of a HO with frequency $\epsilon = \omega$ (solid black), and compare it with the performance of two other HOs, one with the frequency $\epsilon = \Omega_1$ (solid gray), and the other one with $\epsilon = \Omega_2$ (dashed gray). In this panel we set $\Delta = 0$, and $\omega = 1$ in both panels.

4.3.1 Thermometry precision

Since the system is at thermal equilibrium the QFI associated with the temperature is given by the energy variance. Notice that if we diagonalized the Hamiltonian, as we did in Section 3.6, the variance of the full Hamiltonian in such a non-local basis can be written as

$$\begin{aligned}\mathrm{Var}(H) &= \mathrm{Var}(\Omega_1 b_1^\dagger b_1) + \mathrm{Var}(\Omega_2 b_2^\dagger b_2) = \Omega_2\,(N_1[N_1+1]) + \Omega_2\,(N_2[N_2+1]) \\ &= \frac{1}{4}\left\{\left(\frac{\Omega_1}{\sinh\beta\Omega_1}\right)^2 + \left(\frac{\Omega_2}{\sinh\beta\Omega_2}\right)^2\right\}. \end{aligned} \tag{4.22}$$

Here $\Omega_1 = 1 + \left(\Delta - \sqrt{\Delta^2 + (2J)^2}\right)/2$ and $\Omega_2 = 1 + \left(\Delta + \sqrt{\Delta^2 + (2J)^2}\right)/2$. Besides the new basis is connected to the old basis with a Bogoliobov transformation

$$\begin{pmatrix} b_1 \\ b_2 \end{pmatrix} = \begin{pmatrix} \cos\phi & -\sin\phi \\ \sin\phi & \cos\phi \end{pmatrix}\begin{pmatrix} a_1 \\ a_2 \end{pmatrix},$$

with $\phi = \frac{1}{2}\arctan 2J/\Delta$. The QFI is obtained from $\mathcal{F}_T = \mathrm{Var}(H)/T^4$.

In the left panel of Figure 4.2 we plot $\mathcal{F}_T$ versus temperature and for different values of detuning and coupling strength. We first notice that the detuning has a negative effect on the precision. Second, we observe that, increasing the interaction strength boosts the temperature estimation significantly. We deduce that, correlations enhance thermometry precision at low temperatures, a regime that is normally very difficult to estimate. This is easier to explain with the help of the normal mode frequencies. As a result of the interaction J, the normal frequency Ω_1 decreases, hence making it a much more effective thermometer. On the other hand, the other normal mode frequency, Ω_2, increases with J, hence, it effectively gets a worse thermometer. Nevertheless,

the improvement attained from decreasing Ω_1 is so big that it not only compensates for Ω_2, it makes the total system a much more sensitive thermometer as well. See the right panel of Figure 4.2.

4.3.1.1 Local schemes for thermometry

The enhancement in thermometry precision, due to the correlations, is accomplished entirely just by means of global measurements, i.e., those performed on the full Hamiltonian of the bipartite system. Such a global measurement might not be experimentally viable. For this reason, one has to think about local measurements as an inescapable alternative, and explore their sensitivity. Do local measurements also benefit from the enhanced precision offered by quantum correlations? Below, our results reveal that this is surely the case.

We examine the local number operator measurement in either of the wells. This, for the mode j, is given by $\left\langle a_j^\dagger a_j \right\rangle = \left\langle x_j^2 \right\rangle - \frac{1}{2}$. The error associated to this operator is quantified by the error-propagation formula [61],

$$\delta^2(a_j^\dagger a_j; T) = \frac{\left|\partial_T \left\langle a_j^\dagger a_j \right\rangle\right|^2}{\mathrm{Var}(a_j^\dagger a_j)} \equiv \mathcal{F}^{-1}(a_j^\dagger a_j; T). \tag{4.23}$$

Here we define $\mathcal{F}(\hat{O}; T)$ to be the sensitivity of the observable $\hat{O}$ to the parameter T. Without any difficulty, it can be checked out that, for any observable, this quantity is upper bounded by the QFI associated to T, i.e., $\mathcal{F}(\hat{O}; T) \leq \mathcal{F}$. This is obtained from Eq. (4.23), by changing the order of derivative and trace, using the definition of the SLD, followed by the Cauchy-Schwartz inequality.

The sensitivity of $\left\langle a_j^\dagger a_j \right\rangle$ can be evaluated analytically for both wells, but they are cumbersome and we don't present them here. Figure 4.3 pictures the precision of local measurements. Interestingly, they have an overall behavior similar to the optimal one. Namely, the precision boosts by increasing the tunneling rate. Additionally, for comparison, we also depict the QFI per number of oscillators (i.e., $\mathcal{F}_T/2$). It is seen that for vanishing detuning, $\mathcal{F}(a_j^\dagger a_j; T) \approx \mathcal{F}_T/2$. Yet, by increasing the detuning, not only both $\mathcal{F}(a_j^\dagger a_j; T)$ and $\mathcal{F}_T$ start to decrease, but also the local measurements happen to behave differently. Evidently, for the first mode i.e., the one with a smaller frequency we have $\mathcal{F}(a_1^\dagger a_1; T) > \mathcal{F}_T/2$, while for the second mode the direction of the inequality is reversed.

4.3.2 Estimation of the tunneling rate *J*

Putting thermometry aside for a moment, here we aim to explore the limitations on the estimation of the tunneling rate, assuming we know the temperature of the sample accurately. In order

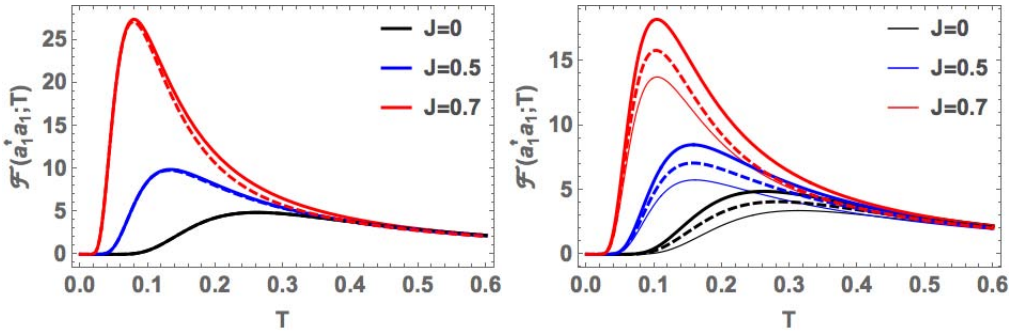

FIGURE 4.3: (Solid thick lines) The sensitivity of local energy measurement $a_1^\dagger a_1$, as given by $\mathcal{F}(a_1^\dagger a_1;T)$, plotted versus temperature. (Solid thin lines), the same for $a_2^\dagger a_2$. Just like the optimal non-local global energy, the correlation among the two oscillators enhances the precision of local measurements as well. For comparison we benchmark the performance of each local measurement with the optimal precision per oscillator $\mathcal{F}_T/2$ (Dashed lines). The **left** panel depicts the case $\Delta = 0$, so that the performance of the two modes are equal. The **right** panel corresponds to $\Delta = 0.2$. In such a case, the frequencies of the normal modes are different causing one oscillator to increase its performance while the other one to decrease it.

to quantify $\mathcal{F}_J$, the ultimate precision on J estimation, one needs to identify the associated SLD: Λ_J. Let us repeat what we mentioned earlier in Section 4.1.1, that classically, the best estimator for J is built up upon the conjugate observable to it, i.e., $A = \partial_J H = -(a_1^\dagger a_2 + a_1 a_2^\dagger)$. Specifically, the susceptibility $\partial_J \langle A \rangle$ is considered to quantify the *linear response* of the system to small perturbations in J. Despite that, in quantum mechanics the observable A as defined here, does not characterize the most informative observable to perturbations in J. This is rather determined by the SLD.

Unlike A, which we discover trivially by taking the derivative of H with respect to J, finding the SLD is not as effortless. The complexity is caused by the fact that $[\partial_J H, H] \neq 0$. Notice that in this model the non-commutativity arises from the detuning Δ, while for $\Delta = 0$ we have $[H_0, H_1] = 0$, and therefore the SLD is $\Lambda_J(\Delta = 0) = -\beta(A - \langle A \rangle)$ [73]. Typically, the non-commutativity does not allow for such an elegant and straightforward relation between the SLD and A. Having said that, the model under study turns out to be immensely exceptional, in some way bridging between non-commutative and commutative models.

Rigorously, by using the results of [74, 75] one can identify the SLD for non-zero detuning to be

$$\begin{aligned}\Lambda_J(\Delta) &= \beta \frac{\tanh(\frac{\Delta}{2T})}{\frac{\Delta}{2T}} \left(a_1^\dagger a_2 + a_1 a_2^\dagger - \left\langle a_1^\dagger a_2 + a_1 a_2^\dagger \right\rangle \right) \\ &= -\beta \frac{\tanh(\frac{\Delta}{2T})}{\frac{\Delta}{2T}} (A - \langle A \rangle). \end{aligned} \tag{4.24}$$

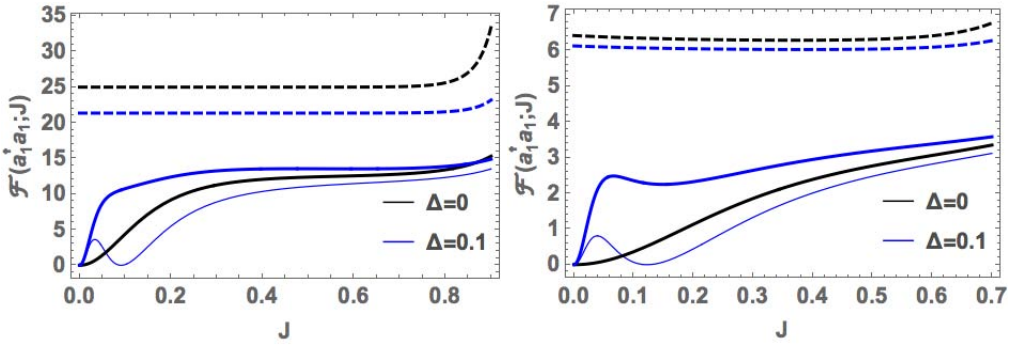

FIGURE 4.4: **Left:** Local estimation of the tunneling rate J. The (solid thin) lines represent precision of $a_1^\dagger a_1$ measurement, while the (solid thick) lines are obtained by measuring $a_2^\dagger a_2$. We benchmark such local measurements against the QFI per oscillator $\mathcal{F}(J)/2$ (dashed lines). For small values of J, local schemes absolutely fail to estimate it. The temperature is set to $T = 0.1$. **Right:** The same as left, but with $T = 0.2$. We observe that the precision of all measurements, being it local or global, is decreased.

The additional coefficient $\frac{\tanh(\frac{\Delta}{2T})}{\frac{\Delta}{2T}}$, which appears in Eq. (4.24), is arising from the non-commutativity. Actually, such contribution is the simplest that can arise from non-commutativity. We recall that, this is true only for a thermal state. Out of equilibrium, the effects of non-commutativity are larger and in such a case, the SLD is not even proportional to $-\beta(A - \langle A\rangle)$. In Section 5.8 we analyze a system with more involved non-commutativity, and in Section 6.2 we analyze the "out of equilibrium" scenario in detail.

Concentrating our efforts on the Λ_J, we obtain that for a thermal state, the QFI is given by

$$\mathcal{F}_J(\Delta) = \mathrm{Tr}\left(\Lambda_J^2(\Delta)\rho\right) = \left(\frac{\tanh(\frac{\Delta}{2T})}{\frac{\Delta}{2T}}\right)^2 \beta^2 \mathrm{Var}(A^2). \tag{4.25}$$

The term in parenthesis is a monotonically decreasing function of $\Delta/2T$, with a maximum value equal to one for $\Delta = 0$. Therefore, the detuning between the frequencies of the two oscillators leads to a less precise estimation of the tunneling rate (however, one should notice that $\mathrm{Var}(A)$ is also a function of Δ, but our results show that for a wide range of parameters it is a decreasing or a constant function with Δ. Nevertheless, the total contribution of Δ decreases the QFI). This can be explained, by bearing in mind that the detuning makes it harder for the two oscillators to exchange energy, as their frequencies are different. While at resonance, exchanging excitation is easier, so that the tunneling term is playing a stronger role, making it easier to be detected.

4.3.2.1 Local estimation of J

Since the interaction coupling is, by definition, a non-local operator, naturally we do not expect to detect it optimally with local measurements. Despite this fact, we would like to

quantify the precision of local measurements, e.g., when global measurements are experimentally unfeasible. Specifically, we study the sensitivity of local number operators $F(a_j^\dagger a_j; J) = \left|\partial_T \left\langle a_j^\dagger a_j \right\rangle\right|^2 / \mathrm{Var}(a_j^\dagger a_j)$. As depicted in Figure 4.4, the local estimations are not very efficient for the estimation of J, and the global measurement notably outperforms them.

4.4 Conclusions

We have analyzed the performance and ultimate limitations of quantum probes for precise thermometry, when the probe thermalizes with the system whose temperature is to be estimated. First, we have rigorously demonstrated that the best individual quantum thermometer is an *effective two-level atom* with a *maximally degenerate* excited state at a specific energy gap, which depends, non-trivially, on the sample temperature. We have shown that there exists a complementary trade-off between the maximum achievable estimation precision, which grows with N, and the specified temperature range in which the estimation is efficient, which shrinks with N. This ultimate precision on thermometry using individual quantum probes is totally model independent. Secondly, we have addressed the role of quantum correlations when using a multipartite system as a probe. By engineering interaction amongst its parties we aim at enhancing our thermometry precision. To this aim, we have analyzed the performance of a thermometer consisting on two coupled harmonic oscillators, and investigated the role of correlations between different partitions in boosting the resolution. We have demonstrated that, when we allow for interaction between the two parties, the QFI gets *super-extensive*. Moreover, since in this case the optimal thermometry protocol requires non-local measurements, we have examined also the precision of more feasible local protocols, and confirm their efficiency. We have shown that even local measurements inherit the boost in precision obtained from the interaction between the two partitions.

Finally, for the system of couple oscillators, in Section 4.3.2, we have also addressed the estimation of the strength of the coupling between the two parties, for a fixed temperature. We observe that increasing the temperature, as well as the detuning between the frequencies of the two oscillators, decreases the precision of estimating the tunneling rate. Besides, we see that local schemes are not efficient in estimation of the tunneling rate, specially when the coupling is small.

The simultaneous estimation of the interaction strength, J, and temperature, T, remains an open problem. In next chapter, we go beyond the bipartite scenario and focus on thermometry and metrology with many-body systems. Parameter estimation out of equilibrium will be also analyzed later in Chapter 6 and Chapter 7.

Chapter 5

Quantum metrolgy in many body systems

As already mention in the chapter Introduction, quantum metrology in strongly correlated systems makes use of criticality to enhance measurement precisions [46, 53]. Despite the fact that quantum phase transitions occur only at zero temperature and in the thermodynamical limit, even at finite temperature, critical effects can be exploit for quantum metrology. Indeed, for low dimensional systems, critical points signaling quantum phase transitions often broaden into *critical regions*. Those regions still separate different phases which keep track of their ground state correlations. Hence, the transition between those phases appear as smooth crossovers [54, 55], nonetheless carrying a footprint of the quantum phase transition occurring at zero temperature. Therefore, even at finite (but small) temperatures, quantum correlations are present and allow for better metrological bounds. For this reason, strongly correlated many-body systems could be used as highly precise magnetometers or thermometers, if tuned close to a critical point [47, 76–79].

In this chapter, we focus on Heisenberg spin models to investigate potential metrological advantages of strongly correlated systems. The quantum Ising model, or XY model in a transverse field, is an integrable model that, unlike the majority of quantum spin models, can be exactly solved by means of a Jordan-Wigner transformation mapping it onto a system of non-interacting fermions and giving access to the full energy spectrum [80]. In Section 5.1 we briefly review the basic properties of the XY spin chain both, at zero and finite temperatures. Our aim is twofold: exploiting strongly correlated systems for both thermometry and estimation of Hamiltonian parameters.

As we discussed extensively in Chapter 4, if the parameter to be estimated is temperature and the system is in thermal equilibrium, the Cramér-Rao bound yields a relation of the form $\delta T \Delta H \geq T^2$, being H the Hamiltonian governing system. The above relation indicates that the minimal

error in temperature estimation of a thermal sample is realized by a projective measurement on its energy eigenbasis. In general, such type of measurements in ultracold lattice gases is not accessible. Instead, information about quantum phases and temperature is usually obtained from momentum and density distributions or from density-density (or spin-spin) correlations. These quantities can be extracted by using destructive methods such as time of flight imaging (the latter via the study of noise correlations [56]) or in-situ imaging, for instance using single site addressability [57, 58]. Despite their huge relevance, these methods might suffer limitations in certain occasions, due to their destructive character. For instance, in order to study spin-spin correlations in currently available setups for single site imaging, one needs to remove all particles from one of the two spin components. In this sense, quantum non demolition (QND) methods can provide clear advantages [59].

Section 5.2 reviews the basic concepts describing the QND Faraday spectroscopy. In Section 5.3, we focus on the thermometry aspects in the XY chain. To this aim, we derive first a closed form of the quantum Fisher information as a function of the temperature for the whole phase diagram. This, in turn, provides the minimal error on the temperature estimation when performing an optimal measurement. Section 5.4 is devoted to the analysis of quantum correlations at finite temperatures with Faraday spectroscopy method. We evaluate, for the whole phase diagram of the model, the signal-to-noise ratio, $T/\delta T$, obtained with a Faraday interface. Remarkably, our results support the suitability of collective quantum correlations as optimal observable for quantum thermometry of strongly correlated systems.

An interesting scenario for metrology arises when the Hamiltonian of interest has a closed algebra, i.e., when the Hamiltonian is of the form $H = \xi_1 H_1 + \xi_2 H_2$ with $[H_1, H_2] = 0$. Whence, the commuting algebra helps to provide the optimal observables that saturate the quantum Cramér-Rao bound. In Section 5.6 we develop the formalism of quantum metrology for closed algebras and in Sec. 5.6 we use as a case study the XX Heisenberg spin model.

In Section 5.7 we propose an iterative feedforward scheme, that exploits criticality to achieve sub-shot-noise metrology at finite temperature. In Section 5.8, we focus on precision magnetometry for Hamiltonians whose algebra do not obey $[H_1, H_2] = 0$, as is the case for the XY model. Since we do not know the optimal measurements analytically, we propose suboptimal metrology scenarios to estimate the unknown parameter. These suboptimal measurements, having a close to optimal yet complicated measurement, are again realized by Faraday spectroscopy. In Section 5.9, we summarize and conclude.

Finally, in the Section 5.8 we develop metrological strategies to tackle precision magnetometry for Hamiltonians whose algebra do not obey $[H_1, H_2] = 0$, as is the case for the XY model. Since for such cases we do not know the optimal measurements analytically, we propose suboptimal

metrology scenarios to estimate the unknown parameter. These suboptimal measurements, having a close performance to the optimal (yet complicated) measurement, are again realized by Faraday spectroscopy. In Section 5.9, we summarize and conclude.

5.1 The model: *XY* spin chain in a transverse field

The *XY* spin-1/2 chain in a transverse field (including the Ising and isotropic *XX* models as particular cases) is an exactly solvable model, and as such, it can be used as a prototype to understand the interplay between quantum and thermal fluctuations. The Hamiltonian governing the system can be written as:

$$H = -J\sum_{l=1}^{N}\left[\frac{1+\gamma}{2}\sigma_l^x\sigma_{l+1}^x + \frac{1-\gamma}{2}\sigma_l^y\sigma_{l+1}^y\right] - h\sum_{l=1}^{N}\sigma_l^z \tag{5.1}$$

where σ_l^α are the usual Pauli matrices at site l, $-1 \leq \gamma \leq 1$ is the parameter that sets the *XY* anisotropy ($\gamma = \pm 1$ and $\gamma = 0$ for the Ising and *XX* models respectively), h is the transverse magnetic field and N is the number of sites of the chain. The coupling constant J can be positive (ferromagnet) or negative (antiferromagnet). Throughout this paper, we will consider only the ferromagnetic case $J > 0$. However, equivalent results can be straightforwardly derived for the antiferromagnetic case $J < 0$. For simplicity, we consider here periodic boundary conditions with an even number of sites, but the results can be easily extended to an odd number of sites or an open chain. However, for large enough chains, one expects such variations not to influence the results [80].

The Hamiltonian (5.1) can be easily diagonalized by mapping it onto a non-interacting fermionic model that provides the full energy spectrum. As it is well known [80, 81] the non-interacting fermionic representation of the *XY* model is obtained by means of the Jordan-Wigner transformation, followed by a unitary Bogoliubov transformation in the quasi-momentum space, yielding:

$$H = \sum_k \epsilon_k \gamma_k^\dagger \gamma_k, \tag{5.2}$$

and the dispersion relation (up to a constant)

$$\epsilon_k = 2|J|\sqrt{(\cos k - h)^2 + (\gamma \sin k)^2}, \tag{5.3}$$

being k the quasi-momentum, $k = \frac{\pi}{N}(2j+1)$, and $j = -N/2, \ldots, N/2-1$. The sign of this energy is arbitrary. Choosing a positive value corresponds to the particle-hole picture for the fermionic quasiparticles, which are defined for $k \in (0,\pi)$ by the following Bogoliubov transformation:

$$\gamma_{\pm k}^\dagger = \cos\theta_k c_{\pm k}^\dagger \pm i \sin\theta_k c_{\mp k}. \tag{5.4}$$

Here, $\cos(2\theta_k) = \gamma \sin k/(\cos k - h)$ for $\theta_k \in (0, \pi/2)$, and $c_k^\dagger$ are the Fourier transform of the on-site fermionic operators that directly relate to the spin operators via the Jordan-Wigner transformation

$$c_l^\dagger = \sigma_l^+ \prod_{l'<l} \sigma_{l'}^z \,, \quad c_l = \sigma_l^- \prod_{l'<l} \sigma_{l'}^z \,. \tag{5.5}$$

The ground state of the system corresponds to the vacuum of the Bogoliubov quasiparticles, and excitations are obtained with creation operators acting on the vacuum. The energy gap between the ground state and the continuum of excited states is thus given by $\Delta E = \min_k(\epsilon_k)$.

Note that the Hamiltonian is symmetric under the exchange $h \leftrightarrow -h$ (by $k \leftrightarrow \pi/2 - k$) and under $\gamma \leftrightarrow -\gamma$ (by $\sigma_x \leftrightarrow \sigma_y$). A sketch of the phase diagram at zero temperature, together with the energy gap ΔE and the energy relation dispersion are displayed in Figure 5.1. The system is always gapped i.e. $\Delta E > 0$, except for the quantum critical lines occurring at $h/J = \pm 1$ (Ising transitions), which separate the paramagnetic phases (PM) from the ferromagnetic (FM) ones (or antiferromagnetic if $J > 0$) and for $\gamma = 0$ and $|h/J| \leq 1$, corresponding to the critical phase in the XX model (anisotropic transition). Moreover, Heisenberg systems with general anisotropies exhibit, for particular values of the couplings, a ground state which is doubly degenerated and which is factorizable as a product of on-site localized wave-functions [82, 83]. In the XY model, for each value of γ, this product ground state corresponds to an external transverse field $h/J = \pm\sqrt{1-\gamma^2}$. The factorized ground state is depicted by a dashed line in phase diagram of Figure 5.1(a).

In the thermodynamic limit (large N), the system in thermal equilibrium at a given temperature T can be described by the density matrix in the macrocanonical ensemble (we set $k_B = 1$):

$$\rho(\gamma, h/J, T) = \frac{e^{-H(\gamma,h/J)/T}}{\mathcal{Z}} = \bigotimes_k \rho^k(\gamma, h/J, T), \tag{5.6}$$

where $\mathcal{Z}$ denotes the partition function of the system. For compactness of notation we write from now on $\rho^k(\gamma, h/J, T)$ simply as $\rho^k(T)$. Since the Hamiltonian (5.2) is separable, the density matrix can be directly written as a tensor product of the density matrices associated to each quasiparticle mode k. These quasiparticles obey fermionic commutation relations, and thus

$$\rho^k(T) = \frac{|0\rangle_k \langle 0| + \mathrm{e}^{-\epsilon_k/T} |1\rangle_k \langle 1|}{1 + \mathrm{e}^{-\epsilon_k/T}}, \tag{5.7}$$

where $|0\rangle_k$ ($|1\rangle_k$) denotes an empty (occupied) quasiparticle state k. We take the above expression as the starting point to study correlations at finite temperatures.

Finally, let us remark that the XY model can be realistically implemented in experiments. In particular, the isotropic XX model directly maps onto a system of hard-core bosons and has been

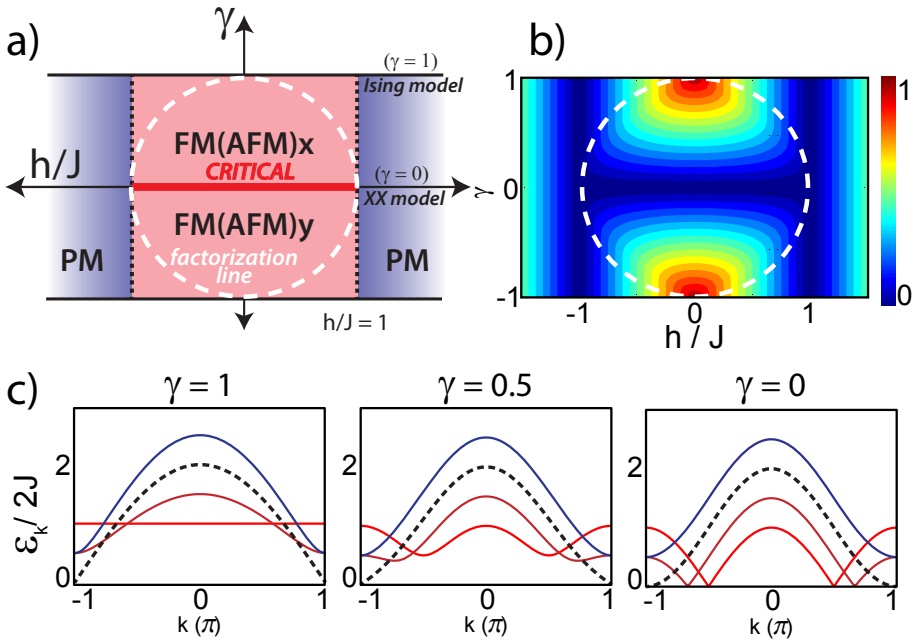

FIGURE 5.1: (Color online) a) Sketch of the phase diagram at zero temperature for the XY model. The $\gamma = 0$ and $\gamma = 1$ lines correspond to the isotropic XX and Ising models respectively. FM(AFM) denote phases with quasi long-range ferro(antiferro)-magnetic order along the x- and y-axis for $\gamma > 0$ and $\gamma < 0$, respectively. PM is the paramagnetic phase. There are second order phase transitions at $h/J = \pm 1$ (Ising transition) and at $\gamma = 0$ (anisotropy transition). The dashed line denotes the factorization ground state for this model. b) Energy gap ΔE to the continuum of excited states (in units of $2J$). The energy spectrum is always gapped except at the critical point $h/J = \pm 1$ and at the critical phase $\gamma = 0$, $|h/J| < 1$. c) Quasiparticle energy dispersion relation for $\gamma = 1$, $\gamma = 0.5$ and $\gamma = 0$, for different values of h/J (dark red: FM phase; red: $h = 0$; blue: PM phase; dashed black: critical point).

experimentally realized with cold atoms in optical lattices [49], while the Ising model has been also engineered with a similar system [84]. Moreover, other models that can be implemented with cold atoms, as the bond-charge Hubbard model, directly map onto the XY model [85].

5.2 Quantum Faraday Spectroscopy

Here, we briefly review a quantum non-demolition scheme for measuring quantum correlations in ultracold atomic lattices. The method is based on a light-matter interface [86] employing the quantum Faraday effect. It was adapted to determine quantum phases of strongly correlated systems in optical lattice systems in [59, 87]. The scheme is extremely versatile and can detect superfluidity, superlattice ordering and itinerant magnetism for fermionic and bosonic lattice gases [88, 89]. It also allows to reconstruct the phase diagram of non-trivial spin chain models [90, 91] and to engineer quantum correlations by suitable post-selection [92]. In the following

we review the basics of the scheme but we point the reader to the previous references for more details.

The basics of a QND Faraday spectroscopy assumes a strongly linearly polarized light beam along e.g. the x-axis propagating on the z-axis and interacting off resonantly with the internal spin degree of freedom of an atomic sample. Due to the atom-photon interaction, the light polarization is rotated by an amount that depends on the magnetic state of the sample. The light can be described by time-integrated canonical operators $X = S_2/\sqrt{N_{ph}}$ and $P = S_3/\sqrt{N_{ph}}$, where $S_{2(3)}$ denote the Stokes operators in the perpendicular directions of the incoming beam while N_{ph} is the total number of photons of the beam. If the atomic sample is confined in an optical lattice, the light can be modulated in a standing wave configuration as schematically depicted in Figure 5.2. After the Faraday interaction has taken place, the integrated equations of motion result into [86]

$$X_{\text{out}} = X_{\text{in}} - \kappa J_z, \tag{5.8}$$

where X_{in} and X_{out} represent, in the input-output formalism, the light quadratures before and after the Faraday interaction. The observable J_z corresponds to the modulated collective angular momentum along z-direction and is defined as:

$$J_z = \sum_l \cos^2\left(k_p l d\right) \sigma_l^z. \tag{5.9}$$

The above sum extends on all lattice sites l, k_p is the wave vector of the probing beam and d is the inter-site distance. Finally, the light-matter coupling constant $\kappa = \sqrt{d_o \eta}$ depends on the optical depth of the atomic sample d_o as well as on the spontaneous emission probability induced by the probe. Typical values of κ are in the range 1-10.

As the light and atom states are initially uncorrelated, it follows that

$$\langle X_{\text{out}} \rangle = -\kappa \langle J_z \rangle, \tag{5.10}$$

$$\text{Var} X_{\text{out}} = \frac{1}{2} + \kappa^2 \text{Var} J_z, \tag{5.11}$$

where we assume the incoming light beam to be in a coherent state with zero mean and variance $1/2$. For the ferromagnetic case ($J > 0$), the output signal is maximum when the wave vector of the probe beam is set to $k_p = \pi/d$ i.e. the light is not modulated. For the antiferromagnetic case ($J < 0$), since the total magnetization of the sample is zero, it is necessary to modulate the incoming beam with half of the frequency $k_p = \pi/2d$.

After the outcoming light quadrature X_{out} has been homodyne measured, the atomic sample is projected onto a subspace of fixed J_z. Owing to the fact that the off resonant interaction with the light does not destroy the sample, we further assume that after the measurement thermalization will take place on such given subspace. Since typical thermalization times for ultracold lattice

gases are on the order of *ms* and the many-body sample is stable on the time scale of seconds, the Faraday interface taking place in the μs regime can be considered as instantaneous. Thus, the Faraday interface could be repeated several times on the same sample preserving its QND character. Finally, we remark that in order to measure the other collective operators J_x and J_y using the same experimental setup, one should apply an appropriate spin rotation to the atomic sample so to map $\sigma^x \to \sigma^z$ or $\sigma^y \to \sigma^z$[93].

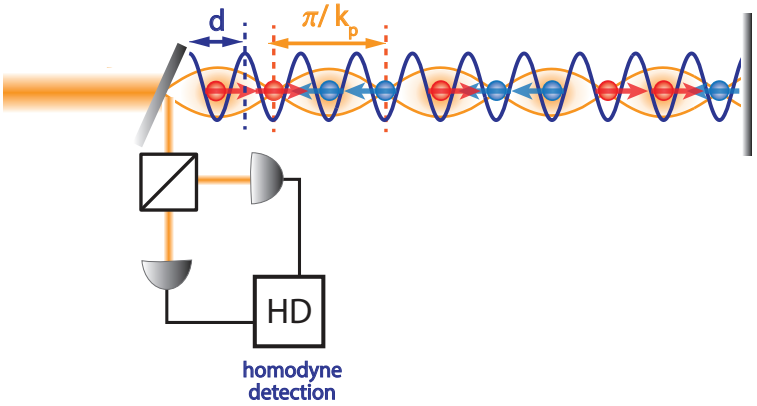

FIGURE 5.2: (Color online). Schematic diagram of the proposed experimental set-up to measure the collective angular momentum imprinted on the light quadratures. The ultracold atomic sample is trapped by an optical lattice potential with wavelength d (blue). An additional strong laser beam (yellow) initially polarized in the x direction is impinging on a beamsplitter. The transmitted part of this probe is propagating through the sample and reflected off a mirror, forming a standing wave with wavevector k_p. After the second pass, the laser beam is outcoupled to a homodyne detector, where the light quadrature is measured and recorded.

5.3 Optimal strategy: lowest bound on the temperature error

Calculation of the QFI becomes straightforward for the XY model due to the simple structure of a thermal state which corresponds to a product state in the fermionic representation (5.6). Therefore we are able to use the additivity of the QFI, which we proved earlier Eq. (2.21) of Section 2.3.1. In particular this allows us to express $\mathcal{F}(T,\rho^T)$ as the sum of the QFI of each individual k state contributing to product state, i.e.

$$\mathcal{F}(T,\rho^T) = \sum_k \mathcal{F}(T,\rho^k(T)) = \frac{(\Delta H)^2}{T^4} = \sum_k \left(\frac{\epsilon_k}{T^2}\right)^2 n_k(1-n_k) \tag{5.12}$$

being $n_k = (1+e^{\epsilon_k/T})^{-1}$ the Fermi-Dirac distribution of the quasiparticles.

Using the above expressions, we focus on the upper bound on the signal-to-noise-ratio, which is given by $(T/\delta T_{\min})^2 = T^2\mathcal{F}(T,\rho^T)$, where we use the index *min* to highlight that the error

obtained from the CRB is minimum over all possible measurements. In the top panels of Figure 5.3, we display this upper bound, normalized by the total number of sites N, for the whole phase diagram at different temperatures. For finite T, this quantity scales linearly with N.

For very small temperatures, e.g. $T/J = 0.05$, the QFI becomes noticeable only close to the critical lines. This is not surprising, since for a gapless system, excitations to the lowest part of the energy spectrum will be created no matter how small the temperature is. Thus, as the uncertainty in energy of the state grows, so does the QFI and accordingly the state becomes very sensitive to thermal fluctuations. In contrast, for a gapped phase, if $T \ll \Delta E_{\text{min}}$, with ΔE_{min} being the minimum energy gap with the ground state, the probability of creating excitations remains low. In such cases, the energy remains well defined, yielding a vanishing value of QFI and correspondingly a large error in temperature estimation. See Section 5.7.1 for details and more quantitative analysis of low temperature behaviour of the system.

On the other hand, for large enough values of the temperature, i.e. $T \geq \Delta E_{\text{min}}$, different modes become excited, and other regions of the phase diagram become more sensitive and optimal for thermometry. In fact, for a given value of T, the accurate estimation of the sample's temperature depend on the energy spectrum but also on the density of states (DOS) as they play a crucial role in the QFI expression (5.12). This can be clearly seen in Figure 5.3, where the value of $(T/\delta T_{\text{min}})^2$ is also plotted for $T/J = 0.2$ and $T/J = 0.8$. The more sensitive regions of the phase diagram are now clearly different than the "zero temperature transition points", i.e. $h = \pm 1$ and $\gamma = 0$ for $|h/J| < 1$.

Finally, in the limit of very large temperatures and as the state tends to be maximally disordered, it is to be expected that the QFI or thermal sensitivity will decay again to zero as shown in Figure 5.5 (solid lines) for some particular cases. We shall return to this point later, in Section 5.4.

5.4 Thermometry in the *XY* model using a Faraday interface

The quantum polarization spectroscopy technique described in the previous section grants access, a priori, to any order of the statistical moments of the collective atomic angular momentum. For certain quantum phases of the model, as for instance the ferromagnetic phase, the mean value of J_z will be enough to infer the temperature of the sample. However, the mean value might vanish for certain observables in an unbroken symmetry phase (e.g. the longitudinal magnetization, J_x, in the Ising model for a thermal state). Instead, this ordering is clearly revealed when looking at the quantum fluctuations or variance of the observable. Here, for reasons that will become clearer later, we focus our study to the mean value of J_z and the variance of J_x. The latter can be written as:

$$\text{Var}J_x = \sum_{l,m} \langle \sigma_l^x \sigma_m^x \rangle - \langle \sigma_l^x \rangle \langle \sigma_m^x, \rangle \tag{5.13}$$

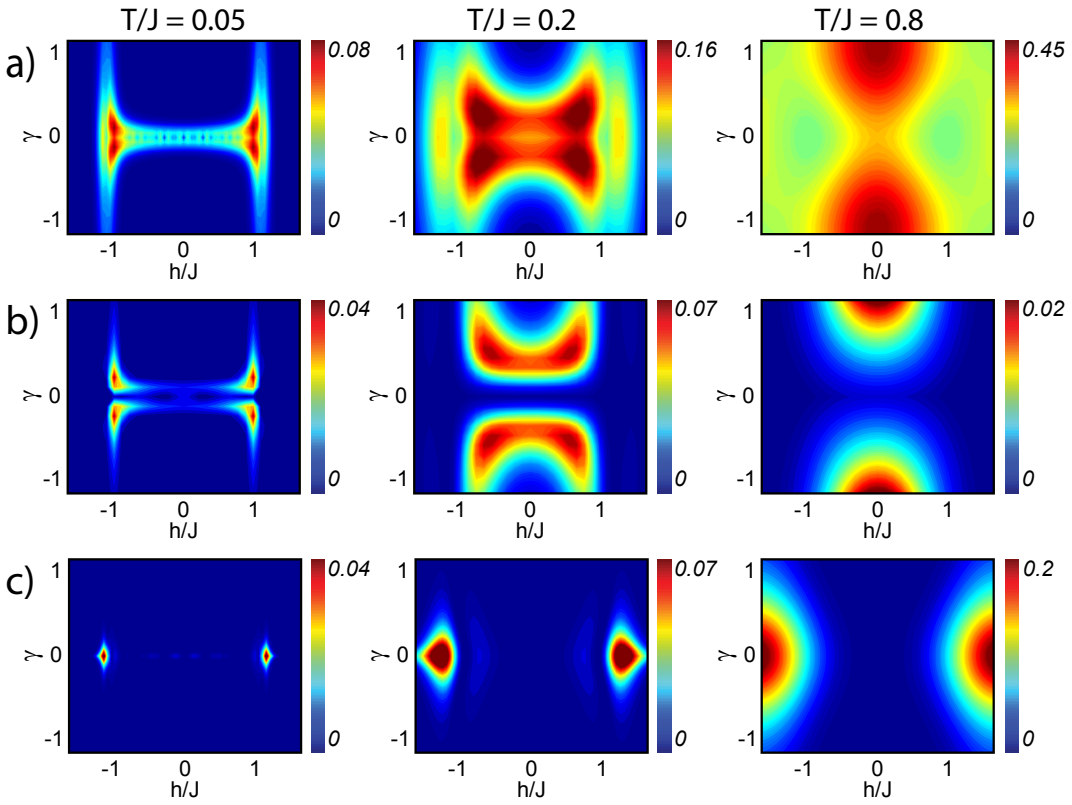

FIGURE 5.3: (Color online). a) Optimal signal-to-noise ratio, $(T/\delta T)^2_{\rm min}$, where δT denotes the temperature uncertainty given by the Cramér-Rao bound when assuming the optimal measurement strategy, plotted as a function of the Hamiltonian parameters and for different values of T/J. At very low T, the thermal sensitivity is larger close to the critical points, whereas when increasing T, the maximum gradually shifts to the Ising ($h = 0$) line. (b) and (c) Signal-to-noise ratio, $(T/\delta T)^2_{\rm F}$, estimated for the Faraday interface for the two mean values of the observables $(J_x - \langle J_x\rangle)^2$ and J_z respectively. The VarJ_x is more sensitive in the FM phase, whereas $\langle J_z\rangle$ works better in the PM phase.

and corresponds to the sum over any two-site correlation function or, equivalently, to the magnetic structure factor at zero quasi-momentum.

We start by analyzing the strength of the output signal when the observable to be measured is VarJ_x (VarJ_y) for $\gamma > 0$ ($\gamma < 0$). We recall that for a coherent input beam, the shot noise is Var$X_{\rm in} = 1/2$. Note that the results for J_y and $\gamma > 0$ are equivalent to those for J_x and $\gamma < 0$. As expected, the variance of the angular momentum associated to the order parameter always exceeds the variance of the angular momentum along the other two directions. Moreover, this is maximal for the Ising model ($\gamma = 1$) and continuously decreases when approaching the XX model ($\gamma = 0$).

A comparison between these two limiting cases ($\gamma = 1$ and $\gamma = 0$) is depicted in Figure 5.4, where in the top panels, we display the output signal VarJ_x/N (assuming $\kappa \approx 1$) divided by the input shot-noise (Var$X_{\rm in}$) as a function of T/J for different values of h/J and two different system sizes $N = 100$ and $N = 200$. At zero temperature, and in the gapped FM phase ($|h/J| < 1$ and

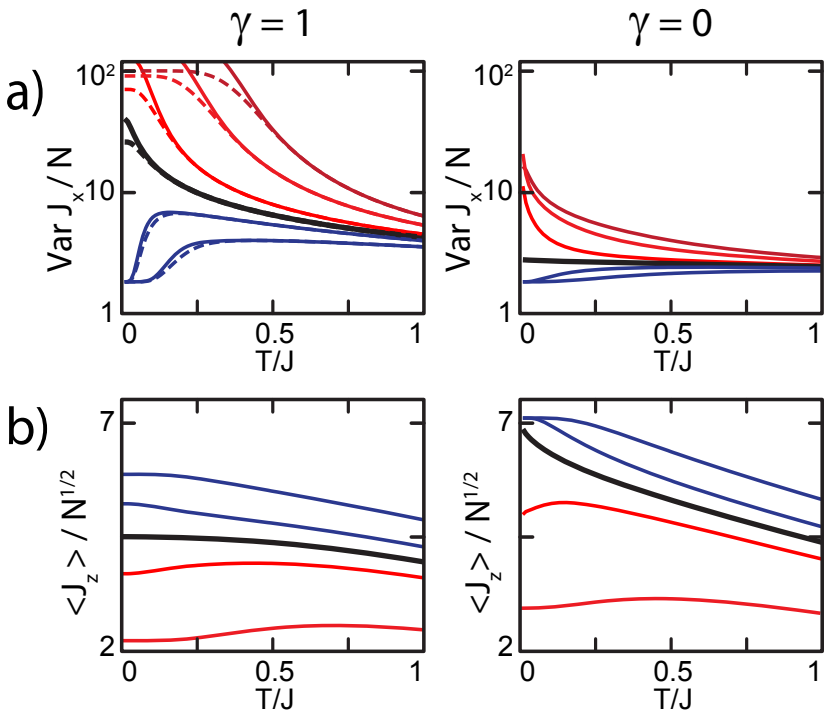

FIGURE 5.4: (Color online). Output signal (assuming $\kappa \approx 1$) as a function of T/J for the two limiting cases $\gamma = 1$ (Ising model) and $\gamma = 0$ (isotropic XX model) for different observables. In red(blue) FM (PM) phase for different values of h/J (a) $\mathrm{Var}J_x/N$, normalized, for comparison, to the incoming beam shot-noise ($\mathrm{Var}X_{\mathrm{in}} = 1/2$). At finite T, $\mathrm{Var}J_x$ scales linearly with N, and the signal is always larger than $\mathrm{Var}X_{\mathrm{in}}$. At low T/J, the signal decreases (increases) with T in the FM (PM) phase. (b) $\langle J_z\rangle/\sqrt{N}$ properly normalized, J_z scales linearly with N, and it shows the opposite behavior with respect to (a). At very low T/J it decreases (increases) in the PM (FM) phase with T. Solid (dashed) lines correspond to $N = 200$ ($N = 100$).

$\gamma \neq 0$), the signal scales as $\kappa^2 N$, whereas in the PM phase ($|h/J| > 1$), it scales as κ^2. Strictly speaking, and since we are dealing with a 1D system, there exists no phase transition at finite temperature. This is reflected in the fact that, at any finite value of T, the signal in the gapped FM phase does not scale anymore as $\kappa^2 N$ but rather as κ^2 and the signal for the two system sizes overlap. Therefore, the plateau depicted in the top panel of in Figure 5.4 is only a finite size effect and it disappears as the system size increases. In this region, the signal is constant with T and thus, it will not be useful for thermometry. The results for any $\gamma \neq 0$ are qualitatively similar to those for the Ising model. Moreover, for any value of the parameters γ and h it is always satisfied that $\mathrm{Var}J_x \geq 1$. If the optical depth d_o is tuned so that $\kappa \geq 1$, the signal of the output beam will be greater than the input beam shot-noise. This is, however, not the case for the other two observables $\mathrm{Var}J_y$ and $\mathrm{Var}J_z$, which go well below the shot noise limit when approaching the XX model.

The output signal, when measuring the mean value of the J_z observable ($\langle J_z\rangle/\sqrt{N}$), is depicted in the bottom panels of Figure 5.4, assuming again $\kappa \approx 1$. In contrast to the former observable, this is maximum (in absolute value) in the PM phase and increases when approaching the $\gamma = 0$ limit.

In order to asses the optimality of measuring collective quantum correlations for thermometry, we focus in the signal-to-noise ratio $(T/\Delta T)^2_{\rm F}$ achievable by using the Faraday interface and compare it with the minimal possible error in temperature estimation provided by the Cramér-Rao bound $(T/\Delta T)^2_{\rm CRB}$.

To this aim, the error performed in measuring temperature using the observable A can be defined as [94]

$$\Delta T \approx \left(\frac{\partial\langle A\rangle}{\partial T}\right)^{-1} \Delta A, \tag{5.14}$$

where ΔA is the standard deviation of the observable or $({\rm Var}A)^{1/2}$. Therefore,

$$\left(\frac{T}{\Delta T}\right)^2_{\rm F} \approx \left(\frac{\partial\langle A\rangle}{\partial T}\right)^2 \frac{1}{{\rm Var}A}, \tag{5.15}$$

For the analyzed model, the variance of the two observables of interest can be evaluated by making extensive use of Wick's theorem. For a better comparison with the optimal signal-to-noise ratio $(T/\Delta T)^2_{\rm CRB}$, in Figure 5.3 we display the signal-to-noise ratio $(T/\Delta T)^2_{\rm F}$ corresponding to the observable $A = (J_x - \langle J_x\rangle)^2$ (middle panels) and $A' = J_z$ (bottom panels) for the whole phase diagram and different values of T/J. Strikingly enough, the behavior of the observable corresponding to the variance of the order parameter is optimal in the FM regions, and follows the same qualitative behavior as $(T/\Delta T)^2_{\rm CRB}$, shifting its maximum value with temperature from the multicritical points ($\gamma = 0$, $|h| = 1$) to the Ising model in absence of transverse field ($\gamma = \pm 1$, $h = 0$). However, it decays faster with T/J than $(\Delta T/T)^2_{\rm CRB}$. In contrast, the observable J_z is optimal in the PM phase and for the $\gamma = 0$ model, and it decays slower with T/J. One could further approach to the value of the former derivative with temperature, which shows a similar behavior with T, by increasing the number of measurements and reduce the variance of the observable.

Our main results are summarized in Figure 5.5, where we fix the value h/J to do a quantitative comparison between the signal-to-noise ratio obtained with the Faraday spectroscopy, $(T/\Delta T)^2_{\rm F}$, and the optimal one provided by the quantum Cramér-Rao bound, $(T/\Delta T)^2_{\rm CRB}$, as a function of T/J. The comparison is performed for $\gamma = 1, 0.3$ and 0, both in the FM phase ($h = 0$) and PM phase ($h = 1.5$). The results clearly show for $T/J \leq 0.35$ the Faraday spectroscopy reading out the observable ${\rm Var}J_x$ provides an almost optimal measurement for thermometry precision in the FM phase in the Ising model and its optimality decreases when approaching the critical XX model ($\gamma = 0$). Instead, in the PM phases, $\langle J_z\rangle$ approaches the ideal bound in the XX model for a temperature range $0 < T/J \leq 0.45$. It is worth to recall that this is indeed the range of temperatures of interest for present experiments with ultracold atomic gases simulating strongly correlated systems [95]

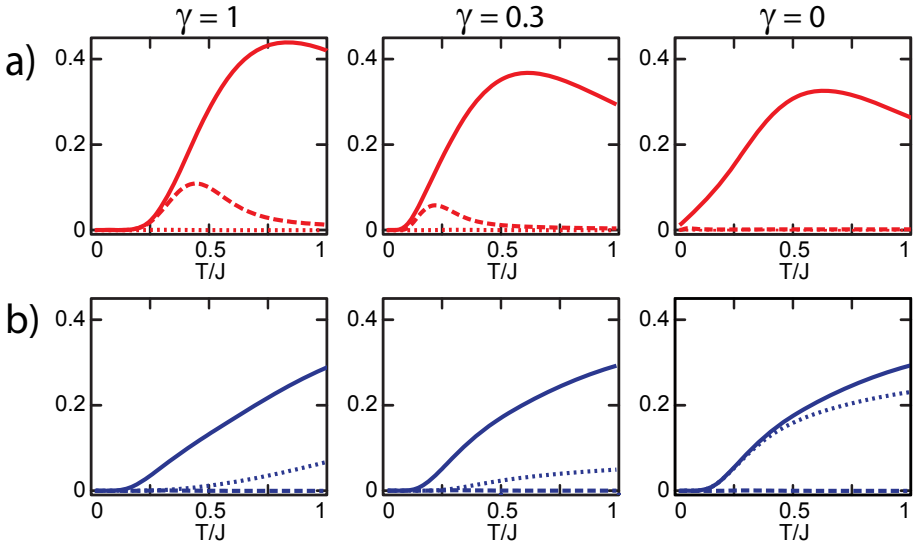

FIGURE 5.5: (Color online). Comparison between the optimal signal-to-noise ratio (solid line), estimated by the Cramér-Rao bound, $(T/\Delta T)^2_{CRB}$, and the signal-to-noise ratio obtained with the Faraday interface using as observables $\mathrm{Var}J_x$ (dashed line) and $\langle J_z\rangle$ (dotted line), for different values of γ and as a function of T/J. (a) $h/J = 0$ (FM phase) and (b) $h/J = 1.5$ (PM phase). $(T/\Delta T)^2_{CRB}$ increases with T/J until it reaches a maximum, decreasing again at very large T/J. $\mathrm{Var}J_x$ is optimal in the FM phase and $\gamma = 1$, whereas $\langle J_z\rangle$ is optimal in the PM phase and $\gamma = 0$. At very large T/J the signal of the Faraday interface becomes less optimal.

5.5 Estimation of the Hamiltonian couplings

The most general form of a many body Hamiltonian is of the type $H = \xi_1 H_1 + \xi_2 H_2$, and the physics of the system is governed by the competition between both terms. Here we firstly focus on the estimation of Hamiltonians that fulfill $[H_1, H_2] = 0$. For such Hamiltonians parameter estimation is directly linked to the (static) *susceptibilities* of the conjugate Hamiltonian term. With the help of Eq. (4.3) of Section 4.1.1, we know that for instance if ξ_1 is the parameter to be estimated, the susceptibility of H_1 is $\chi_{H_1,\xi_1} = \partial_{\xi_1}\langle H_1\rangle$.

Moreover, the corresponding optimal estimator for either of the Hamiltonian parameters ξ_i ($i \in \{1,2\}$) and its corresponding sensitivity, may be easily found from the definitions of the QFI and the SLD, i.e., Eqs. (2.7) and (2.8). One only needs to replace ρ_p with the thermal state $\rho^T \equiv \mathcal{Z}^{-1}\exp(-\beta H)$, and use $\exp(-\beta H) = \exp(-\beta\xi_1 H_1)\exp(-\beta\xi_2 H_2)$. This yields

$$\Lambda_{\xi_i}\rho^T + \rho^T\Lambda_{\xi_i} = -\beta(H_i - \langle H_i\rangle)\rho^T - \beta\rho^T(H_i - \langle H_i\rangle), \tag{5.16}$$

implying that H_i is itself an optimal estimator for ξ_i. In addition, the QFI is straightforwardly evaluated to be

$$\mathcal{F}(\xi_i) = \beta^2\Delta H_i^2. \tag{5.17}$$

Making use of Eqs. (2.6) and (5.17) one may write the uncertainty-type relation $\Delta H_i{}^2 \delta\xi_i^2 \geq \beta^{-2}$. Further, by bearing in mind that $\langle H_i \rangle = -\beta^{-1}\partial_{\xi_i} \log Z$, the maximum ξ_i-sensitivity can be alternatively expressed as

$$\mathcal{F}(\xi_i) = \beta \left| \frac{\partial \langle H_i \rangle}{\partial \xi_i} \right| = \frac{\partial^2 \log Z}{\partial \xi_i^2} = -\beta \frac{\partial^2 A}{\partial \xi_i^2}, \tag{5.18}$$

where $A \equiv -k_B T \log Z$ stands for the Helmholtz free energy. Evidently, the ultimate precision in the estimation of Hamiltonian parameters from thermal states is nothing but a generalized susceptibility. For instance, if the parameter to be estimated is temperature, the specific heat is the relevant figure of merit and, as we shall see below, what limits the sensitivity of a magnetometer is its magnetic susceptibility [46, 53, 60, 70, 96–99].

The connection between susceptibility and QFI has been very recently addressed in reference [60], where it has been shown that $\chi_i = -\beta^2 \partial^2 A / \partial \xi_i^2$ may be cast as $\chi_i = \chi_i^{(\mathrm{el})} + \chi_i^{(vV)}$, where $\chi_i^{(\mathrm{el})}$ is the elastic contribution, also known as the Curie term, and $\chi_i^{(\mathrm{vV})}$ is the van-Vleck term. Furthermore, the QFI can be written as the sum of a classical and a quantum contribution $\mathcal{F}(\xi_i) = \mathcal{F}_{\mathrm{C}}(\xi_i) + \mathcal{F}_{\mathrm{Q}}(\xi_i)$, arising from the parameter-dependence of the eigenvalues and eigenvectors of ρ^T, respectively. It can be seen that (even when $[H_1, H_2] \neq 0$), the susceptibility relates to the QFI as $\chi_i^{(\mathrm{el})} = \beta \Delta H_i{}^2 = \beta \mathcal{F}_{\mathrm{C}}(\xi_i)$. Hence for $[H_1, H_2] = 0$, where both $\chi_i^{(\mathrm{vV})}$ and $\mathcal{F}_{\mathrm{Q}}(\xi_i)$ are zero due to the fact that the eigenstates of the Hamiltonian are independent of the parameter, the Eq. (5.17) is recovered.

5.6 Magnetometry in the XX model

The XX spin chain in a transverse field corresponds to a Heisenberg model with the same coupling for the x and y component of the spin interactions. It can be trivially derived from the XY model by choosing the anisotropy equal to zero, and reads:

$$H_{XX} = -\frac{J}{2} \sum_{l=1}^{N} \left(\sigma_l^{(x)} \sigma_{l+1}^{(x)} + \sigma_l^{(y)} \sigma_{l+1}^{(y)} \right) - h \sum_{l=1}^{N} \sigma_l^{(z)}. \tag{5.19}$$

The energy dispersion for this model reduces to

$$\begin{aligned} \epsilon_p &= 2J(\cos p - h/J), \\ p &= \frac{\pi}{N}(2l+1), \qquad l \in \{-N/2, \cdots, N/2-1\}. \end{aligned} \tag{5.20}$$

It is easy to see that, in Eq. (5.19), the term proportional to J and the term proportional to h commute. Hence, from Section 5.5, we know that the optimal observable for the estimation of h

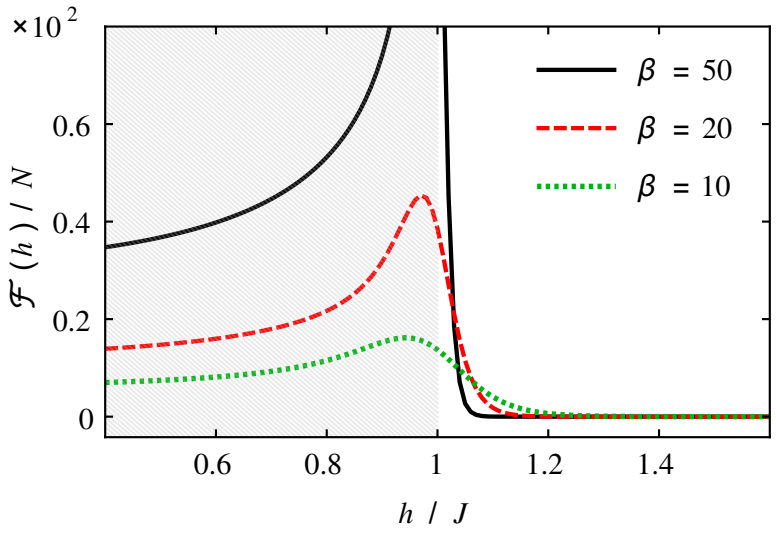

FIGURE 5.6: (color online) *Specific* QFI (i.e. $\mathcal{F}(h)/N$) for the estimation of the magnetic field h in the XX model as a function of h/J, at three different temperatures. The shaded area corresponds to the ferromagnetic region. In the plot $N = 10^5$ and $J = 1$.

is the total magnetization along the z-direction $J_z = \sum_{l=1}^{N} \sigma_l^{(z)}$ and that the corresponding sensitivity is modulated by the static magnetic susceptibility $\mathcal{F}(h) = \beta|\partial_h\langle J_z\rangle| \equiv \beta\chi_h$ [100]. Note that $\langle J_z\rangle$ is a quantity that can be accessed experimentally using Faraday spectroscopy spectroscopy as we already explained in Section 5.2.

For a thermal state ρ^T, Eqs. (5.2) and (5.20) allow to express the magnetization as

$$\langle J_z\rangle = 2\sum_p n_p - N. \tag{5.21}$$

With this expression at hand, and with the help of Eq. (5.18), it is easy to find the explicit formula for $\mathcal{F}(h)$, which reads as

$$\mathcal{F}(h) = \beta\left|\frac{\partial\langle J_z\rangle}{\partial h}\right| = 4\beta^2\sum_p n_p(1-n_p). \tag{5.22}$$

As shown in Figure 5.6, the sensitivity peaks in the ferromagnetic phase, close to the critical point $|h/J| = 1$. This feature becomes sharper as the temperature is cooled down, until $\mathcal{F}(h)$ eventually diverges at criticality in the limit $\beta \to \infty$ [46]. Note as well that $\mathcal{F}(h)$ drops quickly to zero as the probe enters the paramagnetic region (most markedly at low temperatures), whereas it remains non-vanishing within the ferromagnetic phase. This is intuitive, recalling that the paramagnetic ground state is an eigenstate of the estimator J_z and thus, completely insensitive to fluctuations in the field intensity h.

Interestingly, although increasing the equilibrium temperature of the probe significantly reduces the attainable sensitivity for both the ferromagnetic phase and the critical point, thermal mixing

does slightly enhance the sensitivity of paramagnetic samples. This is not so surprising, as an increase in the temperature of the sample populates excited states of H_{XX} (more sensitive than the paramagnetic ground state).

5.7 Sub-shot-noise sensing in the *XX* model

5.7.1 Low-temperature approximation for $\mathcal{F}(h)$

Is it possible to overcome the shot-noise limit in the above occasions. This is what we attack in this section. In what follows we simplify the expression of $\mathcal{F}(h)$ in the ferromagnetic phase, capturing its dependence on N, h/J, and β. Specifically, we are interested in the regime of low temperatures ($\beta \gg 1$) and large N. Inspection of Eq. (5.22) suggests that contributions from $n_p \simeq \{0,1\}$ to $\mathcal{F}(h)$ can be safely neglected. Recalling that $n_p = [1+\exp(\beta\epsilon_p)]^{-1}$, only those terms for which $\beta|\epsilon_p| < \kappa$, where κ is some small positive constant, contribute significantly to the total magnetic sensitivity. From Eq. (5.20) it follows that $-\kappa/\beta < 2J(\cos p - h/J) < \kappa/\beta$, and hence

$$\arccos\left(\frac{h}{J}-\frac{\kappa}{2\beta J}\right) < p < \arccos\left(\frac{h}{J}+\frac{\kappa}{2\beta J}\right). \tag{5.23}$$

One can now perform Taylor expansion to first order in the small parameter κ/β, which yields

$$\arccos\left(\frac{h}{J}\pm\frac{\kappa}{2\beta J}\right) \simeq \arccos(h/J) \mp \frac{\kappa}{2\beta J\sqrt{1-(h/J)^2}}. \tag{5.24}$$

Since N is large, we may assume that the indices p are continuously distributed with a uniform 'density' $N/2\pi$ (recall that $|p| < \pi$). Therefore, the number of energy levels effectively contributing to the sum in Eq. (5.22) would be the product of $N/2\pi$ and the gap between the upper and lower bounds of Eq. (5.23). Taking a constant n_p for all the terms involved in the sum provides with an optimal magnetic sensitivity of

$$\mathcal{F}(h) \simeq \mathcal{F}_{\text{app}}(h) \equiv C\frac{\beta N}{J\sqrt{1-(h/J)^2}}. \tag{5.25}$$

For low enough temperatures and large N, we numerically find the fitting parameter $C \approx 0.64$ to be independent of β, J, and, most importantly, also of the size of the probe N. The close agreement between Eq. (5.25) and $\mathcal{F}(h)$ is showcased in Figure 5.7. As a rule of thumb, we can expect the approximation to hold so long as $k_BT < J-h$. Closer to the critical point, i.e. when $J-k_BT < h < J$, the magnetic sensitivity presents a maximum of approximately $\mathcal{F}_{\text{app}}(h = J-k_BT)$.

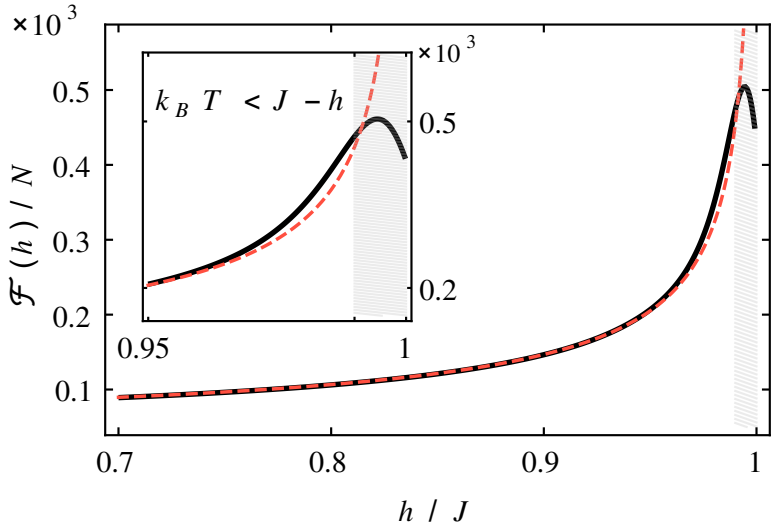

FIGURE 5.7: (color online) (solid black) Specific QFI for magnetic field sensing in the XX model versus h/J. All the plotted area lies within the ferromagnetic phase. (dashed red) Low-temperature approximation of the magnetic sensitivity $\mathcal{F}_{\text{app}}(h)$ from Eq. (5.25). The region $k_BT > J-h$ where the approximation breaks down appears in shaded gray. (inset) Close-up of the neighbourhood of the critical point. The temperature was set to $\beta = 100$, $N = 10^4$, and $J = 1$.

Finally, notice as well that $\mathcal{F}_{\text{app}}(h)$ is linear in N or, in other words, the magnetic sensitivity scales extensively with the probe size. Next, we will show how the scaling of $(\delta h)^{-2}$ may be enhanced by means of a feedforward adaptive protocol that actively exploits quantum criticality.

5.7.2 Adaptive feedforward magnetometry

The expression provided for $\mathcal{F}_{\text{app}}(h)$, i.e. Eq. (5.25), suggests an adaptive protocol to improve the estimation of h. Let us assume, in full generality, that h is known within an interval $h_{\min} < h < h_{\max}$. If the Hamiltonian parameter J is accessible to control, one may start by tuning it to $J = h_{\max}$ to ensure that the spin chain lies in the ferromagnetic side of the transition. After the sample has equilibrated with the new parameters, we can measure its magnetization J_z and come up with the estimate $h \pm \delta h_1$, with 'error bars' $\delta h_1 \simeq 1/\sqrt{\mathcal{F}_1}$, where

$$\mathcal{F}_1 \equiv C \frac{\beta \nu N}{h_{\max}\sqrt{1-(h/h_{\max})}} \equiv A\nu N. \tag{5.26}$$

In Eq. (5.26), we have explicitly accounted for enough repetitions ν of this first step to ensure that $\delta h_1/h \ll 1$. At this point, one can update the interaction strength to $J = h + \delta h_1$ and, again after re-equilibration of the probe, refine the estimate of h according to the outcomes of ν additional magnetization measurements. The error δh_2 after the second iteration is arguably much smaller than δh_1. Note that the protocol is essentially driving the probe towards the critical point, which

drastically increases the sensitivity as shown in Figure 5.7. In particular, $\delta h_2 \simeq 1/\sqrt{\mathcal{F}_2}$, where

$$\mathcal{F}_2 = \left(\frac{C\beta}{\sqrt{2h}}\right)\frac{\nu N}{\sqrt{\delta h_1}} + O\left(\frac{\delta h_1}{h}\right)^{3/2} \simeq B\nu N\mathcal{F}_1^{1/4}, \tag{5.27}$$

where $B \equiv C\beta/\sqrt{2h}$. $\mathcal{F}_2$ As the protocol is repeated further, we find $\delta h_k \simeq 1/\sqrt{\mathcal{F}_k}$, with

$$\begin{aligned}\mathcal{F}_k \simeq B\nu N F_{k-1}^{1/4} &= A^{1/4^{k-1}} B^{1+1/4+\cdots+1/4^{k-2}} (\nu N)^{1+1/4+\cdots+1/4^{k-1}} \\ &= A^{1/4^{k-1}} B^{4/3(1-1/4^{k-1})} (\nu N)^{4/3(1-1/4^k)}.\end{aligned} \tag{5.28}$$

In the limit of large k, the sensitivity scales as $F_k \sim N^{4/3}$ so that $\delta h_k \sim 1/N^{2/3}$, which outperforms the shot-noise scaling by a factor of $1/N^{1/6}$. Hence, the proposed adaptive scheme shows that, at finite temperatures, it is possible to exploit criticality in its wider sense to allow quantum-enhanced sensing and overcome the linear (shot-noise) scaling associated to uncorrelated probes. The reason for such (certainly surprising) fact is that, at each step k of the protocol, the thermal state changes and approaches the quantum crossover point, with its critical behavior. Those changes reflect in a sensitivity that scales super-extensively with the number of particles N. This is the main result of the work presented here.

Two clarifications are in order. To begin with, note that for Eq. (5.25) to remain applicable, we shall always work in the limit $\{\beta, N\} \gg 1$. Recall, however, that the approximation $\mathcal{F}_{\text{app}}(h)$ only holds if $k_B T < J_k - h = \delta h_{k-1}$, so that thermal fluctuations set an effective lower bound for the statistical uncertainty attainable with this iterative scheme: As soon as δh falls below $k_B T$, updating the interaction strength provides no scaling advantage. Indeed, it may even become detrimental if the probe is pushed too close to criticality (see Figure 5.7). Note that this does not mean that uncertainties δh below the level of thermal fluctuations are unattainable, but only that the error decreases no faster than $1/N^{1/2}$ beyond that point.

Secondly, the only metrologically relevant resource considered in our analysis is the number N of spins in the sample. In particular we implicitly assume that the precise adjustment of J, the iteration of the magnetization measurement $\nu \times k$ times, or the re-thermalization of the probe at each step come at no additional cost. Care must be taken, however, as this may be not the case in actual experiments: Practical limitations, like the short lifetime of the sample or the imperfect control of the Hamiltonian parameters, may call for a different assessment of resources, specific to each particular implementation.
Finally, let us mention that a generalization of our adaptive approach has been proposed in [101].

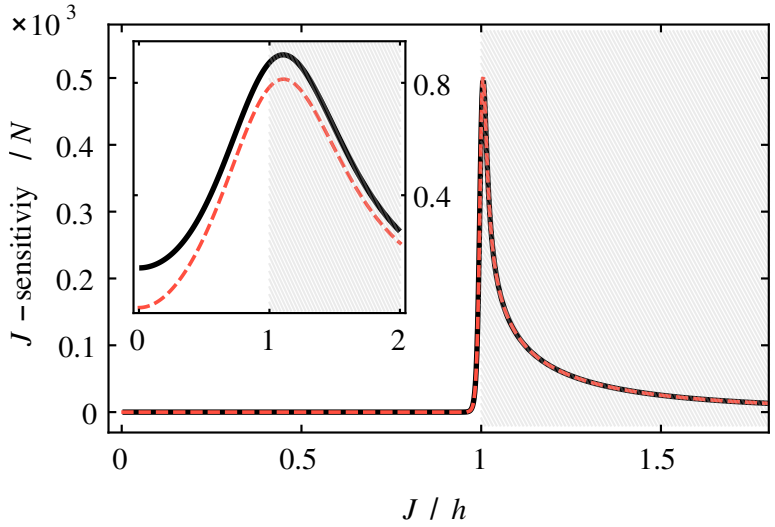

FIGURE 5.8: (color online) (solid black) Specific QFI for the estimation of J in the XX model versus J/h. As in Figure 6.1 the ferromagnetic phase has been shaded. (dashed red) Specific J-sensitivity $F(J;J_z)/N$ of the total magnetization J_z. The temperature was set to $\beta = 100$, $h = 1$, and $N = 10^3$. (inset) Same as in the main plot for the much larger temperature $\beta = 2$. Note that, unlike in the main plot, the vertical axis of the inset is not scaled by the 10^3 factor.

5.7.3 Sub-shot-noise estimation of the coupling J

For completeness we also address the estimation of the Hamiltonian parameter J in the XX model. As we know from Section 5.5, the estimator $O_J \equiv \sum_{l=1}^{N}\left(\sigma_l^{(x)}\sigma_{l+1}^{(x)} + \sigma_l^{(y)}\sigma_{l+1}^{(y)}\right)$ would be optimal in this case. Its sensitivity can be obtained as in Eq. (5.22), which gives

$$\mathcal{F}(J) = 4\beta^2 \sum_p \cos^2 p \; n_p(1-n_p). \tag{5.29}$$

Unfortunately, O_J is not as easy to measure as the total magnetization J_z, since it involves two-body correlations. Although generally sub-optimal, the magnetization is known to be a good estimator for J in the related Ising model (cf. Section 5.8) [47], which motivates us to look at the J-sensitivity $F(J;J_z)$ of this observable. This is plotted alongside $\mathcal{F}(J)$ in Figure 5.8. Note that the abscissa is, in this case, J/h instead of h/J. As in Figure 6.1, $\mathcal{F}(J)$ (solid black) peaks in the ferromagnetic phase close to the critical point. On the other hand, $F(J;J_z)$ (dashed red) is seen to be nearly optimal at low enough temperatures. Most interestingly, $F(J;J_z)$ still remains very close to the optimal sensitivity even at very large temperatures, as illustrated in the inset of Figure 5.8. Hence, J_z can be regarded as a practical alternative for estimating J.

Due to the similarity between Eqs. (5.22) and (5.29), one may proceed as in Section 5.7.1 to come up with the following low-temperature approximation for $\mathcal{F}(J)$ at large N:

$$\mathcal{F}(J) \simeq \mathcal{F}_{\text{app}}(J) \equiv C\frac{h^2\beta N}{J^3\sqrt{1-(h/J)^2}}. \tag{5.30}$$

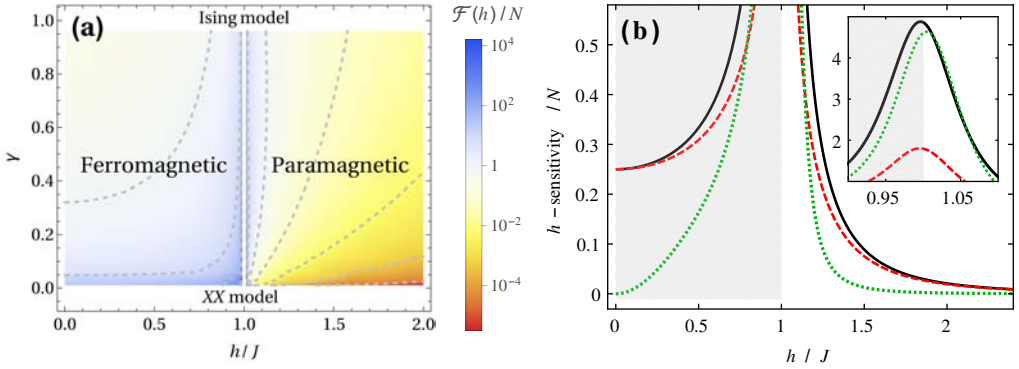

FIGURE 5.9: (color online) (a) Specific QFI (in logarithmic scale) in the XY model as a function of h/J and γ. The critical line appears highlighted in white. Note that $\gamma = 0$ corresponds to the XX model and $\gamma = 1$, to the Ising model. The sensitivity increases with the asymmetry parameter γ in the paramagnetic region, whereas it decreases with γ in the ferromagnetic phase. For this illustration $N = 10^3$, $\beta = 10^3$, and $J = 1$. (b) (solid black) Specific QFI in the Ising model, (dashed red) specific h-sensitivity $F(h; J_z)/N$ of the total magnetization in the z-direction, and (dotted green) specific h-sensitivity $F(h; J_x^2)/N$. (inset) Zoom into the high-sensitivity region, not shown in the main plot. The ferromagnetic phase is highlighted in shaded gray and $N = 40$, $\beta = 100$, and $J = 1$.

Consequently, the exact same line of reasoning of Section 5.7.2 applies to this case: Iteratively updating the value of the external magnetic field h, so as to drive the system towards the critical point, allows, in principle, for sub-shot-noise scaling in the J-sensitivity.

5.8 Magnetometry beyond the *XX* model

We shall now turn our attention back to the Heisenberg XY model, which includes the XX model as a particular case as described by Eq. (5.1). Here the *asymmetry parameter* γ is a resource of non-commutativity, hence $[H_1, H_2] \neq 0$. As a result, we cannot use the results of Section 5.5.

However, just like the thermometry precision, the maximum magnetic sensitivity of the thermal state ρ^T of the XY Hamiltonian can be computed easily by using the additivity of the QFI. Specifically we have $\mathcal{F}(h) = \sum_p \mathcal{F}_p(h)$. Each of the terms contributing to the rhs can be calculated by the help of Eq. (2.17)

$$\mathcal{F}_p(h) = 4 \sum_i \frac{(\partial_h p_i)^2}{p_i} + 2 \sum_{ij} \frac{(p_i - p_j)^2}{p_i + p_j} \left| \langle i_p | \partial_h j_p \rangle \right|^2 \tag{5.31}$$

where $i, j \in \{0, 1\}$, and $p_i = \langle i_p | \rho^p(T) | i_p \rangle$. Notice that unlike thermometry, the state vectors $|i_p\rangle$ do depend on the parameter h. In Figure 5.9(a) the resulting $\mathcal{F}(h)$ is plotted versus h/J and γ. Note that the sensitivity peaks sharply around the critical line $h/J = 1$ (indicated in white) for any γ. Otherwise, in the ferromagnetic phase, the sensitivity decreases as the asymmetry γ is increased, while in the paramagnetic phase, it grows instead.

Note that the two terms in Eq. (5.1) do not commute in general and, consequently, J_z is not necessarily an optimal magnetic field estimator. Even if the QFI can be readily computed, finding the SLD is a much harder task, typically yielding complex non-local optimal estimators. It is therefore important to find good practical estimators, as in Section 5.7.3.

In particular, we shall consider again J_z and the variance $\Delta {J_x}^2$, which can be expressed in terms of two-body correlation functions [77]. Their corresponding h-sensitivities, $F(h;J_z)$ and $F(h;\Delta {J_x}^2)$, are easy to calculate numerically for low N. These are compared to $\mathcal{F}(h)$ in Figure 5.9(b) for $\gamma = 1$ (i.e. in the Ising model). At low temperatures and far from the critical point, J_z turns out to be nearly optimal again. In contrast, close to criticality $\Delta {J_x}^2$ features a magnetic sensitivity much closer to the ultimate bound. At larger temperatures, however, correlations are destroyed by thermal mixing and, consequently, $F(h;\Delta {J_x}^2)$ reduces significantly. On the other hand, $F(h;J_z)$ remains close to optimality even at very large temperatures. Figure 5.9(b) suggests that, in a practical situation, a first estimate $h \pm \delta h_1$ would be best obtained with the more conservative estimator J_z. If the temperature is low enough and J can be tuned to $h + \delta h_1$, further estimates based on $\Delta {J_x}^2$ would subsequently provide much better accuracies.

5.9 Summary and Outlook

In summary, we have proposed a method to estimate the parameters in a strongly correlated spin chain at finite temperatures. Such parameters range from an external magnetic field to atom-atom couplings, to the temperature itself. Our method is based on using collective atomic measurements via a QND Faraday interface. The Faraday interface gives access, a priori, to any order of the statistical moments of the collective atomic angular momentum operators. We have investigated which are the best collective operators to estimate the sample. These depend upon the order of the strongly correlated system (quantum phases) and the temperature range. By borrowing concepts from quantum metrology, we have analytically derived the optimal signal-to-noise ratio for a thermal state governed by the XY Hamiltonian given by the quantum Cramér-Rao bound and we have compared it with the one obtained from the Faraday interface. Remarkable enough, collective atomic correlations can be considered as optimal observables for precision thermometry/magnetometry in the temperature range of interest in present experiments of ultracold lattice gases simulating strongly correlated systems. Our results hold for the XY model, but it remains to be analyzed if the method can be also optimal for other quantum spin models, either integrable or not.

Further we have shown how, even though the magnetic susceptibility, which modulates the magnetic sensitivity, scales extensively in the probe size, sub-shot-noise reduction of the error is still possible through a feedforward adaptive scheme. This sub-shot-noise behaviour can be maintained until the error falls below the level of the environmental noise.

Finally, we have extended our study to more general Hamiltonians where commutative algebra cannot be exploited for metrology; namely, the paradigmatic XY model. There, the sensitivities of different sub-optimal observables have been benchmarked against the practically unattainable ultimate precision bound set by the quantum Fisher information.

Our results may be particularly relevant to practical sub-shot-noise sensing, as we place the focus on the sensitivities achievable with probes prepared in robust thermal states, rather than the fragile highly-entangled pure preparations which are often sought in order to attain better-than-classical error scaling in parameter estimation.

The problem of the simultaneous measurement of several parameters (e.g. h and J) with quantum many-body probes remains an open question that certainly deserves investigation. Although technically very challenging, it would also be interesting to extend this type of analysis to non-integrable thermal spin models, possibly featuring a richer phase diagram. This will be the subject of future work.

Chapter 6

Quantum metrology beyond thermal equilibrium I: Static systems

In this chapter we present our results regarding parameter estimation in systems which are not at thermal equilibrium. The focus is on systems which are at their *stationary state*, so their density matrix does not change with time. By non-equilibrium we specifically mean that the stationary state is *not described by a Gibbs state*. In turn, systems whose density matrices are time dependent (*dynamic*) will be addressed in Chapter 7. We are curious about two particular scenarios that bring on non-equilibrium stationary states:

1. Systems which interact *strongly* with a thermal bath.
2. Systems which interact, simultaneously, with *multiple baths*.

In the first case, the strong coupling produces an unavoidable correlation between the system and the bath, therefore, the Born-Markov approximation is not maintainable anymore. As a consequence, making use of the Lindbladian master equation is ruled out. Notwithstanding, there are multiple paradigms which can be dealt with analytically. Aligned with our particular task of *low temperature thermometry*, we point out the standard Caldeira-Leggett model as an instance of such paradigms. Remarkably, we observe that low temperature thermometry is indeed boosted by strong dissipative interactions, while within quantum technologies, strong dissipation is most often detrimental.

In contrary, when multiple baths appear, the Lindbladian master equation is applicable—provided that the interaction with each bath is weak enough. Nevertheless, the existence of multiple baths poses complications, above all we can not assess a unique temperature to the system. On the bright side, this situation brings up new physics e.g., the rise of stationary heat currents can be exploited to construct an autonomous *quantum heat pump*. Therefore, for our

metrological purposes, it provides various novel opportunities to inquire into. Such opportunities range from exploring the role of temperature gradient in metrology, or estimation of the temperature gradient itself, to probing a quantum heat pump, aiming at acquiring information about the quality of its performance.

The chapter is structured as follows: In Section 6.1 we deal with thermometry of at low temperatures (T), the very same regime where equilibrium probes fail to prove efficient. To tackle this issue we propose coupling the probe strongly to the sample (the heat bath). Our probe is represented by a quantum harmonic oscillator. By studying the stationary state properties of the harmonic oscillator, we observe that the strong coupling definitely improves the precision of thermometry at low T. Further, we propose practically feasible measurements which can achieve fairly close to optimal precision. Finally, we suggest that the spectral density of the probe-system interaction can be set to play a crucial role in low T thermometry.

The rest of the chapter is dedicated to our results in systems which are in contact with multiple baths. Specially, Section 6.2 is devoted to metrology in an interacting bipartite system consisting of two coupled harmonic oscillators, each of which is placed in its local bath. We inquire about the estimation of the temperature gradient between the two local baths, as well as the estimation of the interaction coupling between the two oscillators. Our observations show that the estimation of the coupling between the two oscillators—not to be confused with the coupling with the baths—can be increased quadratically by increasing the temperature gradient. This is achievable merely by global measurements performed on both oscillators, while local protocols fail to acquire any information about the coupling strength. In contrast, we discover that the temperature gradient might be estimated even with local measurements, albeit the optimal measurement is a global one. In addition, we see that unlike the thermal scenario of Section 4.3.1, the coupling between the two oscillators diminishes thermometry precision.

Eventually, Section 6.3 is devoted to quantum heat pumps. First, we review the principle elements of an autonomous quantum heat pump. Whence, we propose the tiniest system, i.e., a two-level atom, to probe a quantum heat pump. Despite the fact that the probe is very small, measuring its steady state reveals notable information about the quantum heat pump. Specially, it detects possible resources of irreversibility, such as heat leaks or internal dissipation. Provided that the irreversibility is negligible, our tiny probe can be used to further estimate the coefficient of performance of the heat pump.

6.1 Thermometry with strongly coupled probes

In what follows, we will show that the thermal sensitivity can indeed improve (at low enough T) as the probe-sample coupling is increased, and the correlations built up among the two eventually allow the probe to sense a 'larger' portion of the sample. Namely, we will find the exact (non-equilibrium) steady-state of a harmonic probe under arbitrarily strong dissipation into an equilibrium environment, to then compute its maximum thermal sensitivity. In order to describe the probe-sample interaction, we adopt the standard Caldeira-Leggett model [102, 103]. As we described in Chapter 3, the Hamiltonian of the probe is just $H_{\rm p} = \frac{1}{2}\omega_0^2 x^2 + \frac{1}{2}p^2$ (where the mass of the probe is $m = 1$), whereas the sample is described as an infinite collection of non-interacting bosonic modes $H_{\rm s} = \sum_\mu \frac{1}{2}\omega_\mu^2 m_\mu x_\mu^2 + \frac{1}{2m_\mu} p_\mu^2$. The probe-sample coupling is realized by a linear term of the form $H_{\rm p\text{–}s} = x\sum_\mu g_\mu x_\mu$. In order to compensate exactly for the 'distortion' caused on the probe by the coupling to the sample, one should replace ω_0^2 with $\omega_0^2 + \omega_R^2$ in $H_{\rm p}$ [102, 103], where the 'renormalization frequency' is $\omega_R^2 := \sum_\mu \frac{g_\mu^2}{m_\mu \omega_\mu^2}$ [1].

The coupling strengths between the probe and each of the sample modes are determined by the 'spectral density' $J(\omega) := \pi \sum_\mu \frac{g_\mu^2}{2m_\mu\omega_\mu}\delta(\omega - \omega_\mu)$, which is given a phenomenological analytical form. To ensure convergence, one must set up a high-frequency cutoff in $J(\omega)$ [103]. In what follows, we shall work with an Ohmic spectral density with Lorentz-Drude cutoff $J(\omega) = 2\gamma\omega\,\omega_c^2/(\omega^2 + \omega_c^2)$, which vanishes for $\omega \gg \omega_c$. Here, γ stands for the dissipation strength and carries the order of magnitude of the couplings g_μ [2].

[1] Splitting the Hamiltonian into a potential and a kinetic term $H = U(x, x_\mu) + K(p, p_\mu)$, one can see that effective potential *felt* by the probe is given by $U(x, x_\mu^\star)$, where $x_\mu^\star = -\frac{g_\mu}{m_\mu\omega_\mu^2}$ [i.e. $\partial_{x_\mu} U = 0$ at $x_\mu^\star$]. This is $U(x, x_\mu^\star) = \frac{1}{2}(\omega_0^2 - \omega_R^2)x^2$. As a result, the high temperature limit of the reduced steady state of the probe obtained from the *bare model* $H = H_{\rm p} + H_{\rm s} + H_{\rm p\text{–}s}$ is $\mathrm{tr}_{\rm s}\rho \propto \exp\left(-\frac{1}{2T}(\omega^2 - \omega_R^2)x^2 - \frac{1}{2T}p^2\right)$, which may differ significantly from the corresponding thermal state $\rho_T = Z^{-1}\exp(-H_{\rm p}/T)$ if the couplings g_μ are strong. To correct this, one must introduce the frequency shift ω_R^2 in $H_{\rm p}$ *ad hoc*.

[2] The need to introduce the cutoff frequency ω_c is related to the fact that even if very large (as compared to the probe), the sample is finite and thus, it has a maximum energy. The non-equilibrium steady state of the central oscillator will unavoidably depend on the choice of ω_c but, as long as $\omega_c \gg \omega_0$, this dependence should be weak and not change its qualitative features [104]. In particular, note that $\omega_R^2 \equiv \frac{2}{\pi}\int_0^\infty \mathrm{d}\omega\,\frac{J(\omega)}{\omega} = 2\gamma\omega_c$.

From the Heisenberg equations of motion to the QLE

We can write down the Heisenberg equations of motion $\left(\frac{d}{dt}A(t) = i[H, A(t)] + \partial_t A(t)\right)$ for all degrees of freedom $\{x, p, x_\mu, p_\mu\}$ of the system $H = H_\mathrm{p} + H_\mathrm{s} + H_\mathrm{p\text{–}s}$. These read

$$\dot{x} = p \tag{6.1a}$$

$$\dot{p} = -\left(\omega_0^2 + \omega_R^2\right)x - \sum\nolimits_\mu g_\mu x_\mu \tag{6.1b}$$

$$\dot{x_\mu} = \frac{p_\mu}{m_\mu} \tag{6.1c}$$

$$\dot{p_\mu} = -m_\mu \omega_\mu^2 x_\mu - g_\mu x. \tag{6.1d}$$

Differentiating Eq. (6.1c) and inserting in it Eq. (6.1d) yields $\ddot{x}_\mu + \omega_\mu^2 x_\mu = -\frac{g_\mu}{m_\mu} x$, which results in

$$x_\mu(t) = x_\mu(t_0)\cos\omega_\mu(t-t_0) + \frac{p_\mu(t_0)}{m_\mu\omega_\mu}\sin\omega_\mu(t-t_0) - \frac{g_\mu}{m_\mu\omega_\mu}\int_{t_0}^{t} \mathrm{d}s \sin\omega_\mu(t-s)\, x(s). \tag{6.2}$$

Similarly, one can differentiate Eq. (6.1a) and use Eqs. (6.1b) and (6.2) to eliminate $\dot{p}$ and x_μ. This results in the following integro-differential equation

$$\begin{aligned}&\ddot{x} + \left(\omega_0^2 + \omega_R^2\right)x - \int_{t_0}^{t} ds \sum\nolimits_\mu \frac{g_\mu^2}{m_\mu\omega_\mu}\sin\omega_\mu(t-s)\, x(s) \\ &= -\sum\nolimits_\mu g_\mu\left(x_\mu(t_0)\cos\omega_\mu(t-t_0) + \frac{p_\mu(t_0)}{m_\mu\omega_\mu}\sin\omega_\mu(t-t_0)\right).\end{aligned} \tag{6.3}$$

This is nothing but the quantum Langevin equation (QLE) of our probe [103, 105]. Since we are interested in the steady state of the central oscillator, we may let $t_0 \to -\infty$ without loss of generality. Defining the stochastic quantum force

$$F(t) := -\sum\nolimits_\mu g_\mu\left(x_\mu(t_0)\cos\omega_\mu(t-t_0) + \frac{p_\mu(t_0)}{m_\mu\omega_\mu}\sin\omega_\mu(t-t_0)\right), \tag{6.4}$$

and the dissipation kernel

$$\chi(t) := \sum\nolimits_\mu \frac{g_\mu^2}{m_\mu\omega_\mu}\sin\omega_\mu t\,\Theta(t) = \frac{2}{\pi}\int_0^\infty \mathrm{d}\omega\; J(\omega)\sin\omega t\;\Theta(t), \tag{6.5}$$

one may rewrite the QLE as

$$\ddot{x}(t) + \left(\omega_0^2 + \omega_R^2\right)x(t) - x(t) * \chi(t) = F(t), \tag{6.6}$$

where $*$ denotes convolution.

In summary, the first two terms in the left-hand side of Eq. (6.6) correspond to the coherent dynamics of a free harmonic oscillator of squared frequency $\omega_0^2 + \omega_R^2$, while the incoherent superposition of all environmental modes, encompassed in $F(t)$, plays the role of a stochastic driving force. Finally, the convolution $x(t) * \chi(t) \coloneqq \int_{-\infty}^{\infty} \mathrm{d}s\, \chi(t-s)x(s)$ brings memory effects into the dissipative dynamics.

It is important to remark that Eq. (6.6) is *exact*. As already advanced, the only assumption that we make is that probe and sample start uncorrelated at $t_0 \to -\infty$, i.e. in $\rho \otimes \sigma_T$, where σ_T is the Gibbs state of the sample at temperature T. The initial state of the probe ρ is arbitrary. However, since the Hamiltonian H is overall bilinear in positions and momenta, its stationary state is Gaussian, and thus, completely determined by its second-order moments $\sigma_{ij}(t',t'') \coloneqq \frac{1}{2}\langle\{R_i(t'), R_j(t'')\}\rangle$, where $R = (x,p)$ [105]. The notation $\langle\cdots\rangle$ stands here for average on the initial state and $\{\ldots\}$ denotes anti-commutator.

One may now take the Fourier transform ($\tilde{f}(\omega) \coloneqq \int_{-\infty}^{\infty} \mathrm{d}t\, f(t) e^{i\omega t}$) in Eq. (6.6), and solve for $\tilde{x}(\omega)$, which yields

$$\tilde{x}(\omega) = [\omega_0^2 + \omega_R^2 - \omega^2 - \tilde{\chi}(\omega)]^{-1} \tilde{F}(\omega) \coloneqq \alpha(\omega)^{-1} \tilde{F}(\omega). \tag{6.7}$$

The position correlator $\sigma_{11}(t',t'')$ can be thus cast as

$$\sigma_{11} = \iint_{-\infty}^{\infty} \frac{\mathrm{d}\omega'\, \mathrm{d}\omega''}{8\pi^2}\, e^{-i(\omega' t' + \omega'' t'')} \langle\{\tilde{x}(\omega'), \tilde{x}(\omega'')\}\rangle, \tag{6.8}$$

whereas σ_{22} may be calculated similarly by noticing that $\langle\{\tilde{p}(\omega')\tilde{p}(\omega'')\}\rangle = -\omega'\omega''\langle\{\tilde{x}(\omega')\tilde{x}(\omega'')\}\rangle$. The two remaining correlators simply vanish ($\sigma_{12} = \sigma_{21} = 0$) (see Appendix C).

Hence, in light of Eqs. (6.7) and (6.8), all we need to know is the power spectrum of the noise $\langle\{\tilde{F}(\omega')\tilde{F}(\omega'')\}\rangle$ and the Fourier transform of the dissipation kernel $\tilde{\chi}(\omega)$. Since the sample was prepared in a Gibbs state, one can show that the noise is connected to the dissipation kernel through the following fluctuation-dissipation relation (see Appendix A.1)

$$\langle\{\tilde{F}(\omega'), \tilde{F}(\omega'')\}\rangle = 4\pi\, \delta(\omega' + \omega'') \coth\left(\tfrac{\omega'}{2T}\right) \mathrm{Im}\tilde{\chi}(\omega'). \tag{6.9}$$

For our specific choice of spectral density $J(\omega)$, $\tilde{\chi}(\omega)$ evaluates to $\tilde{\chi}(\omega) = 2\gamma\omega_c^2/(\omega_c - i\omega)$.

Putting together the pieces from the above paragraphs, we can compute the steady-state covariances $\sigma_{ij}(0,0)$ [104, 106–108] (recall that $t_0 \to -\infty$). These may be collected into the 2×2 covariance matrix $\boldsymbol{\sigma}$, which provides a full description of the (Gaussian) non-equilibrium asymptotic state of our single-mode probe [109]. We can now calculate $\mathcal{F}_T$ from Eq. (**??**), using the fact that the Uhlmann fidelity between two single-mode Gaussian states with covariance matrices $\boldsymbol{\sigma}_1$ and $\boldsymbol{\sigma}_2$ is given by $\mathbb{F}(\boldsymbol{\sigma}_1, \boldsymbol{\sigma}_2) = 2\left(\sqrt{\Delta + \Lambda} - \sqrt{\Lambda}\right)^{-1}$, where $\Delta \coloneqq 4\det(\boldsymbol{\sigma}_1 + \boldsymbol{\sigma}_2)$ and $\Lambda \coloneqq (4\det\boldsymbol{\sigma}_1 - 1)(4\det\boldsymbol{\sigma}_2 - 1)$ [110]. In Figure 6.1(a) we plot the thermal sensitivity $\mathcal{F}_T$ of a

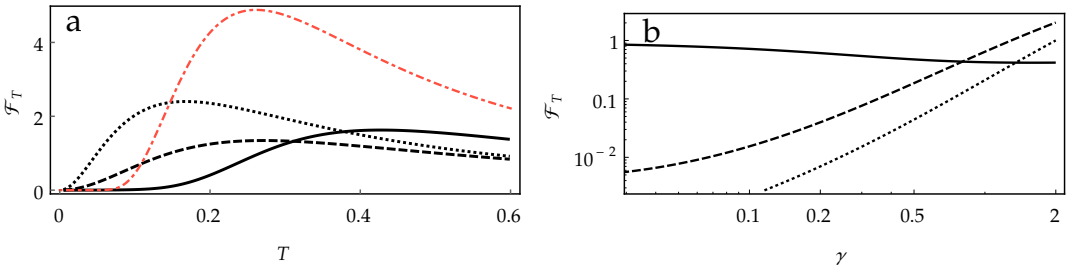

FIGURE 6.1: (color online) (a) Quantum Fisher information $\mathcal{F}_T$ vs. the sample temperature T for different dissipation strengths: (solid black) $\gamma = 0.1$, (dashed black) $\gamma = 1$, and (dotted black) $\gamma = 5$ ($\omega_0 = 1$). The sensitivity of a single-mode probe at thermal equilibrium (dot-dashed red) has been super-imposed for comparison. (b) Log-log plot of $\mathcal{F}_T$ as a function of γ for (solid) $T = 1$, (dashed) $T = 0.1$, and (dotted) $T = 0.05$. In both cases we work in units of $\hbar = k_B = 1$. Here, $\omega_c = 100\,\omega_0$.

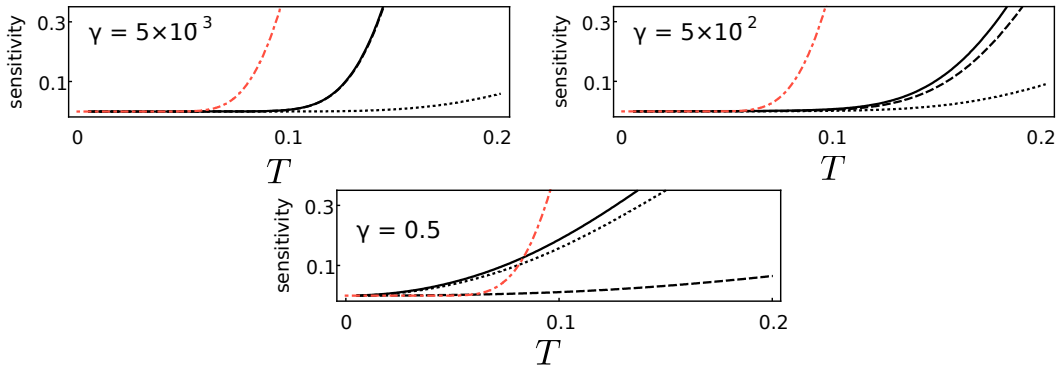

FIGURE 6.2: (color online) Comparison of (solid black) the maximum thermal sensitivity $\mathcal{F}_T$ of the non-equilibrium probe, (dashed black) the sub-optimal sensitivity of the average energy $F_T(H_\mathrm{p})$, (dotted black) the sensitivity of the position covariance $F_T(x^2)$, for different values of the dissipation strength: $\gamma = 5\times10^{-3}$, $\gamma = 5\times10^{-2}$, and $\gamma = 0.5$. Again, the thermal sensitivity of the corresponding equilibrium state has been added for comparison (dot-dashed red), and $\omega_c = 100\,\omega_0$.

harmonic probe as a function of the sample temperature, for several (large) values of the dissipation strength γ. When comparing it with the sensitivity of an equilibrium mode, we can see that, even though the overall maximum attainable sensitivity may be deterred by a stronger probe-sample coupling, the low-temperature QFI does increase significantly as the dissipation strength grows. This is further illustrated in Figure 6.1(b), where we plot $\mathcal{F}_T$ as a function of γ for different temperatures: As shown in the figure, if the sample is cold enough, the sensitivity of the probe increases *monotonically* with the dissipation strength. Hence, the probe-sample coupling can be thought-of as a relevant control parameter in practical low-temperature quantum thermometry. This is our main result.

Thus far, we have shown how strong coupling may improve the ultimate bounds on thermometric precision at low temperatures. However, we have not yet discussed how to saturate those bounds in practice. We therefore need to find observables capable of producing temperature estimates that approach closely the precision bound set by the QFI.

In general, a temperature estimate based on M measurements of some observable O on the steady state of the probe has uncertainty $\delta T \geq 1/\sqrt{M\mathcal{F}_T(O)}$, where $\mathcal{F}_T(O)$ stands for the 'classical Fisher information' of O [111]. This may be lower-bounded by the 'thermal sensitivity' $F_T(O) \coloneqq |\partial_T\langle O\rangle|^2/(\Delta O)^2 \leq \mathcal{F}_T(O) \leq \mathcal{F}_T \equiv \sup_O F_T(O)$ [112]. Here, $\Delta O \coloneqq \sqrt{\langle O^2\rangle - \langle O\rangle^2}$ denotes the uncertainty of O and all averages are taken with respect to the stationary state of the probe.

The observable for which $F_T(O)$ is maximized commutes with the so-called 'symmetric logarithmic derivative' (SLD) L, which satisfies $\partial_T\rho = \frac{1}{2}(L\rho + \rho L)$. For instance, in the case of an equilibrium probe, i.e. $\rho_T \propto \exp(-H_\mathrm{p}/T)$, one has $[L, H_\mathrm{p}] = 0$. Consequently, a complete projective measurement on the energy measurements renders the best temperature estimate. However, as shown in Figure 6.2, when the strength of the interaction with the sample increases, energy measurements become less and less informative about the temperature of the sample: the larger the dissipation strength γ, the smaller $F_T(H_\mathrm{p})/\mathcal{F}_T$. Temperature estimates based on energy measurements seem thus incapable of exploiting the extra low-temperature sensitivity enabled by the strong dissipation. In searching for a more suitable measurement scheme, one can look at the SLD: Since ρ_T is an undisplaced Gaussian (see Appendix A), L will be a quadratic form of x^2 and p^2 [74]. Due to our choice for the probe-sample coupling ($x\sum_\mu g_\mu x_\mu$), the steady state ρ_T becomes squeezed in the position quadrature when the temperature is low enough and the dissipation rate is sufficiently large. Interestingly, we observe that $\langle x^2\rangle$ is much more sensitive to temperature changes in this regime than $\langle p^2\rangle$. We thus take $O = x^2$ as an ansatz for a quasi-optimal temperature estimator. $F_T(x^2)$ is also plotted in Figure 6.2, where we can see how it does approach closely the ultimate bound $\mathcal{F}_T$ as γ grows. Note that the quadratures of e.g. a single trapped ion are either directly measurable [113] or accessible via state tomography [114, 115]. Measuring the variance of the most relevant quadrature of a harmonic thermometer is therefore a practical prescription capable of exploiting the thermometric advantage provided by strong dissipation at low temperatures.

To conclude, we shall give an intuition about the origin of the observed dissipation-driven enhancement. To that end, let us consider not just the marginal of the probe but the global state of probe *and* sample. For simplicity we can model them as a finite N-mode 'star system', comprised of a central harmonic oscillator (playing the role of the probe), linearly coupled to $N-1$ independent peripheral oscillators with arbitrary frequencies (representing the sample). Let us further prepare the N-mode composite in a Gibbs state at the sample temperature T. Indeed, when such linear system is at global thermal equilibrium, and provided that the number of modes N is large enough, the marginal of the central oscillator approximates well the *actual* steady state of the probe, which we have just calculated exactly [116].

It is easy to see that, whatever the distribution of the couplings, the frequencies of the lowermost

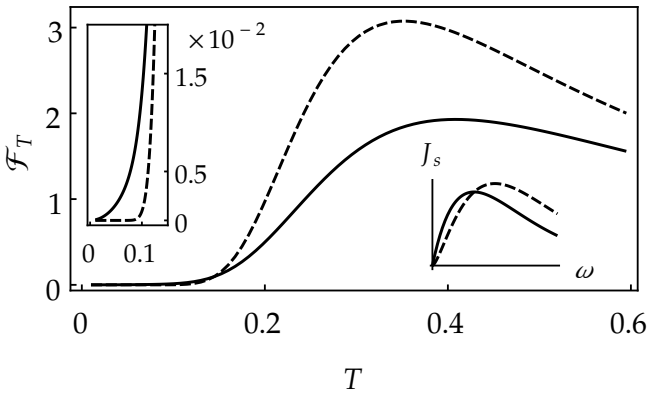

FIGURE 6.3: Quantum Fisher information $\mathcal{F}_T$ as a function of temperature for (solid) Ohmic and (dashed) super-Ohmic spectral density $J_s(\omega)$ with exponential high-frequency cutoff. (top left) Zoom into the low-temperature region of the main plot. (bottom right) comparison of the (solid) Ohmic and (dashed) super-Ohmic spectral densities. In this plots $\omega_0 = 1$, $\gamma = 0.1$, and $\omega_c = 100\omega_0$.

normal modes of the global star system always *decrease monotonically* as the overall magnitude of the coupling strengths increases (see Appendix D). If the temperature T was so low that not even the first harmonic could get thermally populated, the sensitivity of the entire system and, by extension, also that of the central probe, would vanish. However, one could populate the first few normal modes by strengthening the couplings, as their frequencies would then decrease. It is this effect which ultimately enables temperature sensing at low T. The magnitude of the enhancement is dictated by the specific frequency distribution of the probe-sample couplings which, in turn, determines the spectrum of the normal modes of the global system (see Appendix D and Reference [117]).

From the above reasoning it follows that the *shape* of the spectral density $J(\omega)$ could, in principle, be tailored to render more precise low-temperature probes. To see that this is indeed the case, we shall adopt a generic spectral density of the form $J_s(\omega) := \frac{\pi}{2}\gamma\omega^s\omega_c^{1-s}e^{-\omega/\omega_c}$, i.e. with an exponential high-frequency cutoff. We can thus compare the performance of a single-mode thermometer coupled to the sample through an Ohmic ($s = 1$) and a super-Ohmic ($s > 1$) spectral density, e.g. at fixed γ. For this purpose, we resort again to Eqs. (6.7)–(6.9), leading to the exact Gaussian marginal of the probe. Importantly, the dissipation kernel $\tilde{\chi}(\omega)$ needs to be re-calculated due to the change in spectral density (see Appendix B and [108]). Note as well that now $\omega_R = \gamma\omega_c\Gamma(s)$, where $\Gamma(z) := \int_0^\infty \mathrm{d}t\, t^{z-1}e^{-t}$ is Euler's Gamma function. The results are illustrated in Figure 6.3: As we can see, a super-Ohmic spectral density (in our case, with $s = 2$) may allow for a large improvement over an Ohmic one, in terms of maximum achievable thermal sensitivity (also compare with Figure 6.1). On the contrary, when it comes to thermometric precision at low temperatures, the Ohmic spectral density offers a clear advantage. As a final remark, we note that, since the equilibrium state of the probe corresponds to the marginal of a global thermal state [116], we can think of our results as an instance of thermometry on a macroscopic sample through local measurements, as studied in [97].

6.2 Coupled harmonic oscillators with individual local baths

We address the problem of two coupled harmonic oscillators (HO), which could represent a double well, or two cavity modes. The free Hamiltonian of the system is given by

$$H = H_0 + H_I, \text{ with } H_0 = \omega\, a_1^\dagger a_1 + (\omega+\Delta) a_2^\dagger a_2, \text{ and } H_I = -J(a_1^\dagger a_2 + a_1 a_2^\dagger). \tag{6.10}$$

Here a_j and $a_j^\dagger$ represent, respectively, the annihilation and creation operators of the jth HO. Besides, ω is the frequency of the first HO, while the frequency of the second HO is $\omega+\Delta$. In addition, J is the coupling between the two modes, which we assume to be constant. (See Section 7.2.2 for the time dependent tunneling.) Further, we assume that each of the oscillators is coupled to individual thermal baths with two different temperatures T_1 and T_2. By working in the weak coupling limit, and after Born-Markov approximation, followed by the rotating wave approximation, the master equation describing the reduced state of the oscillators is found to be [28, 71, 118, 119]

$$\dot\rho(t) = -i[H,\rho(t)] + \sum_{j=\{1,2\}} \mathcal{D}_j[\rho(t)], \tag{6.11}$$

where the dissipators $\mathcal{D}_j$ are given by

$$\begin{aligned}\mathcal{D}_j[\rho(t)] \quad &= \gamma(N_j+1)\Big(a_j\rho(t)a_j^\dagger - 1/2\{a_j^\dagger a_j,\rho(t)\}\Big) \\ &\quad +\gamma N_j\Big(a_j^\dagger\rho(t)a_j - 1/2\{a_j a_j^\dagger,\rho(t)\}\Big).\end{aligned} \tag{6.12}$$

Here $N_j = (\exp[\omega_j/T_j]-1)^{-1}$ is the mean number of excitations of the jth oscillator at temperature T, and γ being the dissipation rate. We have assumed the same constant dissipation rate for both oscillators. Obviously, for $J=0$ this dynamic is separable, i.e., under this dynamics the two oscillators evolve independently. Therefore, the stationary state is simply a product state. More precisely, the stationary state is such that each oscillator is at thermal equilibrium with its own bath

$$\rho^\infty_{J=0} = \frac{\mathrm{e}^{-H_1/T_1}}{\mathrm{Tr}[\mathrm{e}^{-H_1/T_1}]} \otimes \frac{\mathrm{e}^{-H_2/T_2}}{\mathrm{Tr}[\mathrm{e}^{-H_2/T_2}]}, \tag{6.13}$$

with $H_j = \omega_j a_j^\dagger a_j$ being the free Hamiltonian of the jth oscillator, and the index "∞" stands for the stationary state. Also notice that the dynamics of this model is quadratic in ladder operators, hence it preserves Gaussianity of quantum states. Thus, one may equivalently describe this system with the covariance matrix. We remind the definition of the quadratures

$$x_j = \frac{1}{\sqrt{2}}(a_j^\dagger + a_j), \qquad p_j = \frac{i}{\sqrt{2}}(a_j^\dagger - a_j), \tag{6.14}$$

which satisfy the commutation relations $[x_j, p_k] = i\delta_{jk}$, and all the other commutations are zero. With these definitions at hand, the covariance matrix σ is defined as a Hermitian matrix, with the elements $\sigma_{lm} = \frac{1}{2}\langle R_l R_m + R_m R_l\rangle - \langle R_l\rangle\langle R_m\rangle$, and $R_l \in \{x_1, x_2, p_1, p_2\}$. The σ corresponding to the density matrix of Eq. (6.13) is the following diagonal matrix

$$\sigma^{\infty}_{J=0} = \begin{pmatrix} N_1 + \frac{1}{2} & 0 & 0 & 0 \\ 0 & N_2 + \frac{1}{2} & 0 & 0 \\ 0 & 0 & N_1 + \frac{1}{2} & 0 \\ 0 & 0 & 0 & N_2 + \frac{1}{2} \end{pmatrix}. \tag{6.15}$$

For a non-zero tunneling, the covariance matrix is not diagonal anymore, as the tunneling establishes correlations amongst the two HOs. It is rather given by the following expression [118],

$$\sigma^{\infty} = \zeta \begin{pmatrix} D + N_1 + \frac{1}{2} & -\Delta C & 0 & \gamma C \\ -\Delta C & D + N_2 + \frac{1}{2} & -\gamma C & 0 \\ 0 & -\gamma C & D + N_1 + \frac{1}{2} & -\Delta C \\ \gamma C & 0 & -\Delta C & D + N_2 + \frac{1}{2} \end{pmatrix}, \tag{6.16}$$

with $\zeta = \frac{\gamma^2+\Delta^2}{4J^2+\gamma^2+\Delta^2}$, $D = \frac{2J^2(N_1+N_2+1)}{\gamma^2+\Delta^2}$, and $C = \frac{J(N_1-N_2)}{\gamma^2+\Delta^2}$.

6.2.1 Estimation of the tunneling strength

We are interested in estimation of the tunneling strength J, when it appears as a perturbation. Specially we aim at finding the ultimate precision of its estimation. Accordingly, we need to identify the SLD associated to J, and whence the corresponding QFI. This is straightforward, as we know that for a Gaussian state, like the one in Eq. (6.16), Λ_J can be expressed as a linear combination of all the second order moments of the quadratures [74, 75], namely

$$\begin{aligned} \Lambda_J = {} & d_1\left(x_1^2 - \sigma^{\infty}_{11}\right) + d_2\left(p_1^2 - \sigma^{\infty}_{33}\right) + d_3\left(x_1 p_1 + p_1 x_1\right) \\ & + d_4\left(x_2^2 - \sigma^{\infty}_{22}\right) + d_5\left(p_2^2 - \sigma^{\infty}_{44}\right) + d_6\left(x_2 p_2 + p_2 x_2\right) \\ & + c_1\left(x_1 x_2 - \sigma^{\infty}_{12}\right) + c_2\left(x_1 p_2 - \sigma^{\infty}_{14}\right) + c_3\left(p_1 x_2 - \sigma^{\infty}_{32}\right) + c_4\left(p_1 p_2 - \sigma^{\infty}_{34}\right), \end{aligned} \tag{6.17}$$

with d_js and c_js being coefficients which are yet to be determined. To this end, we make benefit of the fact that for any observable $\hat{O}$ we have

$$\partial_J \left\langle \hat{O} \right\rangle_{J=0} = \frac{1}{2} \left\langle \Lambda_J \hat{O} + \hat{O} \Lambda_J \right\rangle_{J=0}. \tag{6.18}$$

Note that both sides are evaluated at $J = 0$, as we consider the coupling to appear as a perturbation around zero. Next, we imply this relation to all of the quadratic observables appearing

in (6.17), i.e., we choose $\hat{O} \in \{x_1^2, x_2^2, x_1 p_1 + p_1 x_1, \ldots\}$. With this choice of $\hat{O}$, the left hand side of Eq. (6.18) can be evaluated by taking derivative from the covariance matrix σ^∞. Moreover, by using the Wick's theorem for Gaussian distributions [120], one can easily simplify the right hand side and write it down in terms of the elements of σ^∞ as well. We shall start by focusing on the local terms. As an example, for x_1^2 we have

$$\begin{aligned} \frac{1}{2}\left\langle \Lambda_J x_1^2 + x_1^2 \Lambda_J \right\rangle_{J=0} &= \left(\partial_J \sigma^\infty_{11}\right)_{J=0} \\ \Rightarrow 2d_1 (\sigma^\infty_{11})^2_{J=0} - \frac{d_2}{2} &= 0, \end{aligned} \tag{6.19}$$

where we used the fact that $\sigma^\infty_{J=0}$, has no off-diagonal terms, as stated by Eq. (6.15). For p_1^2 we find a very similar equation, with the change of coefficients $d_1 \leftrightarrow d_2$. This implies that, $d_1 = d_2 = 0$. In the same manner, one can find that $d_4 = d_5 = 0$. For the other two local terms i.e., $\left\{\frac{1}{2}(x_1 p_1 + p_1 x_1), \frac{1}{2}(x_2 p_2 + p_2 x_2)\right\}$ we have

$$d_3 \left[2(\sigma^\infty_{11})_{J=0}(\sigma^\infty_{33})_{J=0} + \frac{1}{2}\right] = 0, \qquad d_6 \left[2(\sigma^\infty_{22})_{J=0}(\sigma^\infty_{44})_{J=0} + \frac{1}{2}\right] = 0, \tag{6.20}$$

whence, $d_3 = d_6 = 0$ as well. This confirms that the coefficients associate to local observables are zero, i.e., $d_i = 0\ \forall i$. Thus, it is impossible to detect the perturbation (in the linear response regime) by local measurements on individual oscillators. In other words, the linear response of any local observable to the perturbation is zero. However, the non-local coefficients are non-zero. For $\{x_1 x_2, x_1 p_2, p_1 x_2, p_1 p_2\}$ we find

$$\begin{aligned} c_1(\sigma^\infty_{11})_{J=0}(\sigma^\infty_{22})_{J=0} &= (\partial_J \sigma^\infty_{12})_{J=0}, \qquad & c_2(\sigma^\infty_{11})_{J=0}(\sigma^\infty_{44})_{J=0} &= (\partial_J \sigma^\infty_{14})_{J=0}, \\ c_3(\sigma^\infty_{33})_{J=0}(\sigma^\infty_{22})_{J=0} &= (\partial_J \sigma^\infty_{32})_{J=0}, \qquad & c_4(\sigma^\infty_{33})_{J=0}(\sigma^\infty_{44})_{J=0} &= (\partial_J \sigma^\infty_{34})_{J=0}. \end{aligned} \tag{6.21}$$

Or, by using the symmetry in the covariance matrix we can simply write down

$$c_1 = c_4 = \left(\frac{\partial_J \sigma^\infty_{12}}{\sigma^\infty_{11}\sigma^\infty_{22}}\right)_{J=0}, \qquad c_2 = -c_3 = \left(\frac{\partial_J \sigma^\infty_{14}}{\sigma^\infty_{11}\sigma^\infty_{44}}\right)_{J=0}. \tag{6.22}$$

In turn, the SLD at $J = 0$ is simply given by

$$\begin{aligned} \Lambda_0 &= c_1(x_1 x_2 + p_1 p_2) + c_2(x_1 p_2 - p_1 x_2) \\ &= (c_1 + i c_2) a_1^\dagger a_2 + h.c. \end{aligned} \tag{6.23}$$

From here one finds the corresponding QFI easily with the help of $\mathcal{F}_J = \mathrm{Tr}\left(\rho\Lambda_J^2\right)$, and again, by using the Wick's theorem

$$\begin{aligned}\mathcal{F}_J &= 2c_1^2\left(\sigma_{11}^{\infty}\sigma_{22}^{\infty} - \frac{1}{4}\right) + 2c_2^2\left(\sigma_{11}^{\infty}\sigma_{44}^{\infty} - \frac{1}{4}\right) \\ &= 2\frac{\sigma_{11}^{\infty}\sigma_{22}^{\infty} - \frac{1}{4}}{(\sigma_{11}^{\infty}\sigma_{22}^{\infty})^2}\left[\left(\partial_J\sigma_{12}^{\infty}\right)^2 + \left(\partial_J\sigma_{14}^{\infty}\right)^2\right] \\ &= \left[\frac{2N_1N_2 + N_1 + N_2}{(N_1+\frac{1}{2})^2(N_2+\frac{1}{2})^2}\right]\frac{(N_1-N_2)^2}{\gamma^2+\Delta^2}. \end{aligned} \tag{6.24}$$

It is interesting to look at a case when the temperature of the baths and the frequencies of the two HOs are close to one another. Concretely, let $T_2 = T_1 + \delta T$, $\delta T \ll T_1 \equiv T$, and $\Delta \ll \omega$. Thus, in Eq. (6.24), for the terms in the bracket, we can replace $N_2 \cong N_1 \equiv N = (e^{\omega/T} - 1)^{-1}$. However, the expression in the parenthesis shall be treated as a differential term, i.e., $N_1 - N_2 \equiv dN$, which depends on two variables, the temperature gradient δT and the frequency detuning Δ. One can write it as

$$\begin{aligned} dN &= -\delta T\partial_T(e^{\omega/T} - 1)^{-1} + \Delta\partial_\omega(e^{\omega/T} - 1)^{-1} \\ &= -\frac{\omega\delta T}{T^2}N(N+1) + \frac{\Delta}{T}N(N+1). \end{aligned} \tag{6.25}$$

Putting everything together, the QFI reads as follows

$$\mathcal{F}_J = 2\frac{N^3(N+1)^3}{(N+\frac{1}{2})^4}\frac{(\Delta - \omega\frac{\delta T}{T})^2}{T^2(\Delta^2+\gamma^2)}. \tag{6.26}$$

One can see that the difference between the detuning and the temperature gradient, i.e., $\Delta - \omega\frac{\delta T}{T}$, plays a crucial role in estimation of J. Particularly, for a fixed δT, the best performance is realized when $\Delta = 0$. This leads to a QFI that increases quadratically with δT (yet we should keep $\delta T \ll T$).

6.2.2 Estimation of temperature gradient between two baths

In Chapter 4 we used the coupled HOs to estimate the temperature of a thermal bath. Specifically, we observed that the coupling between the two oscillators boosts the thermometry precision considerably. Here, we address the same problem, in the non-equilibrium regime. We are particularly interested in identifying the optimal measurement for thermometry, its sensitivity, and how the correlation between the two HOs enters the problem.

Concretely, let $T_2 = T_1 + \delta T$, whence, our task is to estimate δT i.e., the temperature gradient. For simplicity, we work in the regime where $\Delta \ll \omega = 1$, and $\delta T \ll T_1 \equiv T$, but we do not put any limit on the coupling J. In order to find $\Lambda_{\delta T}$, the SLD associated to the temperature gradient,

we rewrite Eq. (6.17), with new coefficients to be determined

$$\begin{aligned}\Lambda_{\delta T} = & d_1'\left(x_1^2-\sigma_{11}^{\infty}\right)+d_2'\left(p_1^2-\sigma_{33}^{\infty}\right)+d_3'\left(x_1p_1+p_1x_1\right)\\ & +d_4'\left(x_2^2-\sigma_{22}^{\infty}\right)+d_5'\left(p_2^2-\sigma_{44}^{\infty}\right)+d_6'\left(x_2p_2+p_2x_2\right)\\ & +c_1'\left(x_1x_2-\sigma_{12}^{\infty}\right)+c_2'\left(x_1p_2-\sigma_{14}^{\infty}\right)+c_3'\left(p_1x_2-\sigma_{32}^{\infty}\right)+c_4'\left(p_1p_2-\sigma_{34}^{\infty}\right).\end{aligned} \tag{6.27}$$

Since the temperature gradient is evaluated around $\delta T = 0$, the off-diagonal terms of $(\sigma^{\infty})_{\delta T=0}$ vanish. Further, similar to the estimation of coupling constant, Eq. (6.18), we shall find the linear response of different observables to δT. For instance for x_1^2 we have the following

$$(\partial_{\delta T}\sigma_{11}^{\infty})_{\delta T=0} = 2d_1'(\sigma_{11}^{\infty})_{\delta T=0}^2 - \frac{d_2'}{2}. \tag{6.28}$$

Analogous expressions can be found for the other diagonal terms. Solving them simultaneously gives

$$d_1' = d_2' = \left(\frac{\partial_{\delta T}\sigma_{11}^{\infty}}{2(\sigma_{11}^{\infty})^2-\frac{1}{2}}\right)_{\delta T=0}, \qquad d_4' = d_5' = \left(\frac{\partial_{\delta T}\sigma_{22}^{\infty}}{2(\sigma_{22}^{\infty})^2-\frac{1}{2}}\right)_{\delta T=0}. \tag{6.29}$$

For the local off-diagonal terms, such as $x_1p_1 + h.c.$ one finds

$$(\partial_{\delta T}\sigma_{13}^{\infty})_{\delta T=0} = d_3'\left[2\left(\sigma_{11}^{\infty}\ \sigma_{33}^{\infty}\right)_{\delta T=0}+\frac{1}{2}\right] \Rightarrow d_3' = 0. \tag{6.30}$$

Therefore $d_3' = d_6' = 0$. It remains to determine the off-diagonal non-local terms. These are easily evaluated as follows

$$(\partial_{\delta T}\sigma_{12}^{\infty})_{\delta T=0} = c_1'\left(\sigma_{11}^{\infty}\ \sigma_{22}^{\infty}\right)_{\delta T=0} \Rightarrow c_1' = \left(\frac{\partial_{\delta T}\sigma_{12}^{\infty}}{\sigma_{11}^{\infty}\ \sigma_{22}^{\infty}}\right)_{\delta T=0}. \tag{6.31}$$

Putting everything together, the SLD simplifies to

$$\Lambda_{\delta T} = d_1'\left(x_1^2+p_1^2-2(\sigma_{11}^{\infty})_{\delta T=0}\right)+d_4'\left(x_2^2+p_2^2-2(\sigma_{22}^{\infty})_{\delta T=0}\right)+c_1'(x_1x_2+p_1p_2)+c_2'(x_1p_2-p_1x_2), \tag{6.32}$$

with the coefficients

$$\begin{aligned} d_1' &= \left(\frac{\partial_{\delta T}\sigma_{11}^{\infty}}{2(\sigma_{11}^{\infty})^2-\frac{1}{2}}\right)_{\delta T=0}, & d_4' &= \left(\frac{\partial_{\delta T}\sigma_{22}^{\infty}}{2(\sigma_{22}^{\infty})^2-\frac{1}{2}}\right)_{\delta T=0},\\ c_1' &= \left(\frac{\partial_{\delta T}\sigma_{12}^{\infty}}{\sigma_{11}^{\infty}\ \sigma_{22}^{\infty}}\right)_{\delta T=0}, & c_2' &= \left(\frac{\partial_{\delta T}\sigma_{14}^{\infty}}{\sigma_{11}^{\infty}\sigma_{22}^{\infty}}\right)_{\delta T=0}. \end{aligned} \tag{6.33}$$

Notice that for a vanishing coupling $J = 0$ only d_4' survives. Hence, the optimal measurement becomes a projective energy measurement of the second oscillator. Indeed, this could be already expected considering our results of Chapter 4, in which a single HO in a thermal bath is treated.

On this occasion, the thermal sensitivity is directly given by Eq. (4.20). For non-zero coupling, however, the global observables, like x_1x_2 and p_1p_2, as well as local observables of the first HO, affect the optimal measurement. The impact of each of these observables is determined by the competition between Δ, γ, and J.

Finally, the quantum Fisher information reads as

$$\begin{aligned}\mathcal{F}_{\delta T} &= 4d_1'^2\left[(\sigma_{11}^{\infty})^2_{\delta T=0}-\frac{1}{4}\right]+4d_4'^2\left[(\sigma_{22}^{\infty})^2_{\delta T=0}-\frac{1}{4}\right]+2c_1'^2(\sigma_{11}^{\infty})_{\delta T=0}(\sigma_{22}^{\infty})_{\delta T=0}+2c_2'^2(\sigma_{11}^{\infty})_{\delta T=0}(\sigma_{22}^{\infty})_{\delta T=0}\\ &=\frac{(\partial_{\delta T}\sigma_{11}^{\infty})^2_{\delta T=0}}{(\sigma_{11}^{\infty})^2_{\delta T=0}-\frac{1}{4}}+\frac{(\partial_{\delta T}\sigma_{22}^{\infty})^2_{\delta T=0}}{(\sigma_{22}^{\infty})^2_{\delta T=0}-\frac{1}{4}}+\frac{2(\partial_{\delta T}\sigma_{12}^{\infty})^2_{\delta T=0}}{(\sigma_{11}^{\infty})_{\delta T=0}(\sigma_{22}^{\infty})_{\delta T=0}}+\frac{2(\partial_{\delta T}\sigma_{14}^{\infty})^2_{\delta T=0}}{(\sigma_{11}^{\infty})_{\delta T=0}(\sigma_{22}^{\infty})_{\delta T=0}}\\ &=\left(\frac{4J^4+(2J^2+\Delta^2+\gamma^2)^2}{(4J^2+\Delta^2+\gamma^2)^2}\right)\frac{1}{4T^4}\sinh^{-2}(\frac{1}{2T})+\left(\frac{2(\Delta J)^2+2(\gamma J)^2}{(4J^2+\Delta^2+\gamma^2)^2}\right)\frac{1}{T^4}\sinh^{-2}(\frac{1}{T}).\end{aligned} \tag{6.34}$$

One can further take the derivative of this function with respect to J, and see that the result is always negative (for $J>0$). As a result, increasing the coupling leads to reduction of the temperature sensitivity. This is in contrast with our result when both HOs interact with a single external bath. In that case, the increase of the coupling leads to the enhancement of thermometry precision.

Time evolution of quadratures For our discussions later in Section 7.2, we also address the time evolution of all the second moments under the uncoupled Hamiltonian H_0. We remind the time evolution of local quadratures are given by Eq. (3.56), since the unperturbed dynamics does not mix the modes. These for the jth mode read as

$$\begin{aligned}x_j^2(t) &= e^{-\gamma t}\left(\cos^2(\omega_j t)x_j^2+\sin^2(\omega_j t)p_j^2+\frac{\sin(2\omega_j t)}{2}(x_jp_j+p_jx_j)\right)\\ &\quad+(N_j+\tfrac{1}{2})(1-e^{-\gamma t}),\\ p_j^2(t) &= e^{-\gamma t}\left(\sin^2(\omega_j t)x_j^2+\cos^2(\omega_j t)p_j^2-\frac{\sin(2\omega_j t)}{2}(x_jp_j+p_jx_j)\right)\\ &\quad+(N_j+\tfrac{1}{2})(1-e^{-\gamma t}),\\ \Big(p_jx_j(t)+x_jp_j(t)\Big) &= e^{-\gamma t}\Big(\cos(2\omega_j t)\Big(x_jp_j+p_jx_j\Big)-\sin(2\omega_j t)\Big(x_j^2-p_j^2\Big)\Big).\end{aligned} \tag{6.35}$$

On top of that, for the non-local terms, by using

$$\begin{aligned}x_j(t) &= \frac{1}{\sqrt{2}}(a_j^{\dagger}(t)+a_j(t)) = \mathrm{e}^{-\gamma/2t}\Big(\cos(\omega_j t)x_j+\sin(\omega_j t)p_j\Big)\\ p_j(t) &= \frac{i}{\sqrt{2}}(a_j^{\dagger}(t)-a_j(t)) = \mathrm{e}^{-\gamma/2t}\Big(-\sin(\omega_j t)x_j+\cos(\omega_j t)p_j\Big),\end{aligned} \tag{6.36}$$

we can easily conclude that

$$
\begin{aligned}
x_1x_2(t) &= \mathrm{e}^{-\gamma t}\Big(\cos(\omega_1 t)\cos(\omega_2 t)x_1x_2 + \cos(\omega_1 t)\sin(\omega_2 t)x_1p_2 \\
&\quad + \sin(\omega_1 t)\cos(\omega_2 t)p_1x_2 + \sin(\omega_1 t)\sin(\omega_2 t)p_1p_2\Big), \\
x_1p_2(t) &= \mathrm{e}^{-\gamma t}\Big(-\cos(\omega_1 t)\sin(\omega_2 t)x_1x_2 + \cos(\omega_1 t)\cos(\omega_2 t)x_1p_2 \\
&\quad - \sin(\omega_1 t)\sin(\omega_2 t)p_1x_2 + \sin(\omega_1 t)\cos(\omega_2 t)p_1p_2\Big), \\
p_1x_2(t) &= \mathrm{e}^{-\gamma t}\Big(-\sin(\omega_1 t)\cos(\omega_2 t)x_1x_2 - \sin(\omega_1 t)\sin(\omega_2 t)x_1p_2 \\
&\quad + \cos(\omega_1 t)\cos(\omega_2 t)p_1x_2 + \cos(\omega_1 t)\sin(\omega_2 t)p_1p_2\Big), \\
p_1p_2(t) &= \mathrm{e}^{-\gamma t}\Big(\sin(\omega_1 t)\sin(\omega_2 t)x_1x_2 - \sin(\omega_1 t)\cos(\omega_2 t)x_1p_2 \\
&\quad - \cos(\omega_1 t)\sin(\omega_2 t)p_1x_2 + \cos(\omega_1 t)\cos(\omega_2 t)p_1p_2\Big).
\end{aligned}
\tag{6.37}
$$

We shall come back to this problem in Section 7.2, where we develop our fluctuation dissipation theory to explore the estimation of a time dependent coupling rate $J(t)$.

6.3 Quantum heat pumps

In the previous section, we dealt with a system simultaneously interacting with two different thermal reservoirs. We saw that the stationary state of such a system is not at thermal equilibrium any more. Such non equilibrium systems, which gives rise to stationary state heat currents, might be used to build a (quantum) heat pump. By quantum heat pump we mean any multi-level device which operates between several heat baths, and is capable of realizing energy-conversion cycles like a refrigerator, or a heat transformer.

6.3.1 Endoreversible and irreversible heat pumps

The simplest quantum heat device is a three or a four-level system, which is simultaneously in contact with three external baths: the 'work', the 'hot', and the 'cold' baths with temperatures $T_w > T_h > T_c$ respectively. In what follows, the heat pump will be either endoreversible (three-level system) or irreversible (four-level system), as schematically shown in Figure 6.4. The total Hamiltonian of the system including the heat pump plus all the baths is given by

$$
H = H_{hp} + \sum_{\alpha\in\{w,h,c\}} H_I^\alpha + \sum_{\alpha\in\{w,h,c\}} H_B^\alpha, \tag{6.38}
$$

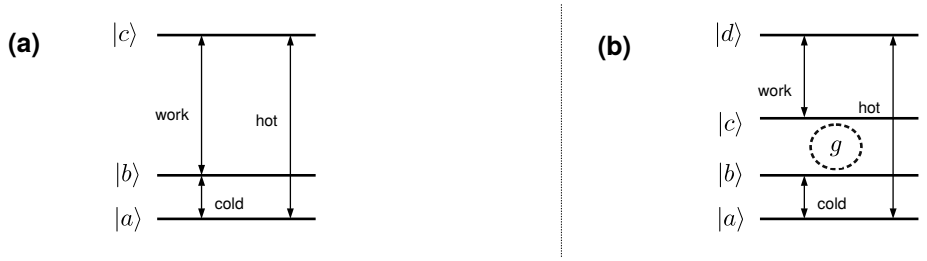

FIGURE 6.4: Schematic illustration of **(a)** a three-level heat pump and **(b)** a four-level irreversible device. The three external heat baths ('work', 'hot' and 'cold') have temperatures $T_w > T_h > T_c$. The arrows indicate *dissipative* coupling between a given heat bath and the corresponding transition. The internal parameter g in the four-level device controls its 'degree of irreversibility' (see text for details).

H_{hp}, being the heat pump Hamiltonian. For the three-level system (also called maser) it is given by

$$H_3 = \omega_c |b\rangle\langle b| + \omega_h |c\rangle\langle c|, \tag{6.39}$$

while for the four-level device it reads as

$$H_4 = \omega_c(|b\rangle\langle b| + |c\rangle\langle c|) + \omega_h |d\rangle\langle d| + g(|b\rangle\langle c| + |c\rangle\langle b|). \tag{6.40}$$

The free Hamiltonian of the bath α, is given by the usual bosonic model

$$H_B^\alpha = \sum_k \omega_{\alpha,k} b_{\alpha,k}^\dagger b_{\alpha,k}. \tag{6.41}$$

Here $\alpha \in \{c,h,w\}$, and the index α,k refers to the mode k of the bath α. Further, we consider three independent interaction terms H_I^α between the heat pump and each bath. The interactions keep the same structure as Eq. (3.43), with $\sigma_x \to \left|\downarrow^\alpha\right\rangle\left\langle\uparrow^\alpha\right| + h.c.$, where $\left|\uparrow^\alpha\right\rangle$ and $\left|\downarrow^\alpha\right\rangle$ represent the two energy levels of heat pump, which are coupled to the bath α. For instance, regarding the maser of Figure 6.4 we have $\left|\downarrow^c\right\rangle = |a\rangle$, and $\left|\uparrow^c\right\rangle = |b\rangle$, and so on. Therefore the interaction with each bath is $H_B^\alpha = \left|\downarrow^\alpha\right\rangle\left\langle\uparrow^\alpha\right| \otimes \mathcal{B}_\alpha + h.c.$, with $\mathcal{B}_\alpha = \sum_k g_{\alpha,k}(b_{\alpha,k} + b_{\alpha,k}^\dagger)$. The corresponding master equation in the interaction picture, under the usual Born-Markov, and the rotating wave approximations, is given by

$$\begin{aligned}
\dot{\rho}_{hp} &= \sum_{\alpha\in\{c,h,w\}} \mathcal{D}_\alpha \rho_{hp} \\
&= \sum_{\alpha\in\{c,h,w\}} \sum_{\omega_\alpha} \Gamma_{\alpha,\omega_\alpha} \left(A_{\alpha,\omega_\alpha} \rho_{hp} A_{\alpha,\omega_\alpha}^\dagger - \tfrac{1}{2} \left\{ A_{\alpha,\omega_\alpha}^\dagger A_{\alpha,\omega_\alpha}, \rho_{hp} \right\} \right) \\
&\quad + e^{-\omega_\alpha/T_\alpha} \Gamma_{\alpha,\omega_\alpha} \left(A_{\alpha,\omega_\alpha}^\dagger \rho_{hp} A_{\alpha,\omega_\alpha} - \tfrac{1}{2} \left\{ A_{\alpha,\omega_\alpha} A_{\alpha,\omega_\alpha}^\dagger, \rho_{hp} \right\} \right).
\end{aligned} \tag{6.42}$$

Hence we have one dissipator $\mathcal{D}_\alpha$ per bath. As we discussed earlier in this chapter, each dissipator may include contributions from several open decay channels at frequencies $\{\omega_\alpha\}$. It is

easy to check that the maser has only one open decay channel per bath. The corresponding jump operators of the maser are $A_c = |a\rangle\langle b|$ with ω_c, $A_h = |a\rangle\langle c|$ with ω_h, and $A_w = |b\rangle\langle c|$ with $\omega_w = \omega_h - \omega_c$. For the four-level device, however, this is not the case, since there are two open decay channels in the cold bath and two open decay channels in the work bath [121].

The presence of multiple thermal reservoirs in the master equation (6.42) results in a non-equilibrium stationary state ρ_∞. This non-equilibrium state means that there are some heat currents from the heat devise to each bath. The heat current from the bath α is defined as $\dot{Q}_\alpha = \mathrm{Tr}(H_3 \mathcal{D}_\alpha(\rho_\infty))$. It is not difficult to check that

$$\dot{Q}_\alpha = \sum_{\omega_\alpha} \Gamma_{\alpha,\omega_\alpha}\ \omega_\alpha (e^{-\omega_\alpha/T_\alpha} p_\downarrow^{\alpha,\omega_\alpha} - p_\uparrow^{\alpha,\omega_\alpha}), \tag{6.43}$$

where $p_\uparrow^{\alpha,\omega_\alpha} = \mathrm{Tr}(A_{\alpha,\omega_\alpha}^\dagger A_{\alpha,\omega_\alpha}\rho_\infty)$, and $p_\downarrow^{\alpha,\omega_\alpha} = \mathrm{Tr}(A_{\alpha,\omega_\alpha} A_{\alpha,\omega_\alpha}^\dagger \rho_\infty)$ are the stationary state populations of the energy levels involved in the transition governed by A_{α,ω_α}. Then, Eq. (6.42) dictates that $\sum_\alpha \dot{Q}_\alpha = 0$, which is the first law of thermodynamics. In addition, the second law of thermodynamics implies that $S = \sum_\alpha \dot{Q}_\alpha / T_\alpha \leq 0$, i.e., the entropy of the system never decreases.

It is instructive to define τ_α the internal spin-temperatures (a.k.a. virtual temperature) associated to each transition of open decay channels []. This reads as

$$\tau_\alpha = \frac{\omega_\alpha}{\log(p_\downarrow^{\alpha,\omega_\alpha}/p_\uparrow^{\alpha,\omega_\alpha})}. \tag{6.44}$$

For models with one open decay channel per bath, like the maser, one might confirm that $T_\alpha > \tau_\alpha$ implies $\dot{Q}_\alpha > 0$, i.e, the heat flows from the bath α to the heat pump. In contrast, for $T_\alpha < \tau_\alpha$ the heat flows in the opposite direction, from the heat pump to the bath. This makes the definition of internal temperature more insightful. If the bath is hotter than the corresponding internal temperature, the heat pump absorbs the energy, and vice versa. In addition, if a bath has the same temperature as the internal temperature, the heat current from that bath is zero. One might easily show that a global equilibrium, (i.e., $\dot{Q}_\alpha = \ \forall\alpha$) is possible. We just need to choose the cold transition frequency to satisfy $\omega_c = \omega_h \frac{T_c(T_w - T_h)}{T_h(T_w - T_c)} \equiv \omega_c^{rev}$. Here we label this frequency with the index *rev*, since the entropy production is zero, and the process is *reversible*. Generally speaking, for models with one open decay channel per heat bath, we can always find a reversibility criteria. Therefore these models, whose source of irreversibility is only due to a mismatch between the external and internal temperatures, are referred to as *endoriverssible*. In contrary, in case of multiple open decay channels for a bath, like the cold and warm baths in the four-level device, there are multiple internal temperatures as well. As a result, the bath temperature might not be equal to all of the internal temperatures simultaneously, posing a problem for achieving reversibility. Such heat devices are referred to as *irreversible*.

For an endoreversible heat pump, by choosing $\omega_c < \omega_c^{rev}$, it is guaranteed that the system performs as a refrigerator with $\dot{Q}_c > 0$, $\dot{Q}_w > 0$, and $\dot{Q}_h < 0$. In contrary, for $\omega_c > \omega_c^{rev}$ the device

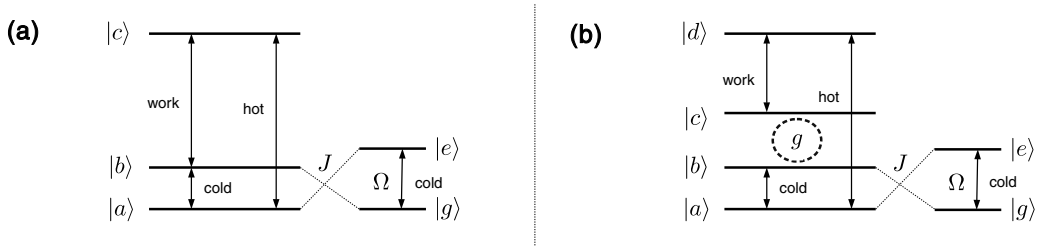

FIGURE 6.5: Schematic illustration of **(a)** a three-level heat pump and **(b)** a four-level irreversible device coupled to a tunable two-level probe of frequency Ω, with coupling strength J. The three external heat baths ('work', 'hot' and 'cold') have temperatures $T_w > T_h > T_c$. The arrows indicate *dissipative* coupling between a given heat bath and the corresponding transition. The internal parameter g in the four-level device controls its 'degree of irreversibility' (see text for details).

operates as a heat transformer with $\dot{Q}_c < 0$, $\dot{Q}_w < 0$, and $\dot{Q}_h > 0$.

In what follows we focus on answering some relevant questions regarding the performance of a quantum heat pump. Namely, is it an irreversible device, or it is just endoreversible? Is it performing as a heat transformer, or as a refrigerator? And is it possible to estimate its coefficient of performance?

6.3.2 Probing a quantum heat pump

In this section we propose a protocol for probing a quantum heat pump, in order to answer to the questions which were arose in the previous section. To this end, we couple the heat device to the simplest possible probe, a two-level spin, as depicted in Figure 6.5. We label the ground state of the spin by $|g\rangle$, and its excited state by $|e\rangle$. Let the energy gap of the two-levels be Ω, such that the free Hamiltonian of the probe reads as $H_p = \Omega|e\rangle\langle e|$.

The interaction between the probe and the heat device is realized by a flip-flop term, corresponding to any of the transitions of the system. The probe independently interacts with the corresponding bath as well. In the rest of this section we place the probe in the cold bath, and couple it to the heat pump transition between the levels $|a\rangle$ and $|b\rangle$, as illustrated in Figure 6.5. The system Hamiltonian is

$$H_S = H_{hp} + H_p + J(|a,e\rangle\langle b,g| + |b,g\rangle\langle a,e|), \tag{6.45}$$

where we assume J, the interaction strength, to be weak enough not to disturb the heat pump significantly. Keep in mind that we refer to the heat pump plus the probe as *system*. The idea is to find the system's stationary state. Then by tracing out the heat pump, and measuring only the probe, we collect necessary information about the device.

The rest of our analysis is model dependent, and we address the maser and the four-level heat device separately.

Probing the endoreversible maser

First we focus on probing the endoreversible maser. The free Hamiltonian of the system, including the maser and the spin is

$$H_{3,p} = \omega_c |b\rangle\langle b| + \omega_h |c\rangle\langle c| + \Omega |e\rangle\langle e| + J(|a,e\rangle\langle b,g| + |b,g\rangle\langle a,e|). \tag{6.46}$$

Together with the baths and their interactions with the system, one might write down the total Hamiltonian

$$\begin{aligned} H = \sum_{\alpha\in\{c,w,h\}} H_B^\alpha + H_{3,p} + (|a\rangle\langle b| + |g\rangle\langle e| + h.c.)\otimes\mathcal{B}_c \\ + (|b\rangle\langle c| + h.c.)\otimes\mathcal{B}_w + (|a\rangle\langle c| + h.c.)\otimes\mathcal{B}_h. \end{aligned} \tag{6.47}$$

In order to find the jump operators of the Lindbladian master equation, we need to expand the system interaction operators, i.e., those appearing in the parenthesis in Eq. (6.47), in the system's basis. First, notice that the eigenvalues of $H_{3,p}$ are $E_1 = 0$, $E_2 = \frac{1}{2}\left(\omega_c + \Omega - \sqrt{4J^2 + (\omega_c - \Omega)^2}\right)$, $E_3 = \frac{1}{2}\left(\omega_c + \Omega + \sqrt{4J^2 + (\omega_c - \Omega)^2}\right)$, $E_4 = \omega_c + \Omega$, $E_5 = \omega_h$, and $E_6 = \omega_h + \Omega$, while the corresponding eigenvectors are $|1\rangle = |a,g\rangle$, $|2\rangle = \mathcal{N}_2^{-1}\left[(E_2 - \omega_c)|a,e\rangle + J|b,g\rangle\right]$, $|3\rangle = \mathcal{N}_3^{-1}\left[(E_3 - \omega_c)|a,e\rangle + J|b,g\rangle\right]$, $|4\rangle = |b,e\rangle$, $|5\rangle = |c,g\rangle$, and $|6\rangle = |c,e\rangle$ ($\mathcal{N}_2$ and $\mathcal{N}_3$ are just normalization constants). It thus follows that the work bath interacts with the maser-spin system at the Bohr frequencies $\omega_h - E_2$, $\omega_h - E_3$ and $\omega_h - \omega_c$, which correspond to jump operators $A_{w,\omega_h - E_2} = \langle 2|b,g\rangle|2\rangle\langle 5|$, $A_{w,\omega_h - E_3} = \langle 3|b,g\rangle|3\rangle\langle 5|$, and $A_{w,\omega_h - \omega_c} = |6\rangle\langle 4|$. Likewise, the hot bath contributes with three decay channels to the master equation: $A_{h,\omega_h} = |1\rangle\langle 5|$, $A_{h,\omega_h + \Omega - E_2} = \langle 2|a,e\rangle|2\rangle\langle 6|$, and $A_{h,\omega_h + \Omega - E_3} = \langle 3|a,e\rangle|3\rangle\langle 6|$. There are also five transitions between energy eigenstates coupled to the cold bath, namely $|1\rangle \leftrightarrow |2\rangle$, $|3\rangle \leftrightarrow |4\rangle$, $|1\rangle \leftrightarrow |3\rangle$, $|2\rangle \leftrightarrow |4\rangle$, and $|5\rangle \leftrightarrow |6\rangle$. However, transitions $|1\rangle \leftrightarrow |2\rangle$ and $|3\rangle \leftrightarrow |4\rangle$ have the *same* associated Bohr frequency E_2. As a result, both are accounted for by a single jump operator $A_{c,E_2} = (\langle a,e|2\rangle + \langle b,g|2\rangle)|1\rangle\langle 2| + (\langle 3|a,e\rangle + \langle 3|b,g\rangle)|3\rangle\langle 4|$. In the case of transitions $|1\rangle \leftrightarrow |3\rangle$ and $|2\rangle \leftrightarrow |4\rangle$, these enter the master equation through the operator $A_{c,E_3} = (\langle a,e|3\rangle + \langle b,g|3\rangle)|1\rangle\langle 3| + (\langle 2|a,e\rangle + \langle 2|b,g\rangle)|2\rangle\langle 4|$. Finally, the process $|5\rangle \leftrightarrow |6\rangle$ is represented simply by $A_{c,\Omega} = |5\rangle\langle 6|$. It remains to address the decay rates, $\Gamma_{\alpha,\omega_\alpha}$. We use the expression for an electromagnetic radiation field at thermal equilibrium in a three dimensional box, thus $\Gamma_{\alpha,\omega_\alpha} = \gamma\omega_\alpha^3(1 + N_{\omega_\alpha,T_\alpha})$, where $N_{\omega_\alpha,T_\alpha} = (e^{\omega_\alpha/T_\alpha} - 1)^{-1}$ is the bosonic thermal occupation number [28].

With all of these at hand, one might solve the stationary state $\rho_{3,p}^\infty$ of the maser-probe system. Therefore, as already mentioned, after tracing out the heat-pump (the maser), we have the stationary state of the probe $\rho_p^\infty = \mathrm{Tr}_3(\rho_{3,p}^\infty)$. In general, this density matrix is not diagonal in the energy basis, and coherence is present. However, we limit ourselves to population measurements in the energy basis (therefore we are not performing the most precise measurement, since

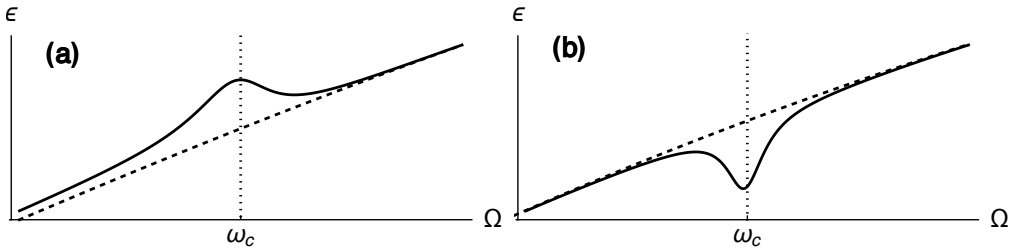

FIGURE 6.6: (solid line) Polarization bias ϵ of the two-level probe as a function of its frequency Ω, while scanning the 'cold transition' of a three-level maser [cf. Figure 6.5(a)] **(a)** in the chiller mode ($\omega_c = 3/4\,\omega_{c,\mathrm{rev}}$), and **(b)** in the heat transformer mode ($\omega_c = 5/4\,\omega_{c,\mathrm{rev}}$). The dashed lines indicate the corresponding equilibrium polarization bias at temperature T_c, and the vertical dotted lines highlight the resonance condition $\Omega = \omega_c$. Specifically, in these plots $T_w = 30$, $T_h = 20$, $T_c = 10$, $\omega_h = 40$, and $J = 0.1$, in units of $\hbar = k_B = 1$. See text for discussion.

we ignore the information registered in the off-diagonal of the ρ_p^∞). Specifically, we study the polarization bias of the spin, $\epsilon \equiv \langle g|\rho_p^\infty|g\rangle - \langle e|\rho_p^\infty|e\rangle$, and compare it with its equilibrium value, $\epsilon_{eq} = (e^{\Omega/Tc} - 1)/(e^{\Omega/Tc} + 1)$. In Figure 6.6 we plot both, versus the frequency Ω in two different regimes. Panel (**a**) corresponds to $\omega_c < \omega_{c,rev}$, and the heat pump performs as a refrigerator. In this case, the polarization bias is slightly larger than its equilibrium value, with a significant pick only close to $\Omega \approx \omega_c$. In contrast, panel (**b**), with $\omega_c > \omega_{c,rev}$, corresponds to a heat transformer. The polarization bias is slightly smaller than its equilibrium value, with a significant drop only close to $\Omega \approx \omega_c$.

Both figures suggest that the energy exchange between the probe and the heat device is efficient only if Ω is close to resonance with ω_c. Otherwise, the probe thermalizes with the cold bath, as if it was not interacting with the heat pump.

Further, one can explain why the polarization bias falls above/below the equilibrium polarization for the refrigerator/heat transformer. For instance, in the refrigeration regime, the probing spin might be considered as an intermediate systems between the bath at T_c, and the *virtual spin* with $\tau_c < T_c$. As a result, the probing spin acquires its own virtual temperature τ_p, defined in terms of its ground and excited state populations. This temperature is between τ_c and T_c, in order to compromise. Since $\tau_p < T_c$, the polarization bias is larger than its equilibrium value at T_c.

Probing the irreversible four-level heat pump

The free Hamiltonian corresponding to the four-level heat devise plus the probing spin (panel **b** in Figure 6.5), is

$$H_{4,p} = \omega_c(|b\rangle\langle b| + |c\rangle\langle c|) + \omega_h|d\rangle\langle d| + g(|b\rangle\langle c| + |c\rangle\langle b|) + \Omega|e\rangle\langle e| + J(|a,e\rangle\langle b,g| + |b,g\rangle\langle a,e|). \tag{6.48}$$

The eigenvalues of this Hamiltonian are $E_1 = 0$, $E_2 = \omega_c + \Omega - g$, $E_3 = \omega_c + \Omega + g$, $E_4 = \omega_h$, $E_5 = \omega_h + \Omega$, and the three real solutions of

$$E_i^3 - (\Omega + 2\omega_c)E_i^2 + (\omega_c^2 + 2\Omega\omega_c - g^2 - J^2)E_i + (g^2\Omega + J^2\omega_c - \Omega\omega_c^2) = 0, \quad i \in \{6,7,8\}. \tag{6.49}$$

The associated eigenvectors write as $|1\rangle = |a,g\rangle$, $|2\rangle = \frac{1}{\sqrt{2}}(|b,e\rangle - |c,e\rangle)$, $|3\rangle = \frac{1}{\sqrt{2}}(|b,e\rangle + |c,e\rangle)$, $|4\rangle = |d,g\rangle$, $|5\rangle = |d,e\rangle$, and $|i\rangle = \mathcal{N}_i^{-1}[((E_i - \omega_c)^2 - g^2)|a,e\rangle + J(E_i - \omega_c)|b,g\rangle + gJ|c,g\rangle]$, where $i \in \{6,7,8\}$, and $\mathcal{N}_i$ are the corresponding normalization constants.

Moreover, the total Hamiltonian of the system plus the baths is

$$H = \sum_{\alpha\in\{c,w,h\}} H_B^\alpha + H_{4,p} + (|a\rangle\langle b| + |g\rangle\langle e| + h.c.)\otimes\mathcal{B}_c + (|c\rangle\langle d| + h.c.)\otimes\mathcal{B}_w + (|a\rangle\langle d| + h.c.)\otimes\mathcal{B}_h. \tag{6.50}$$

In this case, the work, hot and cold baths couple to five, four and ten energy transitions respectively. In general, each of these corresponds to a distinct open decay channel, since they all have different Bohr frequencies[3]. The Lindblad operators are ($i \in \{6,7,8\}$)

$$A_{w,\omega_h-\omega_c+g} = |2\rangle\langle 5|/\sqrt{2}, A_{w,\omega_h-\omega_c-g} = |3\rangle\langle 5|/\sqrt{2}, A_{w,E_i-\omega_h} = \langle c,g|i\rangle|4\rangle\langle i|,$$

$$A_{h,\omega_h} = |1\rangle\langle 4|, A_{h,E_i-\Omega-\omega_h} = \langle a,e|i\rangle|5\rangle\langle i|,$$

$$A_{c,E_i} = (\langle a,e|i\rangle + \langle b,g|i\rangle)|1\rangle\langle i|, A_{c,E_i+g-\Omega-\omega_c} = -(\langle a,e|i\rangle + \langle b,g|i\rangle - \langle c,g|i\rangle)|2\rangle\langle i|/\sqrt{2},$$
$$A_{c,E_i-g-\Omega-\omega_c} = (\langle a,e|i\rangle + \langle b,g|i\rangle + \langle c,g|i\rangle)|3\rangle\langle i|/\sqrt{2}, A_\Omega = |4\rangle\langle 5|.$$

Again, by finding $\rho_{4,p}$, the stationary state of the system, and by tracing out the four-level heat pump, we reach at the stationary state of the probing spin $\rho_p = \mathrm{Tr}_4(\rho_{4,p})$. The polarization bias of the spin, in the refrigeration regime with $\omega_c\omega_{c,rev}$ is illustrated in panel (**a**) of Figure 6.7. One can pinpoint the two open decay channel frequencies at $\omega_c \pm g$. As pointed out in the previous section, the fact that the polarization bias peaks around these frequencies indicates cooperative

[3]However, at $\Omega = \omega_c$ one finds that $E_7 = \omega_c$ and hence, the hot decay channels at frequencies ω_h and $\omega_h + \Omega - E_7$ merge.

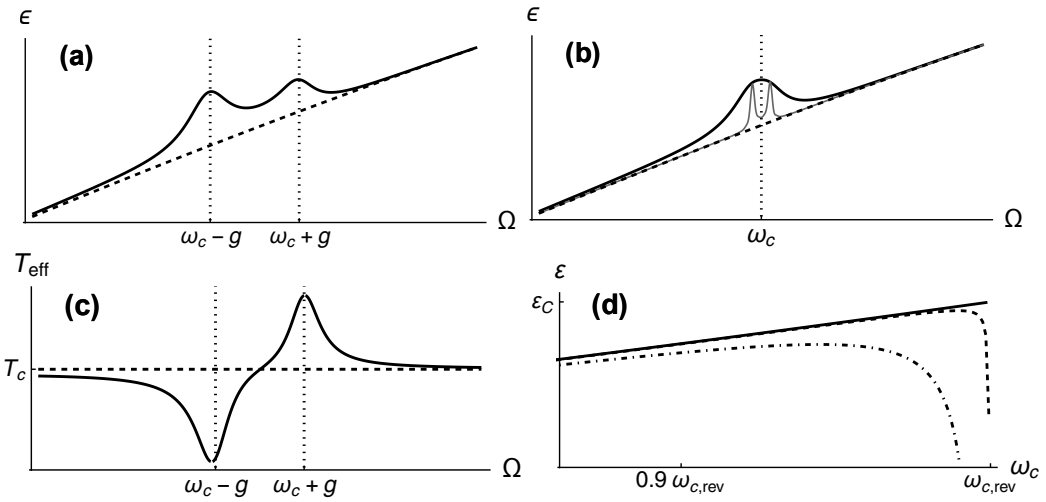

FIGURE 6.7: **(a)** (solid black) Polarization bias ϵ of the auxiliary two-level spin as a function of Ω, when coupled to the cold transition of an irreversible four-level chiller with $g = 0.5$ and $J = 0.1$. The dashed and dotted lines represent the equilibrium bias and the resonance conditions $\Omega = \omega_c \pm g$. **(b)** Same as (a), with $g = 0.1$ and $J = 0.1$. The thin solid gray line stands for the polarization bias resulting from the weaker coupling $J = 0.01$. **(c)** Spin temperature of the probe $T_{\rm eff} = -\Omega/\log[(\epsilon - 1/2)/(\epsilon + 1/2)]$ versus Ω during the scan of an irreversible four-level chiller with $g = 0.5$ at $\omega_c = \omega_{c,\rm rev}$. **(d)** (solid) Coefficient of performance (COP) $\varepsilon = \omega_c/(\omega_h - \omega_c)$ of an endoreversible chiller as a function of ω_c. The dashed and dot-dashed curves correspond to the COP of the irreversible four-level chiller, with $g = 0.1$ and $g = 0.5$, respectively. All other parameters are the same as in Figure 6.6(a).

heat absorption from the cold heat bath by the two detuned elementary cycles conforming the heat device.

However, it may be the case that the separation between open decay channels is smaller or of the order of the spin-device coupling constant J. We may then be unable to resolve the dissipative spectrum. This is illustrated by the solid black curve in panel (**b**) of Figure 6.7. Reducing the coupling J thus allows to increase the resolution of the scan[4] and certify unambiguously the irreversibility of the heat pump. See the thin gray curve in the same figure.

As already mentioned, the existence of decay channels with different frequencies at the interfaces with two or more heat baths gives rise to two distinct effects: The detuning between the various elementary stages that make up the device facilitates the direct heat transfer between baths, i.e. *heat leaks*, and it also results in different stationary rates of energy exchange for each of those constituent stages. As a result, for certain choices of parameters (usually close to $\omega_c = \omega_{c,\rm rev}$) some stages within the device may be operating as absoprtion chillers, while some others may be releasing heat into the cold bath as heat transformers. We refer to this competition as *internal dissipation* [122]. Probing an irreversible heat device may give direct evidence of internal dissipation, as it is the case in Figure 6.7(**c**). There, we plot the stationary spin temperature of the external probe as a function of the probing frequency Ω, precisely at $\omega_c = \omega_{c,\rm rev}$. We can see how the stage at frequency $\omega_c - g$ absorbs heat from the cold reservoir, ultimately

[4]Recall that fixing the dissipation rate γ sets a lower bound on J for consistency with Eq. (6.42).

lowering the spin temperature of the resonant probe, whereas the stage at $\omega_c + g$ is effectively hotter than its environment and thus, releases heat on average. The only reason for choosing T_{eff} instead of ϵ is to graphically accentuate this effect.

6.3.3 Estimating the coefficient of performance of a quantum heat pump

So far we have been able to identify the frequencies of the dissipative spectrum of a multi-level heat device and to assess the direction of its steady-state heat currents. Probing a quantum heat pump with a two-level spin also allows to give an estimate of its *coefficient of performance* (COP), a figure of merit central to thermal engineering. The COP captures the cost-efficiency of the thermodynamic cycle being implemented: For instance, in the case of a quantum absorption refrigerator, it would be defined as $\varepsilon \equiv \dot{Q}_c/\dot{Q}_w$, that is, the 'useful effect' divided by the corresponding 'energy cost'.

In an endoreversible quantum heat device, the stationary rate $\mathcal{I}$ at which energy is exchanged with all three heat baths is identical [123] and the corresponding steady-state heat currents read $\dot{Q}_\alpha = \omega_\alpha \mathcal{I}$. Consequently, the COP of e.g. an endoreversible quantum absorption chiller would be given by just the ratio of the frequencies of the cold and work contact ports $\varepsilon = \omega_c/\omega_w = \omega_c/(\omega_h - \omega_c)$. Hence, estimating the COP of any endoreversible device only takes to probe it through two of its frequency filters so as to find the corresponding decay channels.

If the device does not deviate significantly from endoreversibility, i.e. if the frequencies of its open decay channels do not spread out too much, as it is the case in Figure 6.7(**b**), it will be described reasonably well by an endoreversible model. In particular, its COP may be well approximated as $\varepsilon \simeq \omega_c/(\omega_h - \omega_c)$. This is illustrated in Figure 6.7(**d**), where the COP of an endoreversible three-level chiller (solid line) is compared with the actual ε of two irreversible four-level refrigerators with $g = 0.1$ (dashed line) and $g = 0.5$ (dot-dashed line), as calculated from the exact steady-state heat currents $\dot{Q}_\alpha$. As we can see, for the low-irreversibility setting of Figure 6.7(**b**), the disagreement only becomes important when operating close to the Carnot COP $\varepsilon_C = \frac{T_c(T_w - T_h)}{T_w(T_h - T_c)}$, while for the more irreversible case portrayed in Figure 6.7(**a**), the approximation is much worse, in general. Note as well that the slight shifts of the peaks/wells in the polarization bias, due to the finite spin-device coupling J, are an additional source of error in the estimation of the COP.

6.4 Summary

In this chapter we have analyzed thermometry and metrology for out-of-equilibrium systems in two different scenarios: (A) Strong interactions with a single bath and (B) Simultaneous contact with multiple baths. Regarding (A) our most remarkable results are:

- Low temperature quantum thermometry boosts strong coupling between probe and system.
- The spectral density of the probe-sample coupling plays an important role in this regime.
- Feasible measurement schemes capable of producing nearly optimal temperature estimates are provided.

These findings may be particularly relevant to practical nanoscale thermometry, taking into account the marked decay of the thermometric precision at low temperatures. It is worth emphasizing that all our results are exact, irrespective of the relative ordering of the various time scales involved in the problem. In particular, the second observation calls for a more in-depth analysis of the potential role of reservoir engineering techniques [124, 125] or even dynamical control [126] in enhanced low-temperature quantum thermometry and will be the subject of further investigation.

Regarding (B), we give thought to two distinct projects: (i) Two coupled harmonic oscillators each embedded on its own thermal bath and (ii) Multilevel quantum heat devices with multiple baths. In the case (i), our main results can be summarized as follows

- We provide metrological bounds to both estimation of temperature gradient, δT, and interaction strength J.
- We identify that estimation of J is only possible with non-local measurements and depends on δT.
- Estimation of δT can be performed with local measurements.

In the case (ii), we show how black-box testing of a multi-level quantum heat device can provide relevant information such as the direction of its steady-state heat currents, its degree of irreversibility, and even a good estimate of its coefficient of performance. All this information may be obtained by simply looking at the departure from thermal equilibrium of the steady state of an external two-level probe coupled to one of the contact transitions of the heat device. Crucially, in this testing protocol, no information about the internal structure of the heat device is required.

In particular, it is possible to identify the frequencies of the open decay channels at the interface of the system and each of the heat baths, and thus, to characterize the various elementary thermodynamic cycles that make up the quantum heat pump. We emphasize that all this is possible without knowledge of the Hamiltonian of the multi-level heat device. In some cases, the competition between these elementary stages, which is a signature of internal dissipation, may be directly witnessed.

For our analysis, we have considered the dissipative dynamics of an absorption three-level maser, which realizes the simplest endoreversible thermodynamic cycle, when dissipatively coupled to our external two-level spin. We have further studied the case of a four-level absorption chiller as the paradigm of the more complex irreversible heat devices.

Our results provide a clear and intuitive picture of the inner workings of generic heat-driven thermodynamic cycles, *beyond specific models*, and they may find applications in the design of cost-efficient nano-engineered thermodynamic devices, or in the characterization of the complex energy-conversion processes taking place in mesoscopic biological systems.

Chapter 7

Quantum metrology beyond thermal equilibrium II: Dynamic systems

In this chapter we present our results regarding metrology in systems out of equilibrium, with a dynamic state. The term *dynamic* refers to the time dependence of the density matrix. On this account, the outcomes of measuring the system depend on the time it is interrogated. We point out two distinct frameworks giving rise to dynamic systems:

1. A system underlying a dynamic with a unique stationary state. Any initial preparation of the system ends up in such a stationary state, after a long enough time. Nevertheless, the system might be measured at a finite time before reaching such stationary state.

2. A system which is prepared in the stationary state of a certain dynamic. In principle, it should rest in such a state forever, however, it does not, due to some external (time dependent) perturbation.

The first layout may be employed to survey thermometry with *partially thermalized* systems, a relevant scheme when the total interaction time is insufficient to produce full thermalization. We optimize the estimation protocol by breaking it down into sequential stages of preparation, thermal contact, and measurement. The second scheme is relevant in study of a systems which undergoes a time dependent *quantum map* which, is not necessarily described by a simple Hamiltonian. Aiming at detection of tiniest external forces, which exert a minimum influence on the system, we develop a powerful framework that generalizes the fluctuation dissipation theorem to Markovian systems out of equilibrium.

The structure of this chapter is as follows: Section 7.1, is dedicated to thermometry with a restricted time. This situation needs a slightly different framework than the usual metrology scenarios, as one has to optimize the quantum Fisher information per time, rather than QFI itself

[12, 14]. By taking this contemplation into account, we observe that frequently interrogated probes initialized in their ground state achieve the best performance. Moreover, analogous to the fully thermalized scenario of section 4.2, we see that the precision of thermometry increases by using probes with more energy levels. However one must perform an optimization to find the best energy gap for the system.

In section 7.2 we investigate a system which is subject to a time dependent perturbation, otherwise it would have been resting at the steady state of a Markovian dynamics. To this end, we rigorously derive a generalization of the fluctuation dissipation theorem (FDT), which can be applied to any system with a Markovian quantum evolution. Our FDT is elegantly established with the assistance of the symmetric logarithmic derivative (SLD). We exploit our FDT in the model of two harmonic oscillators, placed in distinct heat baths. Then, by establishing a modulated interaction among the two oscillators, we study the response of the system. We identify the measurement scheme which can detect the tiniest interaction strength. Specifically, we characterize the best observable for detection of the perturbation, the best modulation frequency, and the optimal interrogation time. Finally In section 7.3 we conclude and summarize.

7.1 Thermometry with partially thermalized probes

In section 4.2, we gave thought to a thermometer which reaches thermal equilibrium with the sample. Then we identified which are the optimal probes that maximize the attainable precision in the estimation of the temperature. Here we address the complementary situation in which the probe does not thermalize completely, due to a constraint on the total estimation time (e.g., the sample may be unstable and exists only for times comparable to the dissipation time scale).

On this account, we analyze the dissipative time evolution of the thermometer, in order to make the most effective use of the thermometric protocol. Concretely, we ask ourselves about the optimal breakup of the total running time of the estimation procedure $\mathcal{T}$, into sequential stages of probe preparation, thermal contact during a time interval t, and measurement, so as to optimize the achievable precision Eq. (2.6). Given that we have access to m copies of the thermometer, the total number of independent repeats is $N = m\mathcal{T}/t$. In turn, the QCRB gets the form

$$\delta T \geq \frac{1}{\sqrt{m\mathcal{T}\mathcal{F}_T(t)/t}}, \tag{7.1}$$

with $\mathcal{F}_T(t)$ being the QFI of a single probe at time t. Therefore, the figure of merit to be maximized is the ratio $\mathcal{F}_T(t)/t$ [12, 14]. We need to mention that, for simplicity, we have assumed that after each interrogation the system will be prepared in the same state. In a more general scenario, one could use the information obtained from each measurement to adaptively prepare a more effective thermometer for the next run.

Since we must monitor the time evolution of the thermometer, it is essential to specify the sample and its coupling with the thermometer. To this end, we shall model the sample as a bosonic heat bath linearly coupled to an arbitrary probe, which we introduced in section 3.3. The total Hamiltonian writes as $H_{\rm tot} = H + \sum_\mu \omega_\mu\ b_\mu^\dagger b_\mu + X \otimes \sum_\mu g_\mu (b_\mu + b_\mu^\dagger)$, where b_μ is the annihilation operator of mode ω_μ in the sample. We choose the probe-sample coupling constants to be $g_\mu = (\gamma\omega_\mu)^{1/2}$, implying flat spectral density $J(\omega) \sim \sum_\mu \frac{g_\mu^2}{\omega_\mu}\,\delta(\omega-\omega_\mu) = \gamma$ [103]. This sets the time-scale $\tau_D \sim \gamma^{-1}$ over which $\rho(t)$ varies appreciably. Tracing out the sample from the overall unitary dynamics and assuming a thermal state χ^T for it, leads to an effective equation of motion of the Lindblad-Gorini-Kossakovski-Sudashan type (LGKS) [127], that follows from $\dot\rho = {\rm Tr}_S \frac{d}{dt}\{e^{-iH_{\rm tot}t}\ \rho(0)\otimes\chi^T\ e^{iH_{\rm tot}t}\}$, after sequentially performing the Born, Markov and rotating-wave approximations (see chapter 3 for a detailed derivation). Note that the Born approximation implies that no correlations are ever created between probe and sample, so the latter remains undisturbed throughout the estimation procedure. Note also that, for consistency with the Markov approximation, the temperature of the sample may be not arbitrarily low, as the thermal fluctuations must remain fast compared with τ_D.

In the interaction picture, the master equation can be cast as

$$\dot\rho = \Gamma_{\Omega,T}\left(A_\Omega \rho A_{-\Omega} - \tfrac{1}{2}\{A_{-\Omega}A_\Omega,\rho\}_+\right) + e^{-\Omega/T}\Gamma_{\Omega,T}\left(A_{-\Omega}\rho A_\Omega - \tfrac{1}{2}\{A_\Omega A_{-\Omega},\rho\}_+\right), \tag{7.2}$$

where $A_{\pm\Omega}$ stands for the relaxation/excitation operator associated with the decay channel at frequency Ω. We remind that these follow from the decomposition of $X = \sum_\Omega A_\Omega$ as sum of eigen-operators of the probe Hamiltonian. We also remind that the thermal state $\rho = \mathcal{Z}^{-1}e^{-H/T}$ is a fixed point of Eq. (7.2) and, choosing a suitable coupling operator X, the open dynamics may also be *ergodic*, thus eventually bringing any initial state to thermal equilibrium.

For a two-level thermometer with Hamiltonian $H = \frac{\Omega}{2}\sigma_z$, we can take, for instance, $X = \sigma_x$ from which $A_\Omega = |-\Omega/2\rangle\langle\Omega/2|$, while $A_{-\Omega} = A_\Omega^\dagger$. Here, $|\pm\Omega/2\rangle$ are the corresponding energy eigenstates. Generalizing to the case of an N-level probe with eigenstates $\{|\epsilon_i\rangle\}$, a coupling term like $X = \sum_{i\neq 1}|\epsilon_1\rangle\langle\epsilon_i| + |\epsilon_i\rangle\langle\epsilon_1|$ would also thermalize any preparation, where we have labelled the ground state by $|\epsilon_1\rangle$. The corresponding jump operators are $A_{\epsilon_i-\epsilon_1} = |\epsilon_1\rangle\langle\epsilon_i|$. In particular, to account for our effective two-level systems with maximum excited-state degeneracy we can set $\epsilon_1 = 0$ and take the limit $\epsilon_i \to \Omega$ for $i \neq 1$. Let us finally comment on the decay rates $\Gamma_{\Omega,T}$, which follow from the power spectrum of the bath auto-correlation function $\langle B(t)B(0)\rangle_T \equiv {\rm Tr}[B(t)B(0)\chi^T]$, where $B \equiv \sum_\mu g_\mu(b_\mu + b_\mu^\dagger)$. In the specific case of a quantum probe coupled through dipole interaction to the quantized electromagnetic field in three dimensions, one obtains $\Gamma_{\Omega,T} = \gamma\Omega^3(1-e^{-\Omega/T})^{-1}$ [28].

The problem now goes down to solving Eq. (7.2), transforming the time-evolved state $\rho(t)$ back into the Schrödinger picture (i.e. $\rho \mapsto e^{-iHt}\rho e^{iHt}$), and computing the QFI. Note that besides

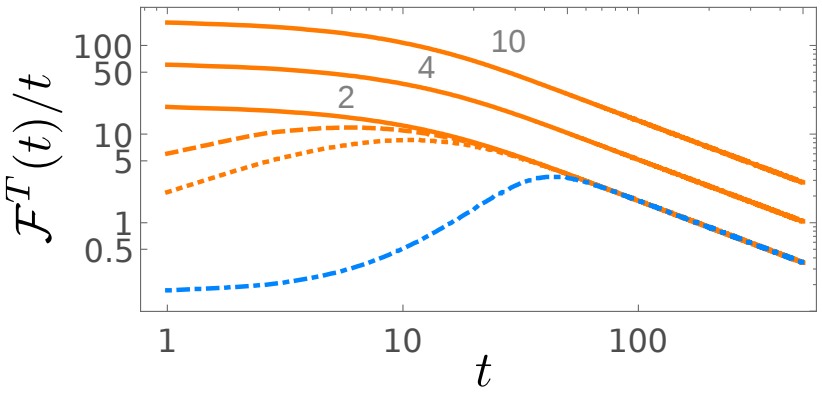

FIGURE 7.1: Log-log plot of $\mathcal{F}^T(t)/t$ as a function of t for different preparations and probe dimensionalities. The continuous orange lines stand for probes with $N = \{2, 4, 10\}$ initialized in the ground state. The dashed and dotted orange curves stand for a two-level probe initialized in a thermal state at temperature 0.8 and 0.9, respectively. The dot-dashed blue curve corresponds to a two-level probe prepared in the maximally coherent state $\rho(0) = |+\rangle\langle+|$ ($\Omega/T = \tilde{x}$, $\gamma = 10^{-3}$, and $T = 1$, in arbitrary units).

comparing the performance of different types of probe, we must now optimize over their initial state too. We start by considering the simplest case of two-level thermometers. Extensive numerical analysis over different initial states shows that ground-state preparations display maximal thermal sensitivity. This indicates that the presence of initial quantum coherence does not provide any significant advantage for thermometry in this setting.

Thus, by choosing $\rho(0) = |0\rangle\langle 0|$ we can combine eqs. (7.2) and (2.7) to compute $\mathcal{F}_2^T(t)$ as a function of the interrogation time t, starting from a ground state preparation:

$$\mathcal{F}_2^T(t) = \frac{x^2\left(e^x\left(e^{t/\tau}-1\right)+(1+e^x)\,\frac{t}{2\tau}\operatorname{csch}\frac{x}{2}\right)^2}{(1+e^x)^2\left(e^{t/\tau}-1\right)\left(1+e^x e^{t/\tau}\right)T^2}, \tag{7.3}$$

where $x = \Omega/T$ and $\tau^{-1} \equiv \gamma\Omega^3 \coth\frac{x}{2}$. Eq. (7.3) shows that the details of the thermal fluctuations of the sample, encoded in $\Gamma_{\Omega,T}$, only enter in the dynamics through the scaling factor τ. Hence, even if our choice of a flat spectral density might seem pretty restrictive at first, changing the probe-sample coupling would just amount to a suitable rescaling of time.

In fig. 7.1 we plot $\mathcal{F}_2^T(t)/t$ for different preparations. As we can see, the sensitivity of a cold thermal probe peaks at some optimal readout time, after which it must be quickly cooled down to start over another relaxation stage in the estimation protocol. In the limiting case of a ground-state preparation, the overall maximum sensitivity is approached as $t \to 0$.

Eq. (7.3) can be generalized to any of our highly degenerate effective two-level probes prepared in the ground state. Just like in the two-level case, their maximum estimation precision follows from the limit

$$\lim_{t\to 0}\frac{\mathcal{F}_N^T(t)}{t} = \frac{\gamma T(N-1)x^5 e^{2x}}{(e^x-1)^3}. \tag{7.4}$$

We now search for the optimal frequency-to-temperature ratio $\tilde{x}$ that sets an ultimate upper bound on the thermal sensitivity in Eq. (7.4). This can be expressed implicitly as $e^{\tilde{x}} = (5 + 2\tilde{x})/(5 - \tilde{x})$, which is independent of N. Interestingly, the specified temperature range for efficient operation does not scale with N, at variance with the fully thermalized case.

For completeness, we examine again here the performance of harmonic probes. Going back to Eq. (7.2), we will set $H = \Omega a^\dagger a$ and $X = a + a^\dagger$, whose corresponding relaxation and excitation operators are trivially $A_\Omega = a$ and $A_{-\Omega} = a^\dagger$, as described in section 3.5. The total Hamiltonian is thus quadratic in positions and momenta and therefore, any Gaussian preparation will preserve its Gaussianity in time [109]. Provided that the initial state also has vanishing first order moments ($\langle x \rangle = \langle p \rangle = 0$), its covariance matrix $\boldsymbol{\sigma}(t)$ alone will be enough for a full description.

In this case, the dynamics may be obtained by using Eq. 3.5, leading to $\boldsymbol{\sigma}(t) = e^{-\Gamma_{\Omega,T} t}\boldsymbol{\sigma}(0) + (1 - e^{-\Gamma_{\Omega,T} t})\boldsymbol{\sigma}_T$ (see [109, 128] as well). Computing the transient QFI is thus straightforward by resorting to Eq. (2.7). In what follows, we shall consider general (undisplaced) single-mode Gaussian states as initial preparations; these can be written as rotated, squeezed thermal states [109, 129]. As it could be expected, ground-state initialization ($\rho(0) = |0\rangle\langle 0|$) provides once again the largest thermal sensitivity. One can ignore the temperature dependence of $\Gamma_{\Omega,T}$ in the solution to the master equation and still get a good approximation to $\lim_{t\to 0} \mathcal{F}^T_{\rm ho}(t)/t$. Surprisingly, we recover Eq. (7.4) with $N = 2$. Indeed, this equivalence of two-level probes and harmonic thermometers extends generally beyond the limits $t \to 0$ and $\rho(0) = |0\rangle\langle 0|$. Therefore, at variance with the fully-thermalized scenario, the specified temperature range of both oscillators and N-level probes in an effective two-level configuration is virtually the same, regardless of N.

7.2 Parameter estimation in Markovian environments

In order to tackle the problem of local parameter estimation in systems out of equilibrium we develop a fluctuation dissipation theorem (FDT). The FDT establishes a relationship between the linear response of a system under a time-dependent perturbation and time correlations of certain observables in equilibrium [130]. Here we derive a generalization of the theorem which can be applied to any Markov quantum system and makes use of the symmetric logarithmic derivative (SLD). There are several important benefits when FDT's are formulated in terms of the SLD. First, such a formulation clarifies the relation between classical and quantum versions of the equilibrium FDT. Second, and more important, it facilitates the extension of the FDT to arbitrary quantum Markovian evolution, as given by quantum maps. Third, it brings out the connection between the FDT and Fisher information, our figure of merit in quantum metrology. In what follows, by adapting the strategy introduced in [131], we prove a generalized FDT for

generic quantum maps, and illustrate these features in the example of two harmonic oscillators with a modulated interaction that was introduced in section 6.2.

We are interested in the well established case of a generic Markovian dynamics. Specifically, we consider $\mathcal{M}_\xi$ be a *completely positive trace preserving* (CPTP) map, as described in Chapter 3. Further, for any *fixed* value of the parameter ξ, the map has a steady state π_ξ. In other words, we have $\mathcal{M}_\xi \pi_\xi = \pi_\xi$, i.e., π_ξ is invariant under the map. The system of our interest is initially given by π_0, which is invariant under $\mathcal{M}_0$. Whence, it evolves by consecutive operation of the map $\mathcal{M}_{\xi(t)}$. Note that we allow the parameter to be time dependent. Taking discrete time steps $t = 1, 2, \ldots$, the evolution of the system is

$$\rho(t) = \Big[\mathcal{M}_{\xi(t)} \circ \mathcal{M}_{\xi(t-1)} \circ \ldots \mathcal{M}_{\xi(1)}\Big]\pi_0. \tag{7.5}$$

Since we work in a regime where ξ appears as a perturbation, our focus shall be on the *linear response* of any observable B. The latter is defined as the deviation of the expectation value of B at time t, from its initial value, and is given by

$$\mathcal{R}_B(t) \equiv \langle B(t)\rangle - \langle B(0)\rangle = \sum_{t'=1}^{t} \phi_B(t-t')\xi(t'). \tag{7.6}$$

Here $\langle B(t)\rangle = \mathrm{Tr}[\rho(t)B]$, identifies the expectation value of the observable B at time t, specially, $\langle B(0)\rangle = \mathrm{Tr}[\pi_0 B]$. In addition, $\phi_B(t)$ is the *response function* of the observable B under the perturbation ξ, and is assumed to vanish for $t < 0$ due to causality. Our aim is mainly to formalize the response function $\phi_B(t)$, independent of the time dependence of $\xi(t)$. By identifying $\phi_B(t)$ one can find the linear response of B to any time dependent perturbation, as Eq. (7.6) suggests.

Before proceeding further, we remark that for a scenario with constant perturbation, $\xi(t) = \xi$, the linear response $\mathcal{R}_B(t)$ is a key element to characterize the sensitivity of the observable B to ξ. In particular, as $t \to \infty$, the linear response reduces to the static susceptibility times the parameter, i.e., $\mathcal{R}_B(\infty) = \xi\, \chi_{B,\xi}$ (See the error-propagation formula (4.23) for comparison). Similarly, for a time dependent perturbation, namely $\xi(t) = |\xi| f(t)$, the linear response characterizes the sensitivity of B to $|\xi|$, the strength of perturbation. Therefore, identification of $\mathcal{R}_B(t)$ is pivotal from a metrological point of view.

One can extend the definition of $\mathcal{R}_B(t)$ to the case of maps acting for a short time Δt. In the continuous limit, $\Delta t \to 0$, the sum in (7.6) is replaced by an integral, such that

$$\mathcal{R}_B(t) = \int_0^t dt'\, \phi_B(t-t')\xi(t'). \tag{7.7}$$

Another important quantity is the *generalized susceptibility* which is defined as the Fourier transform of the response function,

$$\mathcal{X}_{B}(\omega) = \int_0^\infty dt\, \phi_B(t) e^{i\omega t}. \tag{7.8}$$

Again, notice that for a constant perturbation, and for $\omega = 0$, the generalized susceptibility reduces to the static susceptibility via $\mathcal{X}_{B}(0) = \xi\, \chi_{B,\xi}$. The generalized susceptibility has interesting properties, such as the *Kramers-Kronig relation* [8, 103] between its real and imaginary parts: $\mathcal{X}_{B}(\omega) = \mathcal{X}'_{B}(\omega) + i\mathcal{X}''_{B}(\omega)$. When the evolution is unitary under the Hamiltonian $H_0 - \xi(t)A$, the imaginary part $\mathcal{X}''_{B}(\omega)$ is called absorptive part of the susceptibility, since the energy absorbed by the system due to the perturbation is proportional to $\mathcal{X}''_{B}(\omega)$.

To obtain the response function, we need to expand $\rho(t)$ as a power series of $\xi(t)$, and keep up to linear terms. To this end, we write $\mathcal{M}_\xi = \mathcal{M}_0 + \xi\, \mathcal{M}_1 + O(\xi^2)$, where $\mathcal{M}_1$ is not a CPTP map. In addition, the stationary state can be written as $\pi_\xi = \pi_0 + \xi\, \pi_1 + O(\xi^2)$. Again, notice that π_1 is not a density matrix, for instance because it is traceless. The invariance of π_ξ under the map $\mathcal{M}_\xi$ implies

$$\begin{aligned} \left[\mathcal{M}_0 + \xi\, \mathcal{M}_1 + O(\xi^2)\right](\pi_0 + \xi\, \pi_1 + O(\xi^2)) &= \pi_0 + \xi\, \pi_1 + O(\xi^2) \\ \Rightarrow \mathcal{M}_1(\pi_0) + \mathcal{M}_0(\pi_1) &= \pi_1, \end{aligned} \tag{7.9}$$

where we use the fact that $\mathcal{M}_0(\pi_0) = \pi_0$. Furthermore, the SLD of π_ξ associated to ξ (at $\xi = 0$) obeys

$$\begin{aligned} \left(\Lambda_\xi \pi_\xi + \pi_\xi \Lambda_\xi\right)\big|_{\xi=0} &= 2(\partial_\xi \pi_\xi)\big|_{\xi=0} \\ \Rightarrow 2\pi_1 &= \Lambda_0 \pi_0 + \pi_0 \Lambda_0. \end{aligned} \tag{7.10}$$

Expanding the evolution equation (7.5) up to linear terms, we obtain

$$\begin{aligned} \rho(t) &= \mathcal{M}_0^t(\pi_0) + \sum_{t'=1}^{t} \xi(t') \left[\mathcal{M}_0^{t-t'} \circ \mathcal{M}_1 \circ \mathcal{M}_0^{t'-1}\right](\pi_0) \\ &= \pi_0 + \sum_{t'=1}^{t} \xi(t') \left[\mathcal{M}_0^{t-t'} \circ \mathcal{M}_1\right](\pi_0). \end{aligned} \tag{7.11}$$

where we have used the invariance of π_0 under $\mathcal{M}_0$. Therefore, the linear response of B at time t is

$$\mathcal{R}_B(t) = \sum_{t'=1}^{t} \xi(t')\, \mathrm{Tr}\left[B\, \mathcal{M}_0^{t-t'} \circ \mathcal{M}_1\, (\pi_0)\right] \tag{7.12}$$

Comparing (7.12) with (7.6), we immediately identify the response function to be

$$\phi_B(t) = \mathrm{Tr}\Big[B\, \mathcal{M}_0^t \circ \mathcal{M}_1(\pi_0)\Big]. \tag{7.13}$$

Using (7.9) and (7.10) one can further simplify this expression

$$\begin{aligned}
\phi_B(t) &= \mathrm{Tr}\Big[B\, \mathcal{M}_0^t(\pi_1 - \mathcal{M}_0(\pi_1))\Big] \\
&= -\mathrm{Tr}\Big[B\, \mathcal{M}_0^{t+1}(\pi_1) - B\, \mathcal{M}_0^t(\pi_1))\Big] \\
&= -\mathrm{Tr}\left[\Delta B(t)\pi_1\right] \\
&= -\frac{1}{2}\mathrm{Tr}\left[\Delta B(t)(\Lambda_0\pi_0 + \pi_0\Lambda_0)\right] \\
&= -\frac{1}{2}\left\langle \Delta B(t)\Lambda_0 + \Lambda_0 \Delta B(t)\right\rangle_0
\end{aligned} \tag{7.14}$$

with $\langle\bullet\rangle_0 = \mathrm{Tr}[\bullet\pi_0]$ being the expectation value over the initial state. Besides, $\Delta B(t) = B(t+1) - B(t)$ and $B(t) = \widetilde{\mathcal{M}}_0^t(B)$ is the evolution of the observable B in the generalized Heisenberg picture for quantum maps. Here $\widetilde{\mathcal{M}}_0(\bullet)$ is the adjoint map (not necessarily trace preserving) with respect to the scalar product between operators given by the trace, i.e., $\mathrm{Tr}[\circ\mathcal{M}_0(\bullet)] = \mathrm{Tr}[\widetilde{\mathcal{M}}_0(\circ)\bullet]$, for all pair of operators $\circ$ and $\bullet$.

The fluctuation-dissipation relation for the static case is recovered from (7.14) if the two time correlations between $B(t)$ and Λ_0 vanish in the limit $t \to \infty$

$$\begin{aligned}
\chi_{B,\xi} &= \sum_{t'=0}^{\infty} \phi_B(t') \\
&= -\lim_{t\to\infty} \frac{1}{2}\left\langle B(t)\Lambda_0 + \Lambda_0 B(t)\right\rangle + \frac{1}{2}\left\langle B\Lambda_0 + \Lambda_0 B\right\rangle \\
&= \frac{1}{2}\left\langle B\Lambda_0 + \Lambda_0 B\right\rangle.
\end{aligned} \tag{7.15}$$

Finally, the continuous-time version of theorem (7.14) is

$$\phi_B(t) = -\frac{1}{2}\,\frac{d}{dt}\,\left\langle B(t)\Lambda_0 + \Lambda_0 B(t)\right\rangle. \tag{7.16}$$

Eqs. (7.14) and (7.16) are the main result of this section.

7.2.1 Connection with the Kubo relations

Our main results (7.14) and (7.16) are FDR's for generic quantum Markov systems. One can recover the familiar Kubo quantum FDR for states $\pi_\xi = e^{-\beta(H_0 - \xi A)}/\mathcal{Z}$ and Hamiltonian evolution. In this case, the FDR (7.16) reads (as before, we denote by $\phi_B(t)$ the response function of

observable B under the perturbation $-\xi(t)A$):

$$\begin{aligned}\phi_B(t) &= -\frac{1}{2}\left\langle \dot{B}(t)\Lambda_0 + \Lambda_0\dot{B}(t)\right\rangle \\ &= -\frac{i}{2}\left\langle [H_0, B(t)]\Lambda_0 + \Lambda_0[H_0, B(t)]\right\rangle_0 \\ &= -\frac{i}{2}\mathrm{Tr}\left[(\Lambda_0\pi_0 + \pi_0\Lambda_0)[H_0, B(t)]\right] \\ &= -\frac{i}{2}\mathrm{Tr}\left[[\Lambda_0\pi_0 + \pi_0\Lambda_0, H_0]B(t)\right]. \end{aligned} \tag{7.17}$$

Here we use the fact that for a unitary dynamics (we set $\hbar = 1$), $B(t) = \exp(iH_0\ t)B\exp(-iH_0\ t)$, and hence $\dot{B}(t) = i[H_0, B(t)]$. Before taking any further steps, we present an interesting formula for the SLD. To this end, we note that for any real function $g(x)$

$$[H_0 - \xi A, g(H_0 - \xi A)] = 0. \tag{7.18}$$

Differentiating this equation with respect to ξ and setting $\xi = 0$, one gets

$$-[A, g(H_0)] + \left[H_0, \left.\frac{\partial g(H_0 - \xi A)}{\partial \xi}\right|_{\xi=0}\right] = 0. \tag{7.19}$$

In particular, by choosing $g(x) = e^{-\beta x}$ and using the definition of the SLD we obtain

$$[A, \pi_0] = \frac{1}{2}[H_0, \Lambda_0\pi_0 + \pi_0\Lambda_0] \tag{7.20}$$

Substituting this last result into (7.17) leads to

$$\phi_B(t) = i\ \mathrm{Tr}\left[[A, \pi_0]B(t)\right] = i\ \left\langle [B(t), A]\right\rangle, \tag{7.21}$$

which is the standard Kubo formula. Notice that the relationship between the classical FDT and the Kubo formula is not clear at all. On the contrary, our version of the FDT, namely Eqs. (7.14) and (7.16), can be equally applied to classical and quantum systems. This uniform formulation is possible due to the introduction of the SLD. We remind that in the classical case, the SLD coincides with the normal derivative and consequently, for a thermal state with Hamiltonian $H_0 - \xi A$, the SLD is $-\beta(A - \langle A\rangle)$, whereas for a quantum system with $[H_0, A] \neq 0$, the SLD yields a nontrivial conjugated variable as we saw for the two coupled harmonic oscillators in the previous chapters.

7.2.2 Coupled Harmonic Oscillators Out of Equilibrium

With the help of our FDT we are able to investigate, more generally, the system of coupled harmonic oscillators that was described earlier in chapters 4 and 6. In particular, we are interested

in a case where the tunneling between the two oscillators acts as a time dependent perturbation, i.e., $J(t)$. The system is initially identified by Eq. (6.15) (or equivalently Eq. (6.13)), whence, it is quenched/perturbed, by introducing the tunneling between the two oscillators

$$\begin{aligned} H &\to H_0 + H_I \\ H_I &= -J(t)(a_1^\dagger a_2 + a_1 a_2^\dagger). \end{aligned} \tag{7.22}$$

We remark that the difference of this scenario with section 6.2 is twofold: (i) Here, we focus in the response of the system at any time, in contrast to the static case with $t \to \infty$. (ii) In turn, $J(t)$ itself is also time dependent, unlike the static case. On this account, even at $t \to \infty$ the system does not relax to a stationary state.

Further, we demand $|J(t)| \ll \omega$, at any time, such that our linear response remains valid. In order to find $\mathcal{R}_B(t)$, the linear response of the observable B to $J(t)$, we need to identify two key elements as suggested by eqs. (7.7) and (7.16). First, the SLD associated to the tunneling rate $\Lambda_J|_{J=0}$. This is already found analytically in section 6.2, and is given by Eq. (6.23)). The second element is the time evolution of the desired observable under the conjugate map, i.e., $B(t)$. This is also identified by eqs. (6.36) and (6.36) of section 6.2.

With these two elements at hand, the rest is straightforward to proceed. Specifically, one can simply check that the linear response of local observables is zero, i.e., for $B \in \left\{x_j^2, p_j^2, x_j p_j + h.c.\right\}$, we have $\mathcal{R}_B(t) = 0$. This means that the perturbation does not affect local observables, or in other words, the perturbation can not be detected by local measurements. Remember that this is true also for the static case. However, for global observables, i.e., for $B \in \{x_1 x_2, x_1 p_2, p_1 x_2, p_1 p_2\}$, the linear response is nonzero.

Let us first give thought to a constant quench, $J(t) = J_0$, such that we can study the relaxation of the system to its new stationary state. In the left panel of Fig. 7.2 we illustrate, $\mathcal{R}_B(t)/J_0$, for the non-local observables $B \in \{x_1 x_2, x_1 p_2\}$. In the right panel we benchmark the corresponding (square root) sensitivity of these two observables, i.e., $\sqrt{F(B;J_0)} = \mathcal{R}_B(t)/J_0 \sqrt{\mathrm{Var}(B)}$, with that of Λ_J. We discover that the linear response (and hence the sensitivity) experiences some oscillations, before relaxing to the new stationary state, at $t \to \infty$. Interestingly, at certain instances of time, the amplitude of these oscillations might be even bigger than the asymptotic value. By measuring the system at these certain times, one can acquire maximum information about, J_0. Further, from the inset of the left panel, we notice as well, that the sensitivity of $x_1 p_2$ may over perform that of the SLD. But this is not an issue, since the SLD identifies the most sensitive observable for asymptotic measurements.

In general, and more-interestingly, the perturbation is time dependent. With no loss of generality, we focus on a case where $J(t) = J_0(1 - \sin(\nu t))$. The linear response to this perturbation will be equal to the linear response to a constant J_0 minus the linear response to $J_0 \sin(\nu t)$. The latter

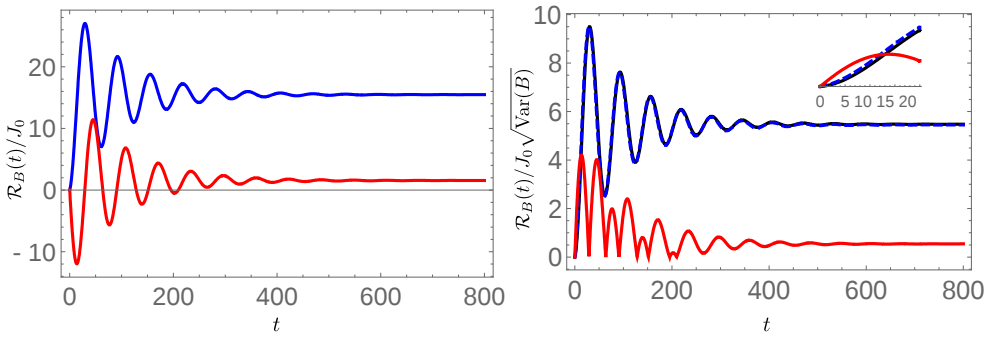

FIGURE 7.2: **Left**) The linear response of the non-equilibrium system to a constant perturbation J_0 for two different observables: x_1x_2 (red), and x_1p_2 (blue). The system relaxes to its new steady state asymptotically, albeit after experiencing some oscillations. The amplitude of such oscillations decays exponentially. Note that, Particularly, at some instances of time, the linear response becomes significantly bigger than its final (static) value. **Right**) The (square root) sensitivity of the same observables as the left panel, benchmarked against the sensitivity of Λ_J (black). We see that the x_1x_2 observable performs very similar to the SLD. As $t \to \infty$ and the system relaxes to its new steady state, the SLD (and approximately x_1x_2) characterizes the most sensitive observable to the perturbation. Its corresponding sensitivity is given by $\sqrt{\mathcal{F}_J}$. Interestingly the sensitivity at some instances of time may get considerably bigger than $\sqrt{\mathcal{F}_J}$. **Inset**) For smaller times, we observe that the sensitivity of x_1p_2 over-performs that of the SLD. Here we set the parameters as follows: $\omega_1 = 1$, $\omega_2 = 1.1$, $T_1 = 1$, $T_2 = 2$, and $\gamma = 0.01$.

is given by $\int_0^t \phi_B(t')\sin(\nu(t-t'))dt'$. Fig 7.3 pictures the linear response to a time dependent perturbation for two different frequencies. On the left panel, we let $\nu = \Delta$, i.e., at resonance with the detuning between the two modes. It is seen that $\mathcal{R}_B(t)/J_0$ may become significantly bigger than the response to a constant perturbation, i.e., with $\nu = 0$ (the black curve). In the right panel of the same figure, we depict the same quantity, but with a larger frequency. We discover that the linear response in this case is also oscillating around the linear response of a constant perturbation. However, due to the small amplitude of these oscillations, one may hardly distinguish this case from a constant perturbation.

The frequency dependence of the linear response raises the idea of modulating the perturbation such that it has a bigger response, hence becoming easier to detect. As a result, from a metrological point of view, characterizing the frequencies with a bigger response sounds essential. To this end we focus on the linear response to the time dependent part of the perturbation, $J_0\sin(\nu t)$:

$$\begin{aligned}\mathcal{R}_B^{\nu}(t) &\equiv \int_0^t \phi_B(t')\sin(\nu(t-t'))dt' \\ &= \sin(\nu t)\int_0^t \phi_B(t')\cos(\nu t')dt' - \cos(\nu t)\int_0^t \phi_B(t')\sin(\nu t')dt'. \end{aligned} \tag{7.23}$$

We also keep in mind that $\phi_B(t') \to 0$ with the speed $\exp(-\gamma t')$ (see eqs. (6.36) and (6.36)). Therefore, for large enough times we can approximate the upper bound of the integral with

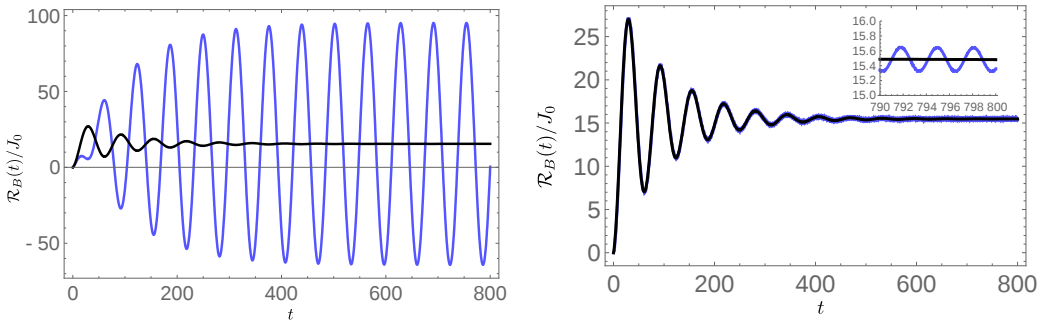

FIGURE 7.3: (**Left**) Blue line) The linear response of the observable x_1x_2 to a time dependent perturbation $J(t) = J_0(1 - \sin(\nu t))$ with $\nu = \Delta$. Black line) The response to the constant perturbation $J(t) = J_0$ is also plotted for comparison. The oscillations of the linear response are so large that the system never gets close to any new stationary state. For metrological tasks, interrogating the system at times with maximum linear response ($t_{\max}$) is essential. (**Right**) Same as left, but with $\nu = 2$. For this frequency, the amplitude of oscillations of the linear response are very small, such that the system can be considered sufficiently close to a stationary state. Therefore, in metrological scenarios, measuring the system at $t_{\max}$ does not significantly enhance the precision of estimation. Here we use the same parameters as in Fig. 7.2.

infinity, which leads to

$$\begin{aligned} \mathcal{R}^{\nu}_{B}(t) &\cong \sin(\nu t)\mathrm{Re}\,\mathcal{X}_{B}(\nu) - \cos(\nu t)\mathrm{Im}\,\mathcal{X}_{B}(\nu) \\ &\cong |\,\mathcal{X}_{B}(\nu)\,|\cos(\nu t + \alpha). \end{aligned} \tag{7.24}$$

Here we benefit from the expression of generalized susceptibility, Eq. (7.8), and define the phase shift $\alpha = \arctan(\mathrm{Re}\,\mathcal{X}_{B}(\nu)/\mathrm{Im}\,\mathcal{X}_{B}(\nu))$. As a result, the magnitude of the generalized susceptibility is equivalent to the amplitude of the oscillations of the linear response at large times. Fig 7.4 shows this amplitude for the observable x_1x_2. It is observed that for $\nu < \Delta$, the generalized susceptibility increases monotonically, and approaches a maximum at $\nu = \Delta$. This is the reason for big oscillations of $\mathcal{R}_B(t)$ in Fig 7.3. However, for $\nu > \Delta$, the generalized susceptibility decreases exponentially. This explains the small oscillations of the linear response for larger frequencies.

Moreover, one can characterize the instances when the linear response has its maximum (at large times):

$$t_{max} = \frac{m\pi - \alpha}{\nu}, \tag{7.25}$$

with m being a (large enough) integer number. Knowing such instances with maximum response is required for being able to detect tinier amounts of J_0. Notice also that $t_{\max}$ does not depend on J_0 itself.

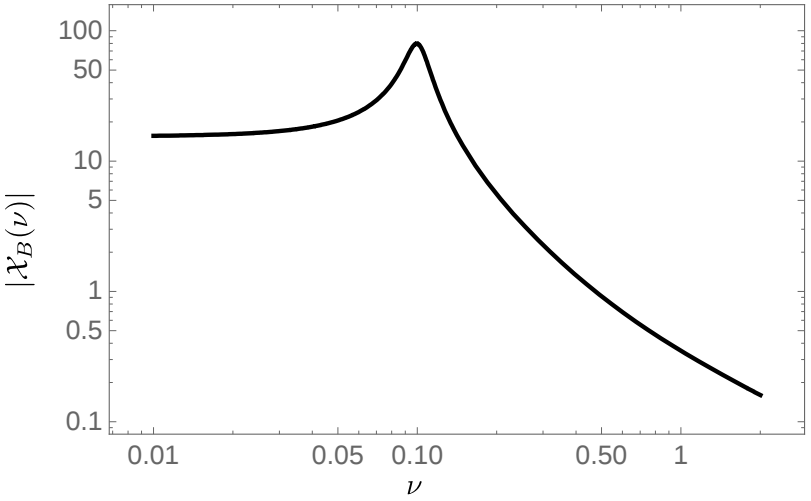

FIGURE 7.4: The magnitude of the generalized susceptibility $|\mathcal{X}_B(\nu)|$ for the observable $x_1 x_2$. We use the same parameters as in Fig. 7.2. For values of ν around the resonance (with $\Delta = 0.1$), and for $\nu < \Delta$, the magnitude of the generalized susceptibility is big. This means that for these frequencies the perturbed system never gets close to a stationary state. For larger frequencies, the generalized susceptibility becomes very small, thus the perturbed system will get close to a final steady state, and keeps oscillating around it for ever. See fig 7.3 as well.

7.3 Summary and conclusions

The aim of this chapter was exploring parameter estimation in *dynamic* systems. For us this is a relevant question in two different scenarios.

The first case is a system which is interrogated before reaching a stationary state. In particular, our study of thermometry with *partially thermalized* probes in section 7.1 lies within this category. We observed that frequently interrogated probes prepared in their ground state provide the largest thermal sensitivity. The maximum thermometry precision scales with N, the number of energy levels, similar to the fully thermalized scenario. However, the specified temperature range—within which the thermometry precision is efficient—is dimension-independent, in contrast to thermalized probes, where this range shrinks with N. These results were obtained by considering a large bosonic sample in thermal equilibrium, weakly coupled to the probe through a linear interaction term, ensuring ergodicity.

The second case that we had to take into account the role of dynamics, was tackling the detection of a time dependent perturbation. Precisely, a system, resting at the fixed point of its dynamics, is affected by a time dependent perturbation. For us it is essential to estimate the strength of this perturbation. To this end, we developed a fluctuation dissipation theory (FDT) for generalized Markovian dynamics. Our FDT connects the linear response of any observable to its correlation with the symmetric logarithmic derivative (SLD). We benefit from this connection, in different

aspects, namely, by clarifying the connection between classical and quantum FDT for equilibrium, by extending the FDT to an arbitrary quantum Markovian dynamic, and by highlighting the connection between the FDT and the QFI for a time dependent parameter.

We applied our FDT by exploring the response of two harmonic oscillators to a perturbation, which exploits interaction amongst them. Particularly, we discovered that in order to detect the strength of such a perturbation, one has to perform global measurements, while local schemes are blind to this perturbation. Wherefore, we quantified the precision of such global measurements. Our results show that there are certain instances of time that the system has a notably bigger response to the perturbation. This suggests that, the system periodically acquires and looses a definite amount of information about the perturbation. That being the case, we characterize the instances of time with the maximum response, and identify that the amount of information is given by generalized dynamical susceptibility.

Appendix A

Solving the QLE for the steady state of the central oscillator

As explained in the main text, any Gaussian state (such as the steady state of the probe) is fully characterized by its first and second-order moments. In the case of a single-mode Gaussian state, these latter can be arranged in the 2×2 real and symmetric covariance matrix $\boldsymbol{\sigma}$. We therefore must be able to compute objects like $\langle\{x(t'),x(t'')\}\rangle$, $\langle\{p(t'),p(t'')\}\rangle$ and $\langle\{x(t'),p(t'')\}\rangle$ from Eq. (6.6). Let us start by taking its Fourier transform, which gives

$$-\omega^2\tilde{x}+(\omega_0^2+\omega_R^2)\tilde{x}+\tilde{x}\tilde{\chi}=\tilde{F}\Rightarrow\tilde{x}(\omega)=\frac{\tilde{F}(\omega)}{\omega_0^2+\omega_R^2-\omega^2-\tilde{\chi}(\omega)}:=\alpha(\omega)^{-1}\tilde{F}(\omega). \tag{A.1}$$

Note that

$$\begin{aligned}\frac{1}{2}\langle\{x(t'),x(t'')\}\rangle&=\frac{1}{2}\int_{-\infty}^{\infty}\frac{\mathrm{d}\omega'}{2\pi}\,e^{-i\omega' t'}\int_{-\infty}^{\infty}\frac{\mathrm{d}\omega''}{2\pi}\,e^{-i\omega'' t''}\langle\{\tilde{x}(\omega'),\tilde{x}(\omega'')\}\rangle\\&=\frac{1}{2}\int_{-\infty}^{\infty}\frac{\mathrm{d}\omega'}{2\pi}\,e^{-i\omega' t'}\int_{-\infty}^{\infty}\frac{\mathrm{d}\omega''}{2\pi}e^{-i\omega'' t''}\,\alpha(\omega')^{-1}\alpha(\omega'')^{-1}\langle\{\tilde{F}(\omega'),\tilde{F}(\omega'')\}\rangle_T.\end{aligned} \tag{A.2}$$

Therefore, all what is left is to find the analytical expression of the power spectrum of the bath $2^{-1}\langle\{\tilde{F}(\omega'),\tilde{F}(\omega'')\}\rangle_T$ and of the Fourier transform of the susceptibility $\tilde{\chi}(\omega)$, which appears in $\alpha(\omega)$. Note that the Fourier transform of all first order moments will be proportional to $\langle\tilde{F}(\omega)\rangle_T$ which is identically zero [cf. Eq. (6.4)]. Hence, the steady states of the central oscillator will be *undisplaced* Gaussians. With the subscript in $\langle\cdots\rangle_T$, we emphasize that the average is taken over the initial Gibbs state of the sample.

A.1 The fluctuation-dissipation relation

Let us start by computing $\frac{1}{2}\langle\{\tilde{F}(\omega'),\tilde{F}(\omega'')\}\rangle_T = \mathrm{Re}\,\langle\tilde{F}(\omega')\tilde{F}(\omega'')\rangle_T$ from Eq. (6.4). Taking into account that $\langle x_\mu(t_0)x'_\mu(t_0)\rangle_T = \delta_{\mu\mu'}(2m_\mu\omega_\mu)^{-1}[1+2n_\mu(T)]$, $\langle p_\mu(t_0)p'_\mu(t_0)\rangle_T = \delta_{\mu\mu'}\frac{1}{2}m_\mu\omega_\mu[1+2n_\mu(T)]$ and $\langle x_\mu(t_0)p_\mu(t_0)\rangle_T = \langle p_\mu(t_0)x_\mu(t_0)\rangle_T^* = i/2$, one has

$$\begin{aligned}\frac{1}{2}\langle\{\tilde{F}(t'),\tilde{F}(t'')\}\rangle_T &= \frac{1}{\pi}\sum_\mu \frac{\pi g_\mu^2}{2m_\mu\omega_\mu}[1+2n_\mu(T)]\\ &\quad\times\Big[\cos\omega_\mu(t'-t_0)\cos\omega_\mu(t''-t_0)+\sin\omega_\mu(t'-t_0)\sin\omega_\mu(t''-t_0)\Big]\\ &= \frac{1}{\pi}\int_0^\infty \mathrm{d}\omega\, J(\omega)\coth\frac{\omega}{2T}\cos\omega(t'-t''),\end{aligned} \tag{A.3}$$

where we have used $2n_\mu(T)+1 = \coth(\omega_\mu/2T)$, which follows from the definition of the bosonic thermal occupation number $n_\mu(T)\equiv[\exp(\omega/2T)-1]^{-1}$. Now, taking the Fourier transform of Eq. (A.3) yields

$$\begin{aligned}\frac{1}{2}\langle\{\tilde{F}(\omega'),\tilde{F}(\omega'')\}\rangle_T &= 2\pi\int_{-\infty}^\infty\frac{\mathrm{d}t'}{2\pi}e^{i\omega' t'}\int_{-\infty}^\infty\frac{\mathrm{d}t''}{2\pi}e^{i\omega'' t''}\int_0^\infty \mathrm{d}\omega\, J(\omega)\coth\frac{\omega}{2T}\left(e^{i\omega(t'-t'')}+e^{-i\omega(t'-t'')}\right)\\ &= 2\pi\int_{-\infty}^\infty\frac{\mathrm{d}t'}{2\pi}\int_{-\infty}^\infty\frac{\mathrm{d}t''}{2\pi}\int_0^\infty \mathrm{d}\omega\, J(\omega)\coth\frac{\omega}{2\pi}\left(e^{it'(\omega+\omega')}e^{it''(\omega''-\omega)}+e^{it'(\omega'-\omega)}e^{it''(\omega''+\omega)}\right)\\ &= 2\pi\int_0^\infty \mathrm{d}\omega\, J(\omega)\coth\frac{\omega}{2T}\Big[\delta(\omega+\omega')\delta(\omega''-\omega)+\delta(\omega'-\omega)\delta(\omega''+\omega)\Big]\\ &= 2\pi\,\delta(\omega'+\omega'')\coth\frac{\omega'}{2T}\Big[J(\omega')\Theta(\omega')-J(-\omega')\Theta(-\omega')\Big],\end{aligned} \tag{A.4}$$

where we have used the identity $\int_{-\infty}^\infty \mathrm{d}t\, e^{i\omega t} = 2\pi\,\delta(\omega)$. On the other hand, we may find $\mathrm{Im}\,\tilde{\chi}(\omega)$ from Eq. (6.5). Note that

$$\begin{aligned}\mathrm{Im}\,\tilde{\chi}(\omega) &= \mathrm{Im}\sum_\mu\frac{g_\mu^2}{m_\mu\omega_\mu}\int_{-\infty}^\infty \mathrm{d}t\, e^{i\omega t}\Theta(t)\sin\omega_\mu t = \sum_\mu\frac{g_\mu^2}{m_\mu\omega_\mu}\int_0^\infty \mathrm{d}t\sin\omega t\sin\omega_\mu t\\ &= \frac{1}{4}\sum_\mu\frac{g_\mu^2}{m_\mu\omega_\mu}\int_0^\infty \mathrm{d}t\,[e^{i(\omega+\omega_\mu)t}-e^{i(\omega-\omega_\mu)t}-e^{i(-\omega+\omega_\mu)t}+e^{-i(\omega+\omega_\mu)t}]\\ &= \frac{1}{4}\sum_\mu\frac{g_\mu^2}{m_\mu\omega_\mu}\left(\int_{-\infty}^\infty \mathrm{d}t\, e^{i(\omega+\omega_\mu)t}-\int_{-\infty}^\infty \mathrm{d}t\, e^{i(\omega-\omega_\mu)t}\right) = \frac{\pi}{2}\sum_\mu\frac{g_\mu^2}{m_\mu\omega_\mu}[\delta(\omega-\omega_\mu)-\delta(\omega+\omega_\mu)]\\ &= \int_0^\infty \mathrm{d}\omega\, J(\omega)[\delta(\omega-\omega_\mu)-\delta(\omega+\omega_\mu)] = J(\omega)\Theta(\omega)-J(-\omega)\Theta(-\omega).\end{aligned} \tag{A.5}$$

Hence the fluctuation-dissipation relation $\langle\{\tilde{F}(t'),\tilde{F}(\omega'')\}\rangle = 4\pi\,\delta(\omega'+\omega'')\coth(\omega'/2T)\,\mathrm{Im}\tilde{\chi}(\omega')$. When it comes to its real part, the calculation is not so straightforward. Recall from Eq. (6.5) that the response function $\chi(t)$ is *causal* due to the accompanying Heaviside step function. Causal response functions have analytic Fourier transform in the upper-half of the complex plane and therefore, the Kramers-Kronig relations hold [103]. In particular

$$\mathrm{Re}\tilde{\chi}(\omega) = \frac{1}{\pi}\,\mathrm{P}\int_{-\infty}^{\infty} d\omega'\,\frac{\mathrm{Im}\tilde{\chi}(\omega)}{\omega'-\omega} \equiv \mathcal{H}\,\mathrm{Im}\tilde{\chi}(\omega), \tag{A.6}$$

where we have introduced the Hilbert transform $g(y) = \mathcal{H}\,f(x) \coloneqq \pi^{-1}\,\mathrm{P}\int_{-\infty}^{\infty} dx\,f(x)/(x-y)$ [132], and P denotes Cauchy principal value.

Appendix B

Dissipation kernel for Ohmic and super-Ohmic spectral densities with exponential cutoff

We will now obtain $\mathrm{Re}\tilde{\chi}(\omega)$ for two instances of the family of spectral densities $J_s(\omega) \coloneqq \frac{\pi}{2}\gamma\omega^s\omega_c^{1-s}e^{-\omega/\omega_c}$, namely $s = 1$ (Ohmic case) and $s = 2$ (super-Ohmic case). To begin with, let us list four useful properties of the Hilbert transform that we shall use in what follows

$$f(-ax) \overset{\mathcal{H}}{\longmapsto} -g(-ay) \qquad a > 0 \qquad \text{(B.1a)}$$

$$xf(x) \overset{\mathcal{H}}{\longmapsto} y\,g(y) + \frac{1}{\pi}\int_{-\infty}^{\infty} dx\, f(x) \qquad \text{(B.1b)}$$

$$\exp(-a|x|) \overset{\mathcal{H}}{\longmapsto} \frac{1}{\pi}\mathrm{sign}\, y\left[\exp(a|y|)\,\mathrm{Ei}(-a|y|) - \exp(-a|y|)\,\overline{\mathrm{Ei}}(a|y|)\right] \qquad a > 0 \qquad \text{(B.1c)}$$

$$\mathrm{sign}\, x \exp(-a|x|) \overset{\mathcal{H}}{\longmapsto} -\frac{1}{\pi}\left[\exp(a|y|)\,\mathrm{Ei}(-a|y|) + \exp(-a|y|)\,\overline{\mathrm{Ei}}(a|y|)\right] \qquad a > 0, \qquad \text{(B.1d)}$$

where $\mathrm{Ei}(x) \equiv -\int_{-x}^{\infty} dt\, t^{-1}e^{-t}$ is the exponential integral, and $\overline{\mathrm{Ei}}(x)$ denotes its principal value.

Ohmic case ($s = 1$)

According to Eqs. (A.6) and (A.5), one has

$$\mathrm{Re}\tilde{\chi}(\omega) = \frac{\pi\gamma}{2}\Big\{\mathcal{H}[\Theta(\omega')\,\omega'\exp(-\omega'/\omega_c)](\omega) - \mathcal{H}[-\Theta(-\omega')\,\omega'\exp(\omega'/\omega_c)](\omega)\Big\}. \qquad \text{(B.2)}$$

Using Eqs. (B.1a) and (B.1b), this rewrites as

$$\begin{aligned}\mathrm{Re}\,\tilde{\chi}(\omega) &= \frac{\pi\gamma}{2}\Big\{\mathcal{H}[\Theta(\omega')\,\omega'\exp(-\omega'/\omega_c)](\omega)+\mathcal{H}[\Theta(\omega')\,\omega'\exp(-\omega'/\omega_c)](-\omega)\Big\}\\ &= \frac{\pi\gamma}{2}\Big\{\omega\mathcal{H}[\Theta(\omega')\exp(-\omega'/\omega_c)](\omega)-\omega\mathcal{H}[\Theta(\omega')\exp(-\omega'/\omega_c)](-\omega)+\frac{2\omega_c}{\pi}\Big\}. \quad \text{(B.3)}\end{aligned}$$

Now, using first Eq. (B.1a), and then Eq. (B.1c), one finds

$$\begin{aligned}\mathrm{Re}\,\tilde{\chi}(\omega) &= \gamma\omega_c+\frac{\pi\gamma}{2}\omega\mathcal{H}[\exp(-|\omega'|/\omega_c)](\omega)\\ &= \gamma\omega_c-\frac{\gamma}{2}\omega\Big[\exp(-\omega/\omega_c)\,\overline{\mathrm{Ei}}(\omega/\omega_c)-\exp(\omega/\omega_c)\,\mathrm{Ei}(-\omega/\omega_c)\Big], \quad \text{(B.4)}\end{aligned}$$

which can also be expressed in terms of the incomplete Euler's Gamma function $\Gamma(0,x) = -\mathrm{Ei}(-x)$.

Super-Ohmic case ($s = 2$)

Using the properties of Eq. (B.1) it is also straightforward to obtain $\mathrm{Re}\,\tilde{\chi}(\omega)$ in the case of $s = 2$:

$$\begin{aligned}\mathrm{Re}\,\tilde{\chi}(\omega) &= \frac{\pi\gamma}{2\omega_c}\Big\{\mathcal{H}[\Theta(\omega')\,\omega'^2\exp(-\omega'/\omega_c)](\omega)-\mathcal{H}[\Theta(-\omega')\,\omega'^2\exp(\omega'/\omega_c)](\omega)\Big\}\\ &= \frac{\pi\gamma}{2\omega_c}\Big\{\mathcal{H}[\Theta(\omega')\,\omega'^2\exp(-\omega'/\omega_c)](\omega)+\mathcal{H}[\Theta(\omega')\,\omega'^2\exp(-\omega'/\omega_c)](-\omega)\Big\}\\ &= \frac{\pi\gamma}{2\omega_c}\Big\{\omega\mathcal{H}[\Theta(\omega')\,\omega'\exp(-\omega'/\omega_c)](\omega)-\omega\mathcal{H}[\Theta(\omega')\,\omega'\exp(-\omega'/\omega_c)](-\omega)+\frac{2\omega_c^2}{\pi}\Big\}\\ &= \gamma\omega_c+\frac{\pi\gamma}{2\omega_c}\Big\{\omega^2\mathcal{H}[\Theta(\omega')\exp(-\omega'/\omega_c)](\omega)+\omega^2\mathcal{H}[\Theta(\omega')\exp(-\omega'/\omega_c)](-\omega)\Big\}\\ &= \gamma\omega_c+\frac{\pi\gamma}{2\omega_c}\omega^2\mathcal{H}[\mathrm{sign}\,\omega\exp(-|\omega'|/\omega_c)](\omega)\\ &= \gamma\omega_c-\frac{\gamma}{2\omega_c}\omega^2\Big[\exp(-\omega/\omega_c)\,\overline{\mathrm{Ei}}(\omega/\omega_c)+\exp(\omega/\omega_c)\,\mathrm{Ei}(-\omega/\omega_c)\Big].\end{aligned} \quad \text{(B.5)}$$

Appendix C

Calculation of the steady-state covariances

Now we have all the ingredients to compute the steady-state covariances of the central oscillator. Note that

$$\frac{1}{2}\langle\{x(t'),x(t'')\}\rangle = \frac{1}{2}\int_{-\infty}^{\infty}\frac{\mathrm{d}\omega'}{2\pi}\,e^{-i\omega' t'}\int_{-\infty}^{\infty}\frac{\mathrm{d}\omega''}{2\pi}\,e^{-i\omega'' t''}\,\alpha(\omega')^{-1}\alpha(\omega'')^{-1}\langle\{\tilde{F}(\omega'),\tilde{F}(\omega'')\}\rangle_T \tag{C.1}$$

$$= \int_{-\infty}^{\infty}\frac{\mathrm{d}\omega'}{2\pi}\,e^{-i\omega' t'}\int_{-\infty}^{\infty}\mathrm{d}\omega''\,e^{-i\omega'' t''}\,\alpha(\omega')^{-1}\alpha(\omega'')^{-1}$$

$$\times[J(\omega')\Theta(\omega') - J(-\omega')\Theta(-\omega')]\coth\frac{\omega'}{2T}\,\delta(\omega'+\omega'')\,\mathrm{Im}\tilde{\chi}(\omega') \tag{C.2}$$

$$= \int_{-\infty}^{\infty}\frac{\mathrm{d}\omega'}{2\pi}\,e^{-i\omega'(t'-t'')}\alpha(\omega')^{-1}\alpha(-\omega')^{-1}$$

$$\times[J(\omega')\Theta(\omega') - J(-\omega')\Theta(-\omega')]\coth\frac{\omega'}{2T}\,\mathrm{Im}\tilde{\chi}(\omega'). \tag{C.3}$$

This gives a closed expression for the position-position covariance. Note that, since $\tilde{p}(\omega) = -i\omega\,\tilde{x}(\omega)$, one has $2^{-1}\langle\{\tilde{p}(\omega'),\tilde{x}(\omega'')\}\rangle = 0$ and

$$\frac{1}{2}\langle\{p(t'),p(t'')\}\rangle = \int_{-\infty}^{\infty}\frac{\mathrm{d}\omega'}{2\pi}\,e^{-i\omega'(t'-t'')}\,\omega'^2\,\alpha(\omega')^{-1}\alpha(-\omega')^{-1}$$

$$\times[J(\omega')\Theta(\omega') - J(-\omega')\Theta(-\omega')]\coth\frac{\omega'}{2T}\,\mathrm{Im}\tilde{\chi}(\omega'). \tag{C.4}$$

Therefore, we have fully characterized the steady state of a single harmonic oscillator in a bosonic bath. Note that the *only* underlying assumption is that the environment was prepared in an equilibrium state at temperature T. Specifically, this was required when evaluating the

correlators $\langle\{x_\mu(t_0), x_\mu(t_0)\}\rangle_T$ and $\langle\{p_\mu(t_0), p_\mu(t_0)\}\rangle_T$ in Eq. (A.3). Otherwise, our calculation is *completely general*. For a non-equilibrium bath, one would only need to recalculate Eqs. (A.3) and (A.4).

Appendix D

Dependence of the normal-mode frequencies on the coupling strength in a 'star system'

Let us consider a finite *star system* with N modes. As already explained in the main text, this will be comprised of a central harmonic oscillator of bare frequency ω_0 (playing the role of the probe), dissipatively coupled to $N-1$ independent peripheral oscillators with arbitrary frequencies $\omega_{\mu\in\{1,\cdots,N-1\}}$ (representing the sample). We will choose linear probe-sample couplings of the form $x\gamma\sum_{\mu=1}^{N-1} g_\mu x_\mu$, were γ carries the order of magnitude of the coupling strengths. Note that we also allow for arbitrary frequency-distribution of the coupling constants g_μ.

Hence, the total N-particle Hamiltonian may be written as $\hat{H} = \frac{1}{2}\bar{x}^{\mathrm{t}}\mathsf{V}\bar{x} + \frac{1}{2}|\bar{p}|^2$, with $\bar{x} = (x, x_1, \cdots, x_{N-1})$ and $\bar{p} = (p, p_1, \cdots, p_{N-1})$. For simplicity of notation, we will take unit mass for all particles. The $N\times N$ interaction matrix V may thus be written as

$$\mathsf{V} = \gamma\begin{pmatrix} \gamma^{-1}\Omega_0^2 & g_1 & g_2 & \cdots & g_{N-2} & g_{N-1} \\ g_1 & \gamma^{-1}\omega_1^2 & 0 & \cdots & 0 & 0 \\ g_2 & 0 & \omega_2^2 & \cdots & 0 & 0 \\ \vdots & \vdots & \vdots & \ddots & \vdots & \vdots \\ g_{N-2} & 0 & 0 & \cdots & \gamma^{-1}\omega_{N-2}^2 & 0 \\ g_{N-1} & 0 & 0 & \cdots & 0 & \gamma^{-1}\omega_{N-1}^2 \end{pmatrix}. \tag{D.1}$$

The frequencies of the normal modes of the system are given by the square root of the N solutions λ_i of $P_N(\lambda_i) = |\mathsf{V} - \lambda_i\mathbb{1}| = 0$. Note that we have shifted the frequency of the central oscillator $\omega_0^2 \to \Omega_0^2 \coloneqq \omega_0^2 + \sum_\mu g_\mu^2/\omega_\mu^2$ to ensure that all $\lambda_i > 0$.

While it is hard to obtain closed expressions for λ_i, one may easily see the following: The frequencies of the modes above Ω_0 increase with the coupling strength, whereas those of the modes below Ω_0 decrease with γ (i.e. $\partial_\gamma \lambda_i > 0$ for $\lambda_i > \Omega_0^2$ and $\partial_\gamma \lambda_i < 0$ for $\lambda_i < \Omega_0^2$). Indeed, expanding $P_N(\lambda)$ by minors along the last row, yields the recurrence relation

$$P_N(\lambda) = (\omega_{N-1}^2 - \lambda) P_{N-1}(\lambda) - \gamma^2 g_{N-1}^2 \Pi_{k=1}^{N-2} (\omega_k^2 - \lambda), \tag{D.2}$$

which allows to rewrite the condition $P_N(\lambda_i) = 0$ as

$$\Omega_0^2 - \lambda_i = \frac{1}{\prod_{l=1}^{N-1} \omega_l^2 - \lambda_i} \sum_{k=1}^{N-1} \gamma^2 g_k^2 \prod_{l=1}^{N-1} \frac{\omega_l^2 - \lambda_i}{\omega_k^2 - \lambda_i} = \sum_{k=1}^{N-1} \frac{\gamma^2 g_k^2}{\omega_k^2 - \lambda_i}. \tag{D.3}$$

Consequently, the derivative of any eigenvalue λ_i with respect to the coupling strength γ evaluates to

$$\partial_\gamma \lambda_i = -\frac{2\gamma \sum_{k=1}^{N-1} g_k^2 (\omega_k^2 - \lambda_i)^{-1}}{1 + \sum_{k=1}^{N-1} \gamma^2 g_k^2 (\omega_k^2 - \lambda_i)^{-2}}. \tag{D.4}$$

Comparing Eqs. (D.3) and (D.4) we can see that $\partial_\gamma \lambda_i > 0$ for $\lambda_i > \Omega_0^2$, and that, on the contrary, $\partial_\gamma \lambda_i < 0$ for $\lambda_i < \Omega_0^2$.

Bibliography

[1] R Wynands and S Weyers. Atomic fountain clocks. Metrologia, 42(3):S64, 2005.

[2] Michael A Lombardi, Lisa M Nelson, Andrew N Novick, and Victor S Zhang. Time and frequency measurements using the global positioning system. Cal Lab: International Journal of Metrology, 8(3):26–33, 2001.

[3] G. Kucsko, P. C. Maurer, N. Y. Yao, M. Kubo, H. J. Noh, P. K. Lo, H. Park, and M. D. Lukin. Nanometre-scale thermometry in a living cell. Nature, 500(7460):54–58, 2013. doi: 10.1038/nature12373.

[4] BP Abbott, R Abbott, TD Abbott, MR Abernathy, F Acernese, K Ackley, C Adams, T Adams, P Addesso, RX Adhikari, et al. Observation of gravitational waves from a binary black hole merger. Physical review letters, 116(6):061102, 2016.

[5] Vittorio Giovannetti, Seth Lloyd, and Lorenzo Maccone. Quantum-enhanced measurements: beating the standard quantum limit. Science, 306(5700):1330–1336, 2004.

[6] Vittorio Giovannetti, Seth Lloyd, and Lorenzo Maccone. Advances in quantum metrology. Nat Photon, 5(4):222–229, apr 2011. ISSN 1749-4885. URL http://dx.doi.org/10.1038/nphoton.2011.35.

[7] Philip R Bevington and D Keith Robinson. Data reduction and error analysis for the physical sciences; 3rd ed. McGraw-Hill, New York, NY, 2003.

[8] H. Cramér. Mathematical methods of statistics, volume 9. Princeton university press, 1999.

[9] Harald Cramer. Mathematical methods of statistics / by Harald Cramer. Princeton University Press Princeton, 1946.

[10] Carl W. Helstrom. Quantum detection and estimation theory. Journal of Statistical Physics, 1(2):231–252, 1969. ISSN 1572-9613. doi: 10.1007/BF01007479. URL http://dx.doi.org/10.1007/BF01007479.

[11] P. Cappellaro, J. Emerson, N. Boulant, C. Ramanathan, S. Lloyd, and D. G. Cory. Entanglement Assisted Metrology. Phys. Rev. Lett., 94:020502, Jan 2005. doi: 10.1103/PhysRevLett.94.020502. URL http://link.aps.org/doi/10.1103/PhysRevLett.94.020502.

[12] S.F. F Huelga, Chiara Macchiavello, T. Pellizzari, a.K. K Ekert, M.B. B Plenio, and J. I Cirac. Improvement of Frequency Standards with Quantum Entanglement. Physical Review Letters, 79(20):3865–3868, 1997. ISSN 0031-9007. doi: 10.1103/PhysRevLett.79.3865. URL http://hdl.handle.net/2299/1048{%}5Cnhttp://link.aps.org/doi/10.1103/PhysRevLett.79.3865.

[13] Rafał Demkowicz-Dobrzański, Jan Kołodyński, and Mdlin GuÅ£. The elusive Heisenberg limit in quantum-enhanced metrology. Nature Communications, 3(2012):1063, 2012. ISSN 2041-1723. doi: 10.1038/ncomms2067. URL http://www.nature.com/doifinder/10.1038/ncomms2067.

[14] Alex W. Chin, Susana F. Huelga, and Martin B. Plenio. Quantum metrology in non-markovian environments. Physical Review Letters, 109(23):1–5, 2012. ISSN 00319007. doi: 10.1103/PhysRevLett.109.233601.

[15] Katarzyna Macieszczak. Zeno limit in frequency estimation with non-markovian environments. Phys. Rev. A, 92:010102, Jul 2015. doi: 10.1103/PhysRevA.92.010102. URL http://link.aps.org/doi/10.1103/PhysRevA.92.010102.

[16] Andrea Smirne, Jan Kołodyński, Susana F. Huelga, and Rafał Demkowicz-Dobrzański. Ultimate precision limits for noisy frequency estimation. Phys. Rev. Lett., 116:120801, Mar 2016. doi: 10.1103/PhysRevLett.116.120801. URL http://link.aps.org/doi/10.1103/PhysRevLett.116.120801.

[17] R. Chaves, J. B. Brask, M. Markiewicz, J. Ko??ody??ski, and A. Ac??n. Noisy metrology beyond the standard quantum limit. Physical Review Letters, 111(12):1–5, 2013. ISSN 00319007. doi: 10.1103/PhysRevLett.111.120401.

[18] J. B. Brask, R. Chaves, and J. Kołodyński. Improved quantum magnetometry beyond the standard quantum limit. Phys. Rev. X, 5:031010, Jul 2015. doi: 10.1103/PhysRevX.5.031010. URL http://link.aps.org/doi/10.1103/PhysRevX.5.031010.

[19] Haidong Yuan. Sequential feedback scheme outperforms the parallel scheme for hamiltonian parameter estimation. Phys. Rev. Lett., 117:160801, Oct 2016. doi: 10.1103/PhysRevLett.117.160801. URL http://link.aps.org/doi/10.1103/PhysRevLett.117.160801.

[20] Tohru Tanaka, Paul Knott, Yuichiro Matsuzaki, Shane Dooley, Hiroshi Yamaguchi, William J. Munro, and Shiro Saito. Proposed robust entanglement-based magnetic field

sensor beyond the standard quantum limit. Phys. Rev. Lett., 115:170801, Oct 2015. doi: 10.1103/PhysRevLett.115.170801. URL http://link.aps.org/doi/10.1103/PhysRevLett.115.170801.

[21] Yuichiro Matsuzaki, Simon C. Benjamin, and Joseph Fitzsimons. Magnetic field sensing beyond the standard quantum limit under the effect of decoherence. Physical Review A - Atomic, Molecular, and Optical Physics, 84(1), 2011. ISSN 10502947. doi: 10.1103/PhysRevA.84.012103.

[22] Mario Napolitano, Marco Koschorreck, Brice Dubost, Naeimeh Behbood, Robert Sewell, and Morgan W. Mitchell. Interaction-based Quantum Metrology Showing Scaling Beyond the Heisenberg Limit. In Research in Optical Sciences, page QW1B.2. Optical Society of America, 2012. doi: 10.1364/QIM.2012.QW1B.2. URL http://www.osapublishing.org/abstract.cfm?URI=QIM-2012-QW1B.2.

[23] B. M. Escher, R. L. de Matos Filho, and L. Davidovich. General framework for estimating the ultimate precision limit in noisy quantum-enhanced metrology. Nature Physics, 7(5): 406–411, 2011. ISSN 1745-2473. doi: 10.1038/nphys1958. URL http://dx.doi.org/10.1038/nphys1958.

[24] Yu Watanabe, Takahiro Sagawa, and Masahito Ueda. Optimal measurement on noisy quantum systems. Phys. Rev. Lett., 104:020401, Jan 2010. doi: 10.1103/PhysRevLett.104.020401. URL http://link.aps.org/doi/10.1103/PhysRevLett.104.020401.

[25] S. Alipour, M. Mehboudi, and A. T. Rezakhani. Quantum Metrology in Open Systems: Dissipative Cramér-Rao Bound. Phys. Rev. Lett., 112:120405, Mar 2014. doi: 10.1103/PhysRevLett.112.120405. URL http://link.aps.org/doi/10.1103/PhysRevLett.112.120405.

[26] R. Yousefjani, S. Salimi, and A. S. Khorashad. A Framework for Estimating the Ultimate Precision Limit in Noisy Metrology. ArXiv e-prints, February 2016.

[27] R Alicki and K Lendi. Quantum dynamical semigroups and applications. Lectures Notes in Physics. Springer, Berlin, 2007.

[28] H. P. Breuer and F. Petruccione. The theory of open quantum systems. Oxford University Press, Great Clarendon Street, 2002.

[29] Nicole Yunger Halpern, Philippe Faist, Jonathan Oppenheim, and Andreas Winter. Microcanonical and resource-theoretic derivations of the thermal state of a quantum system with noncommuting charges. Nature Communications, 7:12051, jul 2016. URL http://dx.doi.org/10.1038/ncomms12051http://10.0.4.14/ncomms12051http://www.nature.com/articles/ncomms12051{#}supplementary-information.

[30] P. Neumann, I. Jakobi, F. Dolde, C. Burk, R. Reuter, G. Waldherr, J. Honert, T. Wolf, A. Brunner, J. H. Shim, et al. High-precision nanoscale temperature sensing using single defects in diamond. Nano Lett., 13(6):2738–2742, 2013. doi: 10.1021/nl401216y.

[31] David M. Toyli, Charles F. de las Casas, David J. Christle, Viatcheslav V. Dobrovitski, and David D. Awschalom. Fluorescence thermometry enhanced by the quantum coherence of single spins in diamond. Proceedings of the National Academy of Sciences, 110 (21):8417–8421, 2013. doi: 10.1073/pnas.1306825110. URL http://www.pnas.org/content/110/21/8417.abstract.

[32] F. Seilmeier, M. Hauck, E. Schubert, G. J. Schinner, S. E. Beavan, and A. Högele. Optical Thermometry of an Electron Reservoir Coupled to a Single Quantum Dot in the Millikelvin Range. Phys. Rev. Applied, 2:024002, Aug 2014. doi: 10.1103/PhysRevApplied.2.024002.

[33] F. Haupt, A. Imamoglu, and M. Kroner. Single Quantum Dot as an Optical Thermometer for Millikelvin Temperatures. Phys. Rev. Applied, 2:024001, Aug 2014. doi: 10.1103/PhysRevApplied.2.024001.

[34] Carlos Sabín, Angela White, Lucia Hackermuller, and Ivette Fuentes. Impurities as a quantum thermometer for a Bose-Einstein condensate. Scientific Reports, 4: 6436, sep 2014. URL http://dx.doi.org/10.1038/srep06436http://10.0.4.14/srep06436.

[35] Matteo Brunelli, Stefano Olivares, and Matteo G. A. Paris. Qubit thermometry for micromechanical resonators. Phys. Rev. A, 84:032105, Sep 2011. doi: 10.1103/PhysRevA.84.032105. URL http://link.aps.org/doi/10.1103/PhysRevA.84.032105.

[36] Matteo Brunelli, Stefano Olivares, Mauro Paternostro, and Matteo G. A. Paris. Qubit-assisted thermometry of a quantum harmonic oscillator. Phys. Rev. A, 86:012125, Jul 2012. doi: 10.1103/PhysRevA.86.012125. URL http://link.aps.org/doi/10.1103/PhysRevA.86.012125.

[37] Kieran D. B. Higgins, Brendon W. Lovett, and Erik M. Gauger. Quantum thermometry using the ac stark shift within the rabi model. Phys. Rev. B, 88:155409, Oct 2013. doi: 10.1103/PhysRevB.88.155409. URL http://link.aps.org/doi/10.1103/PhysRevB.88.155409.

[38] Thomas M. Stace. Quantum limits of thermometry. Phys. Rev. A, 82:011611, Jul 2010. doi: 10.1103/PhysRevA.82.011611. URL http://link.aps.org/doi/10.1103/PhysRevA.82.011611.

[39] Sania Jevtic, David Newman, Terry Rudolph, and T. M. Stace. Single-qubit thermometry. Phys. Rev. A, 91:012331, Jan 2015. doi: 10.1103/PhysRevA.91.012331. URL http://link.aps.org/doi/10.1103/PhysRevA.91.012331.

[40] S. Boixo, A. Datta, M. J. Davis, S. T. Flammia, A. Shaji, and C. M. Caves. Quantum Metrology: Dynamics versus Entanglement. Phys. Rev. Lett., 101:040403, 2008. URL http://journals.aps.org/prl/abstract/10.1103/PhysRevLett.101.040403.

[41] M J Woolley, G J Milburn, and Carlton M Caves. Nonlinear quantum metrology using coupled nanomechanical resonators. New Journal of Physics, 10(12):125018, 2008. URL http://stacks.iop.org/1367-2630/10/i=12/a=125018.

[42] S. Choi and B. Sundaram. Bose-einstein condensate as a nonlinear ramsey interferometer operating beyond the heisenberg limit. Phys. Rev. A, 77:053613, May 2008. doi: 10.1103/PhysRevA.77.053613. URL http://link.aps.org/doi/10.1103/PhysRevA.77.053613.

[43] Sergio Boixo, Steven T. Flammia, Carlton M. Caves, and JM Geremia. Generalized limits for single-parameter quantum estimation. Phys. Rev. Lett., 98:090401, Feb 2007. doi: 10.1103/PhysRevLett.98.090401. URL http://link.aps.org/doi/10.1103/PhysRevLett.98.090401.

[44] Alfredo Luis. Nonlinear transformations and the Heisenberg limit. Physics Letters A, 329(1–2):8–13, 2004. ISSN 0375-9601. doi: 10.1016/j.physleta.2004.06.080. URL http://www.sciencedirect.com/science/article/pii/S0375960104009090.

[45] S. M. Roy and Samuel L. Braunstein. Exponentially enhanced quantum metrology. Phys. Rev. Lett., 100:220501, Jun 2008. doi: 10.1103/PhysRevLett.100.220501. URL http://link.aps.org/doi/10.1103/PhysRevLett.100.220501.

[46] Paolo Zanardi, Matteo G. A. Paris, and Lorenzo Campos Venuti. Quantum criticality as a resource for quantum estimation. Phys. Rev. A, 78:042105, Oct 2008. doi: 10.1103/PhysRevA.78.042105. URL http://link.aps.org/doi/10.1103/PhysRevA.78.042105.

[47] Carmen Invernizzi, Michael Korbman, Lorenzo Campos Venuti, and Matteo G. A. Paris. Optimal quantum estimation in spin systems at criticality. Phys. Rev. A, 78:042106, Oct 2008. doi: 10.1103/PhysRevA.78.042106. URL http://link.aps.org/doi/10.1103/PhysRevA.78.042106.

[48] Michael Skotiniotis, Pavel Sekatski, and Wolfgang Dür. Quantum metrology for the Ising Hamiltonian with transverse magnetic field. New Journal of Physics, 17(7):073032, 2015. URL http://stacks.iop.org/1367-2630/17/i=7/a=073032.

[49] B. Paredes, A. Widera, V. Murg, O. Mandel, S. Fölling, I. Cirac, G. V. Shlyapnikov, Th. W. Hänsch, and I. Bloch. Tonksgirardeau gas of ultracold atoms in an optical lattice. Nature, 429:277–281, 2004. URL http://www.nature.com/nature/journal/v429/n6989/full/nature02530.html.

[50] M. Lewenstein, A. Sanpera, V. Ahufinger, B. Damski, A. Sen, and U. Sen. Ultracold atomic gases in optical lattices: mimicking condensed matter physics and beyond. Adv. Phys., 56(2):243–379, 2007. doi: 10.1080/00018730701223200.

[51] J. Simon, W. S. Bakr, R. Ma, M. E. Tai, P. M. Preiss, and M. Greiner. Quantum simulation of antiferromagnetic spin chains in an optical lattice. nat, 472:307–312, April 2011. doi: 10.1038/nature09994. URL http://www.nature.com/nature/journal/v472/n7343/full/nature09994.html.

[52] R Toskovic, R van den Berg, A Spinelli, I S Eliens, B van den Toorn, B Bryant, J.-S. Caux, and A F Otte. Atomic spin-chain realization of a model for quantum criticality. Nat Phys, advance on, apr 2016. ISSN 1745-2481. URL http://dx.doi.org/10.1038/nphys372210.1038/nphys3722http://www.nature.com/nphys/journal/vaop/ncurrent/abs/nphys3722.html{#}supplementary-information.

[53] Ugo Marzolino and Daniel Braun. Precision measurements of temperature and chemical potential of quantum gases. Phys. Rev. A, 88:063609, Dec 2013. doi: 10.1103/PhysRevA.88.063609. URL http://link.aps.org/doi/10.1103/PhysRevA.88.063609.

[54] N. D. Mermin and H. Wagner. Absence of ferromagnetism or antiferromagnetism in one- or two-dimensional isotropic heisenberg models. Phys. Rev. Lett., 17:1133, 1966. URL http://journals.aps.org/prl/abstract/10.1103/PhysRevLett.17.1133.

[55] P. C. Hohenberg. Existence of long-range order in one and two dimensions. Phys. Rev., 158:383, 1967. URL http://journals.aps.org/pr/abstract/10.1103/PhysRev.158.383.

[56] S. Fölling, F. Gerbier, A. Widera, O. Mandel, T. Gericke, and I. Bloch. Spatial quantum noise interferometry in expanding ultracold atom clouds. Nature, 434:481–484, 2005. URL http://www.nature.com/nature/journal/v434/n7032/abs/nature03500.html.

[57] J. F. Sherson, Ch. Weitenberg, M. Endres, M. Cheneau, I. Bloch, and S. Kuhr. Single-atom-resolved fluorescence imaging of an atomic mott insulator. Nature, 467:68–72, 2010. URL http://www.nature.com/nature/journal/v467/n7311/abs/nature09378.html.

[58] W. S. Bakr, A. Peng, M. E. Tai, R. Ma, J. Simon, J. I. Gillen, S. Fölling, L. Pollet, and M. Greiner. Probing the superfluidtomott insulator transition at the single-atom

level. Science, 329:547–550, 2010. URL http://www.sciencemag.org/content/329/5991/547.abstract.

[59] K. Eckert, O. Romero-Isart, M. Rodriguez, M. Lewenstein, E. S. Polzik, and A. Sanpera. Quantum non-demolition detection of strongly correlated systems. Nat. Phys., 4:50–54, 2008. URL http://www.nature.com/nphys/journal/v4/n1/abs/nphys776.html.

[60] Philipp Hauke, Markus Heyl, Luca Tagliacozzo, and Peter Zoller. Measuring multipartite entanglement through dynamic susceptibilities. (March):2–7, 2016. doi: 10.1038/NPHYS3700.

[61] Gza Tth and Iagoba Apellaniz. Quantum metrology from a quantum information science perspective. Journal of Physics A: Mathematical and Theoretical, 47(42):424006, 2014. URL http://stacks.iop.org/1751-8121/47/i=42/a=424006.

[62] V. Giovannetti, S. Lloyd, and L. Maccone. Advances in quantum metrology. Nat. Phys., 5:222–229, 2011. URL http://www.nature.com/nphoton/journal/v5/n4/full/nphoton.2011.35.html.

[63] M. G. A. Paris. Quantum estimation for quantum technology. Int. J. Quant. Inf., 07:125, 2009. URL http://www.worldscientific.com/doi/abs/10.1142/S0219749909004839.

[64] S. Alipour and A. T. Rezakhani. Extended convexity of quantum fisher information in quantum metrology. Phys. Rev. A, 91:042104, Apr 2015. doi: 10.1103/PhysRevA.91.042104. URL https://link.aps.org/doi/10.1103/PhysRevA.91.042104.

[65] M. A. Nielsen and I. L. Chuang. Quantum Computation and Quantum Information. Cambridge University Press, Cambridge, England, 2010.

[66] Mark M. Wilde. Quantum Information Theory. Cambridge University Press, New York, NY, USA, 1st edition, 2013. ISBN 1107034256, 9781107034259.

[67] Hans-Jürgen Sommers and Karol Zyczkowski. Bures volume of the set of mixed quantum states. Journal of Physics A: Mathematical and General, 36(39):10083, 2003. URL http://stacks.iop.org/0305-4470/36/i=39/a=308.

[68] Sj Gu. doi: 10.1142/S0217979210056335.

[69] Paolo Zanardi, Lorenzo Campos Venuti, and Paolo Giorda. Bures metric over thermal state manifolds and quantum criticality. Phys. Rev. A, 76:062318, Dec 2007. doi: 10.1103/PhysRevA.76.062318. URL http://link.aps.org/doi/10.1103/PhysRevA.76.062318.

[70] Paolo Zanardi, H. T. Quan, Xiaoguang Wang, and C. P. Sun. Mixed-state fidelity and quantum criticality at finite temperature. Phys. Rev. A, 75:032109, Mar 2007. doi: 10.1103/PhysRevA.75.032109. URL https://link.aps.org/doi/10.1103/PhysRevA.75.032109.

[71] Howard M Wiseman and Gerard J Milburn. Quantum Measurement and Control. Cambridge University Press, Leiden, 2009.

[72] T. Jahnke, S. Lanéry, and G. Mahler. Operational approach to fluctuations of thermodynamic variables in finite quantum systems. Phys. Rev. E, 83:011109, Jan 2011. doi: 10.1103/PhysRevE.83.011109. URL https://link.aps.org/doi/10.1103/PhysRevE.83.011109.

[73] Mohammad Mehboudi, Luis A. Correa, and Anna Sanpera. Achieving sub-shot-noise sensing at finite temperatures. Phys. Rev. A, 94:042121, Oct 2016. doi: 10.1103/PhysRevA.94.042121. URL http://link.aps.org/doi/10.1103/PhysRevA.94.042121.

[74] A. Monras. Phase space formalism for quantum estimation of Gaussian states. arXiv preprint arXiv:1303.3682, 2013. URL http://arxiv.org/abs/1303.3682.

[75] Zhang Jiang. Quantum fisher information for states in exponential form. Phys. Rev. A, 89:032128, Mar 2014. doi: 10.1103/PhysRevA.89.032128. URL http://link.aps.org/doi/10.1103/PhysRevA.89.032128.

[76] Giulio Salvatori, Antonio Mandarino, and Matteo G. A. Paris. Quantum metrology in Lipkin-Meshkov-Glick critical systems. Phys. Rev. A, 90:022111, Aug 2014. doi: 10.1103/PhysRevA.90.022111. URL http://link.aps.org/doi/10.1103/PhysRevA.90.022111.

[77] M Mehboudi, M Moreno-Cardoner, G De Chiara, and A Sanpera. Thermometry precision in strongly correlated ultracold lattice gases. New Journal of Physics, 17(5):055020, 2015. URL http://stacks.iop.org/1367-2630/17/i=5/a=055020.

[78] Antonella De Pasquale, Davide Rossini, Rosario Fazio, and Vittorio Giovannetti. Local quantum thermal susceptibility. Nature Communications, 7:12782, sep 2016. URL http://dx.doi.org/10.1038/ncomms12782http://10.0.4.14/ncomms12782http://www.nature.com/articles/ncomms12782{#}supplementary-information.

[79] Li-Sha Guo, Bao-Ming Xu, Jian Zou, and Bin Shao. Improved thermometry of low-temperature quantum systems by a ring-structure probe. Phys. Rev. A, 92:052112, Nov 2015. doi: 10.1103/PhysRevA.92.052112. URL http://link.aps.org/doi/10.1103/PhysRevA.92.052112.

[80] E. Lieb, Th. Schultz, and D. Mattis. Two soluble models of an antiferromagnetic chain. Ann. Phys. (NY), 16:407–466, 1961. URL http://www.sciencedirect.com/science/article/pii/0003491661901154.

[81] Hans-Jürgen Mikeska and Alexei K. Kolezhuk. One-dimensional magnetism. In Ulrich Schollwöck, Johannes Richter, DamianJ.J. Farnell, and RaymodF. Bishop, editors, Quantum Magnetism, volume 645 of Lecture Notes in Physics, pages 1–83. Springer Berlin Heidelberg, 2004. ISBN 978-3-540-21422-9. doi: 10.1007/BFb0119591. URL http://dx.doi.org/10.1007/BFb0119591.

[82] J. Kurmann and H. Thomas. Antiferromagnetic long-range order in the anisotropic quantum spin chain. Physica A, 112:235–255, 1981. URL http://www.sciencedirect.com/science/article/pii/0378437182902175.

[83] S. M. Giampaolo, G. Adesso, and F. Illuminati. Theory of ground state factorization in quantum cooperative systems. Phys. Rev. Lett., 100:197201, 2008. URL http://journals.aps.org/prl/abstract/10.1103/PhysRevLett.100.197201.

[84] J. Simon, W. S. Bakr, R. Ma, M. E. Tai, Ph. M. Preiss, and M. Greiner. Quantum simulation of antiferromagnetic spin chains in an optical lattice. Nature, 472:307–312, 2011. URL http://www.nature.com/nature/journal/v472/n7343/full/nature09994.html.

[85] M. Roncaglia, C. D. E. Boschi, and A. Montorsi. Hidden xy structure of the bond-charge hubbard model. Phys. Rev. B, 82:233105, 2010. URL http://journals.aps.org/prb/abstract/10.1103/PhysRevB.82.233105.

[86] D. Kupriyanov, O. Mishina, I. Sokolov, B. Julsgaard, and E. Polzik. Multimode entanglement of light and atomic ensembles via off-resonant coherent forward scattering. Phys. Rev. A, 71:032348, Mar 2005. doi: 10.1103/PhysRevA.71.032348. URL http://link.aps.org/doi/10.1103/PhysRevA.71.032348.

[87] K. Eckert, L. Zawitkowski, A. Sanpera, M. Lewenstein, and E.S. Polzik. Quantum polarization spectroscopy of ultracold spinor gases. Phys. Rev. Lett., 98:100404, 2007. URL http://journals.aps.org/prl/abstract/10.1103/PhysRevLett.98.100404.

[88] T. Roscilde, M. Rodriguez, K. Eckert, O. Romero-Isart, M. E. Lewenstein, Polzik, and A. Sanpera. Quantum polarization spectroscopy of correlations in attractive fermionic gases. New. J. Phys., 11:055041, 2009. URL http://iopscience.iop.org/1367-2630/11/5/055041.

[89] B. Rogers, M. Paternostro, J. F. Sherson, and G. De Chiara. Characterization of bose-hubbard models with quantum nondemolition measurements. Phys. Rev. A, 90:043618,

2014. URL http://journals.aps.org/pra/abstract/10.1103/PhysRevA.90.043618.

[90] G. De Chiara, O. Romero-Isart, and A. Sanpera. Probing magnetic order in ultracold lattice gases. Phys. Rev. A, 83:021604(R), 2011. URL http://journals.aps.org/pra/abstract/10.1103/PhysRevA.83.021604.

[91] G. De Chiara and A. Sanpera. Detection of entanglement in ultracold lattice gases. J. Low Temp. Phys., 165:292–305, 2011.

[92] P. Hauke, R. J. Sewell, M. W. Mitchell, and M. Lewenstein. Quantum control of spin correlations in ultracold lattice gases. Phys. Rev. A, 87:021601, 2013. URL http://journals.aps.org/pra/abstract/10.1103/PhysRevA.87.021601.

[93] G. Toth and Morgan W Mitchell. Generation of macroscopic singlet states in atomic ensembles. New Journal of Physics, 12(5):053007, 2010. URL http://stacks.iop.org/1367-2630/12/i=5/a=053007.

[94] S. L. Braunstein and C. M. Caves. Statistical distance and the geometry of quantum states. Phys. Rev. Lett., 72:3439, 1994. URL http://journals.aps.org/prl/abstract/10.1103/PhysRevLett.72.3439.

[95] L. Tarruell, D. Greif, T. Uehlinger, G. Jotzu, and T. Esslinger. Creating, moving and merging dirac points with a fermi gas in a tunable honeycomb lattice. Nature, 483:302–305, 2012. URL http://www.nature.com/nature/journal/v483/n7389/nature10871/metrics/blogs.

[96] L. A. Correa, M. Mehboudi, G. Adesso, and A. Sanpera. Individual Quantum Probes for Optimal Thermometry. Phys. Rev. Lett., 114:220405, Jun 2015. doi: 10.1103/PhysRevLett.114.220405.

[97] A. De Pasquale, D. Rossini, R. Fazio, and V. Giovannetti. Local quantum thermal susceptibility. Nat. Commun., 7:12782, September 2016. doi: 10.1038/ncomms12782. URL http://dx.doi.org/10.1038/ncomms12782.

[98] Wen-Long You, Ying-Wai Li, and Shi-Jian Gu. Fidelity, dynamic structure factor, and susceptibility in critical phenomena. Phys. Rev. E, 76:022101, Aug 2007. doi: 10.1103/PhysRevE.76.022101. URL https://link.aps.org/doi/10.1103/PhysRevE.76.022101.

[99] Lorenzo Campos Venuti and Paolo Zanardi. Quantum critical scaling of the geometric tensors. Phys. Rev. Lett., 99:095701, Aug 2007. doi: 10.1103/PhysRevLett.99.095701. URL https://link.aps.org/doi/10.1103/PhysRevLett.99.095701.

[100] H. T. Quan. Finite-temperature scaling of magnetic susceptibility and the geometric phase in the XY spin chain. Journal of Physics A Mathematical General, 42:395002, October 2009. doi: 10.1088/1751-8113/42/39/395002.

[101] D. Braun, G. Adesso, F. Benatti, R. Floreanini, U. Marzolino, M. W. Mitchell, and S. Pirandola. Quantum enhanced measurements without entanglement. arXiv e-prints, January 2017.

[102] A. O. Caldeira and A. J. Leggett. Path integral approach to quantum Brownian motion. Phys. A, 121:587–616, 1983. doi: 10.1016/0378-4371(83)90013-4.

[103] U. Weiss. Quantum dissipative systems, volume 13. World Scientific Pub Co Inc, 2008.

[104] L. A. Correa, A. A. Valido, and D. Alonso. Asymptotic discord and entanglement of nonresonant harmonic oscillators under weak and strong dissipation. Phys. Rev. A, 86: 012110, Jul 2012. doi: 10.1103/PhysRevA.86.012110.

[105] H. Grabert, U. Weiss, and P. Talkner. Quantum theory of the damped harmonic oscillator. Z. Phys. B, 55(1):87–94, 1984. doi: 10.1007/BF01307505.

[106] A. A. Valido, L. A. Correa, and D. Alonso. Gaussian tripartite entanglement out of equilibrium. Phys. Rev. A, 88:012309, Jul 2013. doi: 10.1103/PhysRevA.88.012309.

[107] A. A. Valido, D. Alonso, and S. Kohler. Gaussian entanglement induced by an extended thermal environment. Phys. Rev. A, 88:042303, Oct 2013. doi: 10.1103/PhysRevA.88.042303.

[108] A. A. Valido, A. Ruiz, and D. Alonso. Quantum correlations and energy currents across three dissipative oscillators. Phys. Rev. E, 91:062123, Jun 2015. doi: 10.1103/PhysRevE.91.062123.

[109] A. Ferraro, S. Olivares, and M. G. A. Paris. Gaussian states in continuous variable quantum information. Bibliopolis, Napoli, 2005. URL https://arxiv.org/abs/quant-ph/0503237.

[110] H. Scutaru. Fidelity for displaced squeezed thermal states and the oscillator semigroup. J. Phys. A: Math. Gen., 31(15):3659, 1998. doi: 10.1088/0305-4470/31/15/025.

[111] O. E. Barndorff-Nielsen and R. D. Gill. Fisher information in quantum statistics. J. Phys. A, 33(24):4481, 2000. doi: 10.1088/0305-4470/33/24/306.

[112] S. L. Braunstein and C. M. Caves. Statistical distance and the geometry of quantum states. Phys. Rev. Lett., 72:3439–3443, May 1994. doi: 10.1103/PhysRevLett.72.3439.

[113] T. Bastin, J. von Zanthier, and E. Solano. Measure of phonon-number moments and motional quadratures through infinitesimal-time probing of trapped ions. J. Phys. B: At. Mol. Opt. Phys., 39(3):685, 2006. doi: 10.1088/0953-4075/39/3/020.

[114] C. D'Helon and G. J. Milburn. Reconstructing the vibrational state of a trapped ion. Phys. Rev. A, 54:R25–R28, Jul 1996. doi: 10.1103/PhysRevA.54.R25.

[115] J. F. Poyatos, R. Walser, J. I. Cirac, P. Zoller, and R. Blatt. Motion tomography of a single trapped ion. Phys. Rev. A, 53:R1966–R1969, Apr 1996. doi: 10.1103/PhysRevA.53.R1966.

[116] Y. Subaşı, C. H. Fleming, J. M. Taylor, and B. L. Hu. Equilibrium states of open quantum systems in the strong coupling regime. Phys. Rev. E, 86:061132, Dec 2012. doi: 10.1103/PhysRevE.86.061132.

[117] L. A. Correa, M. Perarnau-Llobet, K. V. Hovhannisyan, S. Hernández-Santana, M. Mehboudi, and A. Sanpera. Low-temperature thermometry enhanced by strong coupling. arXiv e-prints, November 2016.

[118] Steve Campbell, Gabriele De Chiara, and Mauro Paternostro. Equilibration and non-classicality of a double-well potential. Scientific Reports, 6:19730, jan 2016. URL http://dx.doi.org/10.1038/srep19730http://10.0.4.14/srep19730.

[119] P Zoller and C W Gardiner. Quantum Noise in Quantum Optics: the Stochastic Schrdinger Equation. (quant-ph/9702030), 1997.

[120] William H Louisell. Quantum statistical properties of radiation. Wiley series in pure and applied optics. Wiley, New York, NY, 1973.

[121] Luis A Correa, José P Palao, and Daniel Alonso. Internal dissipation and heat leaks in quantum thermodynamic cycles. Physical Review E, 92(3):032136, 2015.

[122] Luis A. Correa, José P. Palao, and Daniel Alonso. Internal dissipation and heat leaks in quantum thermodynamic cycles. Phys. Rev. E, 92:032136, Sep 2015. doi: 10.1103/PhysRevE.92.032136. URL https://link.aps.org/doi/10.1103/PhysRevE.92.032136.

[123] J. E. Geusic, E. O. Schulz-DuBios, and H. E. D. Scovil. Quantum equivalent of the carnot cycle. Phys. Rev., 156:343–351, Apr 1967. doi: 10.1103/PhysRev.156.343. URL http://link.aps.org/doi/10.1103/PhysRev.156.343.

[124] A. G. Kofman, G. Kurizki, and B. Sherman. Spontaneous and induced atomic decay in photonic band structures. J. Mod. Opt., 41(2):353–384, 1994. doi: 10.1080/09500349414550381.

[125] J. F. Poyatos, J. I. Cirac, and P. Zoller. Quantum Reservoir Engineering with Laser Cooled Trapped Ions. Phys. Rev. Lett., 77:4728–4731, Dec 1996. doi: 10.1103/PhysRevLett.77.4728.

[126] A. Zwick, G. A. Álvarez, and G. Kurizki. Maximizing Information on the Environment by Dynamically Controlled Qubit Probes. Phys. Rev. Applied, 5:014007, Jan 2016. doi: 10.1103/PhysRevApplied.5.014007.

[127] G. Lindblad. On the generators of quantum dynamical semigroups. Communications in Mathematical Physics, 48(2):119–130, 1976. ISSN 1432-0916. doi: 10.1007/BF01608499. URL http://dx.doi.org/10.1007/BF01608499.

[128] Matteo G. A. Paris, Fabrizio Illuminati, Alessio Serafini, and Silvio De Siena. Purity of gaussian states: Measurement schemes and time evolution in noisy channels. Phys. Rev. A, 68:012314, Jul 2003. doi: 10.1103/PhysRevA.68.012314. URL https://link.aps.org/doi/10.1103/PhysRevA.68.012314.

[129] Gerardo Adesso, Sammy Ragy, and Antony R Lee. Continuous variable quantum information: Gaussian states and beyond. Open Systems & Information Dynamics, 21 (01n02):1440001, 2014.

[130] Herbert B. Callen and Theodore A. Welton. Irreversibility and generalized noise. Phys. Rev., 83:34–40, Jul 1951. doi: 10.1103/PhysRev.83.34. URL http://link.aps.org/doi/10.1103/PhysRev.83.34.

[131] J. Prost, J. F. Joanny, and J. M R Parrondo. Generalized fluctuation-dissipation theorem for steady-state systems. Physical Review Letters, 103(9):1–4, 2009. ISSN 00319007. doi: 10.1103/PhysRevLett.103.090601.

[132] H. Bateman. Tables of integral transforms (vol. II). California Institute of Technology Bateman Manuscript Project, New York: McGraw-Hill, 1954, edited by Erdelyi, Arthur, 1, 1954.